2009

Design of Sea Water Heat Exchanger for Miniature Vapor Compression Cycle

James Hughes
University of Central Florida

DESIGN OF SEA WATER HEAT EXCHANGER FOR MINIATURE VAPOR COMPRESSION CYCLE

by

JAMES HUGHES
B.S. University of Central Florida, 2006

A thesis submitted in partial fulfillment of the requirements
for the degree of Master of Science
in the Department of Mechanical, Materials and Aerospace Engineering
in the College of Engineering and Computer Science
at the University of Central Florida
Orlando, Florida

Fall Term
2009

Major Professor: Louis Chow

ABSTRACT

Recent advances in the development of miniature vapor compression cycle components have created unique opportunities for heating and cooling applications, specifically to human physiological requirements that arise in extreme environments. Diving in very cold water between 1.7 and 5°C requires active heating because passive thermal insulation has proven inadequate for long durations. To maintain diver mobility and cognitive performance, it is desirable to provide 250 to 300 W of heat from an un-tethered power source. The use of a miniature vapor compression cycle reduces the amount of power (batteries or fuel cell) that the diver must carry by 2.5 times over a standard resistive heater. This study develops the compact evaporator used to extract heat from the sea water to provide heat to the diver. The performance is calculated through the application of traditional single-phase and two-phase heat transfer correlations using numerical methods. Fabrication methods were investigated and then a prototype was manufactured. A test stand was developed to fully characterize the evaporator at various conditions. The evaporator is then evaluated for the conditions of interest. Test results suggest the correlations applied over predict performance up to 20%. The evaporator tested meets the performance specifications and design criteria and is ready for system integration.

I dedicate this work to my loving wife Kate. Without her support, encouragement, and faith I would not be where I am today. I would also like to thank my parents, Larry and Marian for providing inspiration and nurturing my creativity and interest in engineering.

I would also like to dedicate this to my brother Dan Hughes who passed away in 2004 for his friendship, guidance, and courage. You are greatly missed by many.

ACKNOWLEDGMENTS

I would like to thank Dr. Louis Chow for the opportunities he provided as well as his encouragement and academic advisement throughout my undergraduate and graduate years. I would also like to thank Dr. Daniel Rini and Ben Saarloos for technical advisement and funding. Special thanks are extended to my advisory committee members, Dr. Olusegun Ilegbusi and Dr. David Nicholson.

TABLE OF CONTENTS

LIST OF FIGURES

LIST OF TABLES

NOMENCLATURE

B	Friction factor relationship constant	[-]
C	Turbulent-Viscous constant	[-]
Cp	Specific Heat	[J/kg*K]
D	Diameter	[m]
D_h	Hydraulic diameter	[m]
E	Modulus of elasticity	[Pa]
f	Friction factor	[-]
F_{cr}	Critical force	[N]
F_{ReAR}	Reynolds number aspect ratio factor	[-]
F_{Xtt}	Collier empirical correlation	[-]
G	Mass flux	[kg/m^2*s]
Gr	Grashof number	[-]
h	Heat transfer coefficient	[W/m^2*K]
h	Enthalpy	[J/kg*K]
H	Head loss	[Pa/m]
k	Thermal conductivity	[W/m*K]
L	Length	[m]
LMTD	Log mean temperature difference	[K]
n_b	Number of buckling lobes	[-]
Nu	Nusselt number	[-]
P	Pressure	[Pa]
P_{cr}	Critical buckling pressure	[Pa]
Pr	Prandtl number	[-]
Q	Heat rate	[W]
r	Radius	[m]
Re	Reynolds number	[-]
t	Thickness	[m]
t_{bcl}	Minimum cylinder thickness for buckling	[m]
T	Temperature	[K]
V_{dot}	Volumetric flow rate	[m^3/s]
x	Quality	[-]
X	Martinelli parameter	[-]
β	Volumetric expansion coefficient	[1/K]
λ	Thinness ratio	[-]
μ	Viscosity	[kg/m*s]
v	Kinematic viscosity	[m^2/s]
v	Poisson's ratio	[-]
ρ	Density	[kg/m^3]
σ_{sat}	Saturated liquid surface tension	[N/m]
σ_{yp}	Tensile yield strength	[Pa]
φ	Phase	[-]

Subscripts and Abbreviations

0	Initial
al	Aluminum
amb	Ambient
ch	channel
f	Liquid
g	Vapor
i	Inner
o	Outer
R134a	1,1,1,2-Tetrafluoroethane haloalkane refrigerant
ref	Reference
sat	Saturation
sur	Surface

CHAPTER ONE: INTRODUCTION

The passive thermal protection used for divers in temperature extremes and hazardous water conditions is inadequate for long duration dives. Currently, closed cell neoprene insulation is used to protect the diver in cold water for short periods of time. This is the same material used in commercially available wet suits. In order to increase the thermal resistance, the insulation thickness is increased, which limits the diver's mobility. Another draw back to the closed-cell insulation is a reduction in thermal resistance with depth. As the diver descends and pressure increases, the closed cells of gas in the insulation are compressed, reducing the thermal resistance by 50% at 15 msw (meters of seawater)[1], and thus reducing the overall effectiveness of the insulation. In addition to heating in cold water, cooling of the diver is needed in warm water dives to prevent heat stress as well as increase diver capability. This need is magnified for contaminated water dives because the diver must don a dry suit as personal protective equipment (PPE) even in warm water.

To maintain thermal neutrality in extreme hot and cold water conditions, **active thermal management is required**. The level of heating/cooling required to maintain safe skin and core body temperatures varies with the ambient water temperature. Studies have been performed and reported by Bardy et al.[2], as shown in Figure 1. In these studies "thermal neutrality" resulted in the subject remaining still in the water and staying within the defined "safe" thermal limits[3] for an extended period of time. The target performance for heating (**300 W in 1.7°C water**) is selected to exceed the 6.5 mm thick wetsuit data at the extreme temperature conditions. Coupled with additional body heat

generated from physical activity, it is anticipated that the unit will meet a diver's heating needs with a 3-mm wetsuit as well.

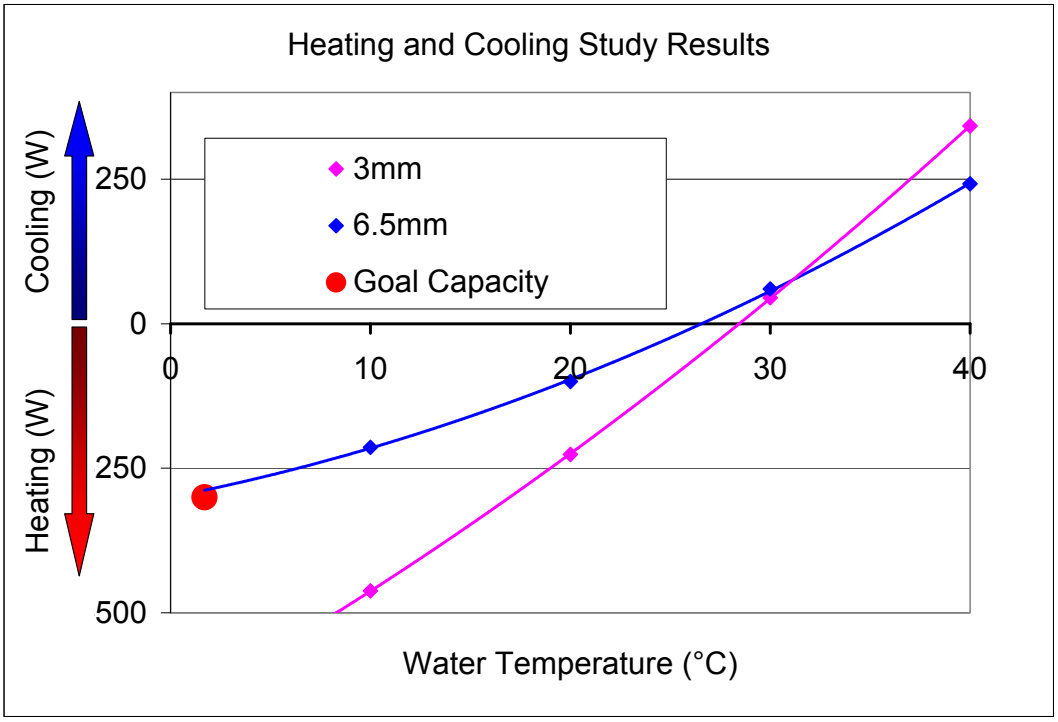

Figure 1: Heating and cooling requirements

The diver target heating/cooling load range is one that fits in the area between efficient conventional vapor compression cycle technology and the "micro"-cooling loads often cooled with Thermo-Electric Coolers (TECs). Figure 2 illustrates the cooling ranges that currently available devices such as TECs and commercial heat pumps operate at optimum efficiency.

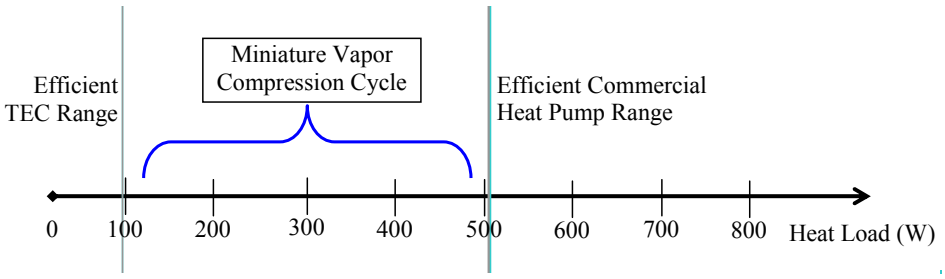

Figure 2: Target heat pump range for greatest efficiency

In the past, diver heating systems have utilized inefficient resistive heaters to help the diver maintain thermal equilibrium. Resistive heaters at best can provide only the amount of power consumed as heat (Coefficient of Performance, COP = 1.0). This is a very inefficient way to provide heat and it cannot provide cooling in warm water. Thermo-electrics can provide both heating and cooling, however they are also very inefficient in the target heating/cooling range. The use of a custom Miniature Vapor Compression Cycle (MVCC) will provide both heating and cooling with a COP around 2.5 in a similar manner that a residential home's heat pump can provide heating in the winter and cooling in the summer. The MVCC is coupled with a small water loop connected to a tube-suit garment to heat or cool the diver. A MVCC for heating the diver is shown in Figure 3. The low pressure vapor (arrow 1), enters the rotary compressor and is compressed to high pressure, high temperature vapor (arrow 2). The high pressure vapor is then condensed in the internal heat exchanger, adding heat to the water that circulates to the diver, thus heating the diver. The condensed high pressure refrigerant (arrow 3) is then expanded to a low pressure, low temperature 2-phase mixture of liquid and vapor (arrow 4). The 2-phase flow then takes in heat from the ambient ocean water through the external heat exchanger and evaporates to low pressure vapor (arrow 1), completing the MVCC. This continues in a steady-state fashion.

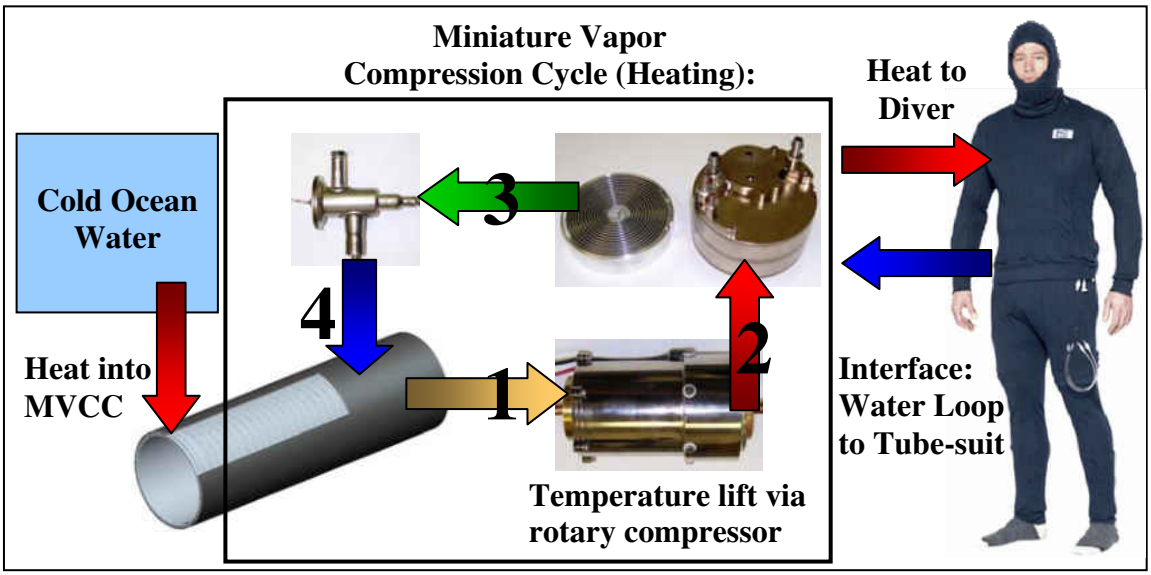

Figure 3: MVCC heating cycle, taking heat from ocean and heating diver

The MVCC is purposefully targeted to heat loads so "small" that conventional heat pumps are simply too bulky and heavy, and so "large" that TECs are too inefficient. In general, TEC coefficient of performance diminish to less than 1 with cooling loads exceeding 100 W (with temperature lifts greater than 10°C) meaning more electrical power is consumed than cooling is supplied. Conversely, conventional heat pump technology that is efficient and relatively lightweight for multi-kW heat loads quickly becomes excessively heavy in the sub-kW range. **Neither technology is well-suited to the application at hand**.

In MVCC, as in any vapor compression cycle, an important component affecting overall weight and efficiency is the compressor. Over the past six years, Rini Technologies, Inc. (RINI) has been developing the miniature rotary compressor shown in Figure 4, as part of a lightweight MVCC for portable personal cooling (with funding from ARMY, DARPA, DHS, NASA, ONR). The rotary compressor has a number of key attributes which make it more suitable for use in diving applications than other

compressor types. In particular, RINI's compressor possesses the following attributes which meet the Navy's needs:

- **Orientation Independence** due to lack of compressor oil reservoir; a key feature since divers are not always "up right". The RINI compressor is the **only** miniature refrigeration compressor on the market today that is orientation independent.
- **Variable Lift and Load Capability** by controlling and varying the operating speed to minimize power consumption and maximize performance under all conditions.
- **High Temperature Lift** due to high compression ratio of the positive displacement motion of the rotor and a unique compressor valve design.
- **Highly Efficient Compression & Compact Design** due to compression via rotary motion instead of reciprocating parts.
- **Versatile Design.** Simple changes to the rotor allow the compressor displacement to be fine-tuned to match a desired motor operating speed for maximum efficiency.
- **Reliable Performance** has been demonstrated by maintaining performance within 10% for over 1000 hours of run time.

Figure 4: RINI rotary compressor

In addition to the compressor, RINI has developed a water pump and condenser. The condenser, shown in Figure 5, exchanges heat between the refrigerant and small water loop that heats the diver. The water pump provides the flow for the small water loop through the condenser and diver's tube-suit. The water pump is shown in Figure 6.

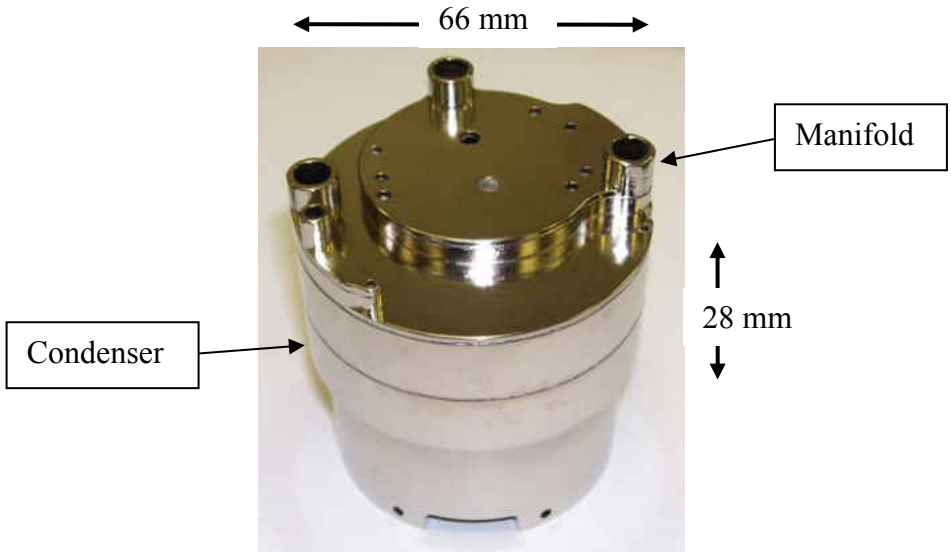

Figure 5: RINI Condenser

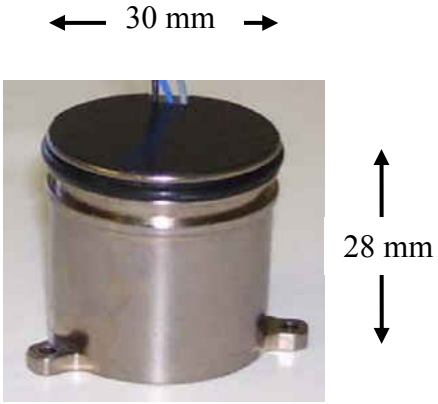

Figure 6: RINI water pump

With these existing components developed through other efforts, an evaporator design is needed to implement the MVCC for cold water diving. The focus of this study is to develop, test and evaluate an evaporator to be incorporated with the existing MVCC components.

CHAPTER TWO: HEAT EXCHANGER DESIGN

Design Requirements

Although a sea-water heat exchanger can be applied to various marine heating and cooling applications, this specific diver heat pump application has several specific criteria defined by the Navy and the remaining components. The thermal requirements are determined from the heating and cooling report presented in Figure 1. These requirements include reliability, environmental resistance, off-gas testing, and depth rating.

A primary requirement desired is to have the smallest volume packaging for the heat pump. The heat pump should not interfere with the diver's range of motion and minimally impedes the diver's ability to carry equipment such as communications, ammunition, and weaponry. Thus the heat exchanger must be the smallest possible envelope volume while encasing the other components of the heat pump. The envelope volume is defined by the largest diameter and major length. The heat pump components that the heat exchanger will encase will restrict the minimum dimensions to a diameter of 81 mm by 190 mm long.

The environment resistance requirement necessitates the material and coating options capable of with standing salt water environments and abrasion. The heat exchanger will be used in water consisting of particulate, chemical, and biological contaminates typically found in ocean water and fresh water lakes for durations up to 12 hours. Thus it must be highly corrosion resistant and easy to decontaminate.

The material and coating selection is further limited by the off-gas requirements set by NAVSEA P-9290. The off-gas requirements are necessary for bringing the unit onto a submarine where anything that the heat exchanger off gasses enters the breathing loop.

The unit must also be capable of operating at a depth rating of 91 meters of sea water (MSW). For the average density of seawater (1027 kg/m^3) the pressure is 916 Pa (134 PSI). This will require analysis of the end plates used to seal the heat exchanger as well as buckling analysis of the heat exchanger.

It is desirable for the unit to be neutrally buoyant in sea water. Knowing the weight of the internal components of the system 1.7 kg (3.8 lbs), the displacement required for neutral buoyancy is calculated to be 1.68 L (102 in^3). The minimum volume of the core (81 mm diameter by 190 mm length) however, is only 0.99 L (2.2 lbs), thus the unit starts out with a buoyancy of -1.6 lbs. Since the volume of the unit is a higher design priority, the weight of the evaporator will be minimized to limit the negative buoyancy of the system. The priority of the design requirements is listed in Table 1.

Table 1: Summary of design requirements applicable to heat exchanger

1. Enclose 81 mm diameter by 190 mm length
2. Provide 300 W of heat
3. Supply water temperature 35°C (95°F)
4. Provide minimum envelope volume
5. Pass environmental resistance testing
6. Pass off-gas test (P-9290)
7. Pass depth rating of 91 m
8. Provide neutral buoyancy

The thermal requirements are driven by the Navy's system requirements and efficiency of the compressor and condenser. The Navy requires that the system provide 300 W of heat to the diver in 1.7°C (35°F) water. Thermodynamic analysis of the system

determines the approximate heat load required. The temperature-entropy diagram to be analyzed is shown in Figure 7. The compressor is an existing specialized miniature rotary compressor with known efficiencies across a range of operating conditions. In order to know the compressor isentropic efficiency, the inlet pressure, temperature lift, and mass flow must be known. With this information, correlations to compressor test data determine the isentropic efficiency of the compressor.

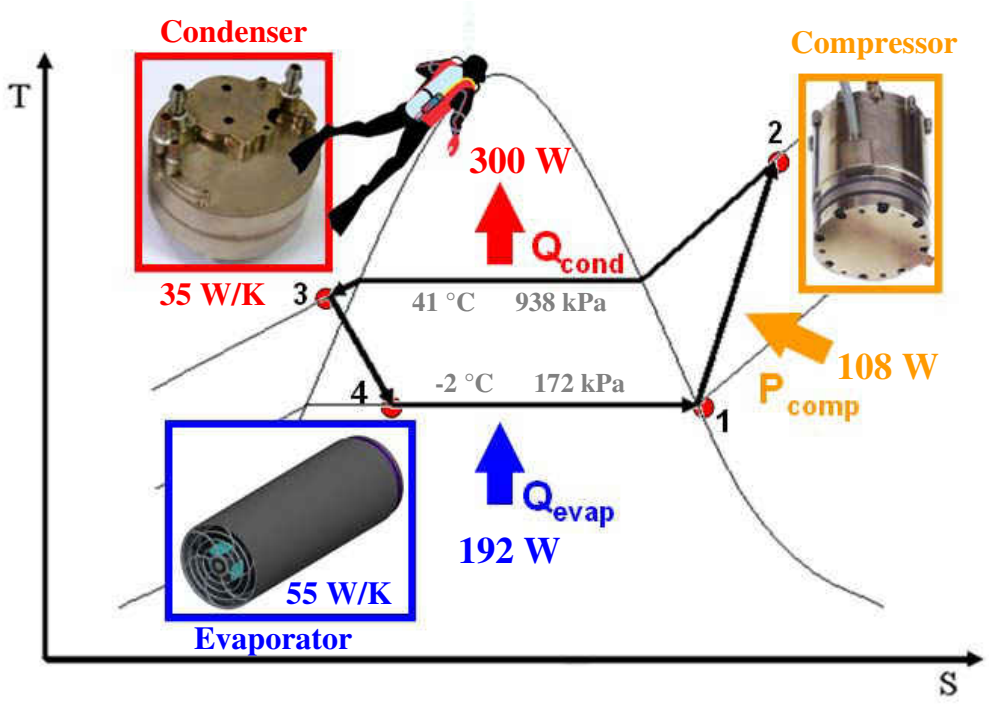

Figure 7: Preliminary temperature-entropy diagram

Starting with the 300 W of heating to the diver and 35°C supply water temperature needed from the condenser, the condensing pressure and mass flow rate required can be determined based on the known performance.

Table 2: Condenser analysis

Cycle Stage	Condenser Analysis	
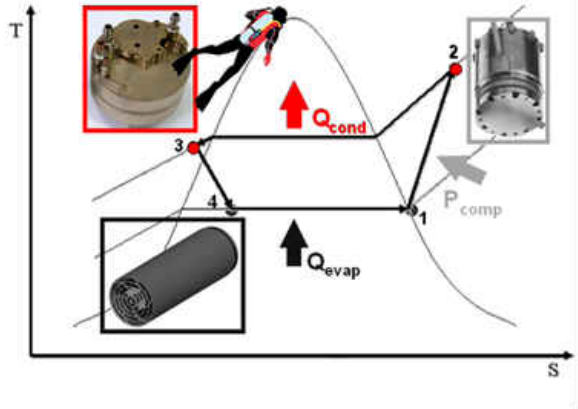	Heat Exchange:	300 W
	Weight:	0.14 kg
	Maximum Diameter:	66 mm
	Length:	28 mm
	Performance:	35 W/K
	Water Pressure Drop:	13.8 kPa
	Water Flow Rate:	12.6 cc/s
	Water Pump Power:	6 W
	Water Outlet Temperature:	35 °C
	Saturation Temperature:	41 °C
	Saturation Pressure:	938 kPa

With the condenser requirements determined, using the ambient water temperature and an estimated evaporator performance, the required heat absorption and saturation pressure can be determined.

Table 3: Estimated evaporator thermal requirements

Cycle Stage	Evaporator Analysis	
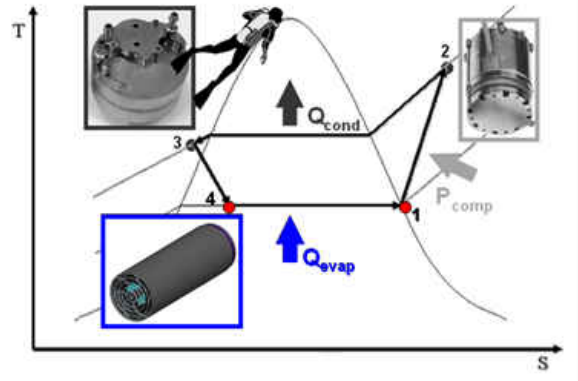	Performance (est.):	55 W/K
	Ambient Sea Temperature:	1.7 °C
	Heat Absorption:	192 W
	Saturation Temperature:	-1.8 °C
	Saturation Pressure:	172 kPa

Using the results obtained from the thermodynamic analyses of the condenser and estimated evaporator, it was then possible to approximately identify the requirements of the compressor. The compressor and motor requirements are listed below in Table 4, which include a motor efficiency of 83% and a maximum component length of 84 mm and diameter of 66 mm.

Table 4: Approximate compressor component requirements

Cycle Stage	Compressor Analysis	
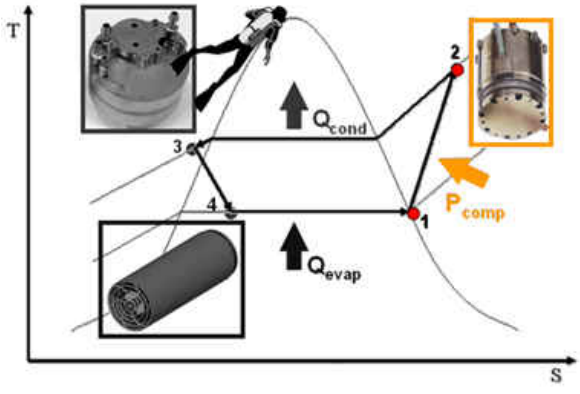	Electrical Power:	108 W
	Mass Flow Rate:	1.29 gm/s
	Weight:	1.1 kg
	Maximum Diameter:	66 mm
	Length:	84 mm
	Motor Efficiency:	83 %
	Isentropic Efficiency:	41%

Due to the variability in water temperature and heat rate required of the unit, a fixed expansion device such as a capillary tube will not suffice. A thermostatic expansion valve (TXV) actively controls the restriction such that a constant superheat is maintained. This maximizes evaporator performance which in turn minimizes compressor lift and power over a much wider range of conditions than allowed by a fixed restriction. The TXV senses the temperature of the evaporator outlet gas through a remote bulb attached to the evaporator outlet. A commercially available TXV is shown in Figure 8.

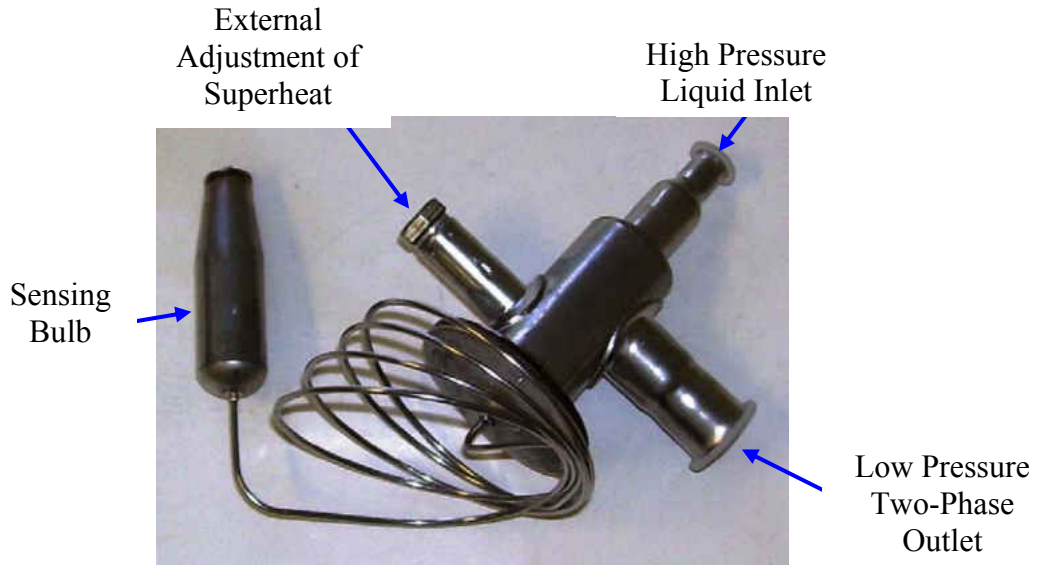

Figure 8: Thermostatic expansion valve (TXV)

The final major component of the heating unit will be the water pump providing the flow through the condenser and tube-suit, which is analyzed in Table 5. The custom high efficiency pump is positive displacement and self-priming.

Table 5: FDHS Water Pump

Water Pump	Water Pump Analysis	
	Flow Rate:	12.6 cc/s
	Lift:	70 kPa
	Electrical Power:	6 W
	Motor Efficiency:	80%
	Length:	28 mm
	Diameter:	30 mm

Conceptual Design

Determination Of Minimum Volume

Minimizing the total system volume is the driving constraint in determining the size of the evaporator. The compressor, condenser, water pump, expansion valve (TXV)

and ancillary electronics must be packaged within the evaporator. These components make up the "core" of the system as illustrated in Figure 9. This design layout was chosen to utilize the pressure vessel enclosing the "core" as the heat transfer device for absorbing heat from the ocean. This would minimize the number of parts and help with operation in contaminated water. Extensive Computer Aided Design (CAD) work was performed to package the "core" within the evaporator to minimize the volume.

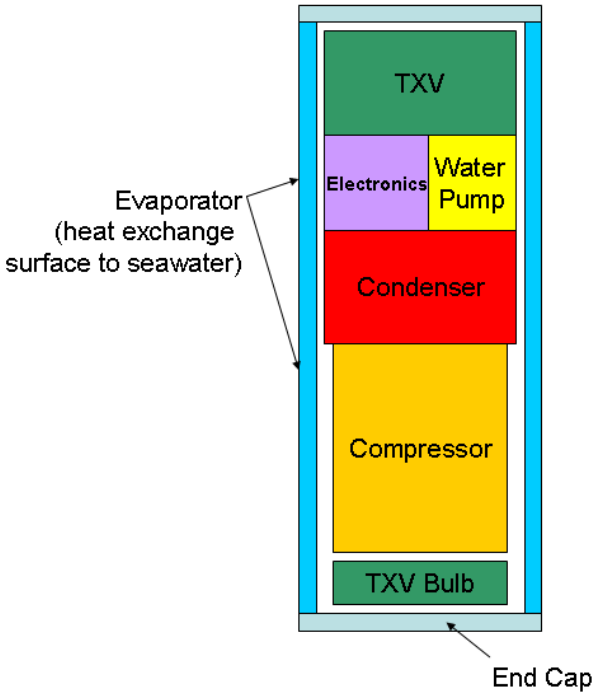

Figure 9: Layout of system with outer spiral evaporator

The assembly process is also important in determining the size of the evaporator. Assembly of the "core" will be performed separately from the evaporator. The fully assembled "core" is then assembled into the evaporator. A solder connection is then made on each end to connect the refrigeration tubes. This assembly process allows the evaporator volume to be minimized by requiring minimal work space to make a solder

connection on each end. Thus the minimum volume the evaporator must enclose is defined at 81 mm diameter by 190 mm length.

Heat Exchange Method

To meet the contaminated water requirements, it is desirable to use a plain cylinder shell as the main heat transfer surface of the evaporator. As seen in Figure 10, a spiral would be used for the refrigerant to travel underneath the shell, pulling heat out of the ambient water through free (natural) convection. The heat flow is illustrated in Figure 11. This would provide a simple and clean design, thus the free convection on the surface was investigated.

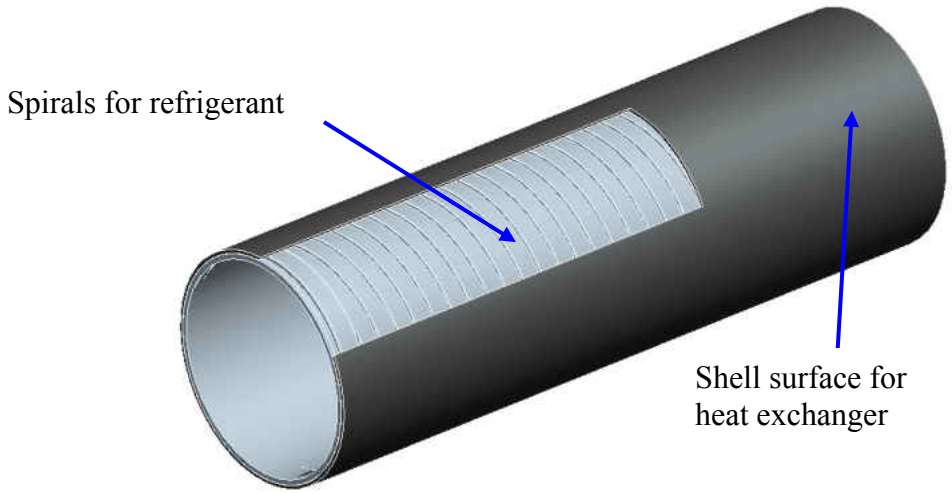

Figure 10: Spiral shell heat exchanger cut away

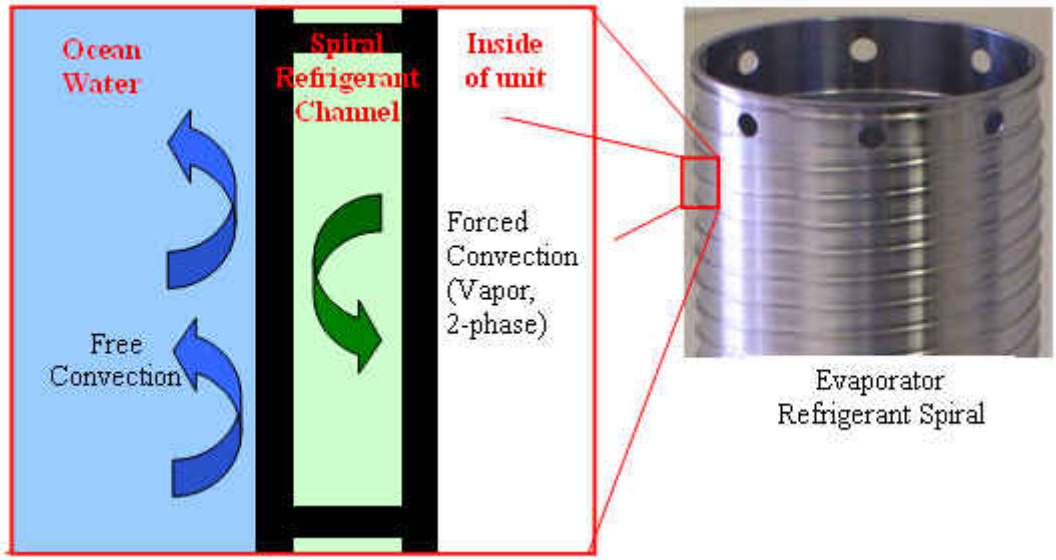

Figure 11: Evaporator heat exchange illustration

For a cylindrical wall, the heat transfer is modeled using the capacitance method [4].

$$q = \frac{T_{amb} - T_{ref}}{\frac{1}{h_{ref} \cdot \pi \cdot D_o \cdot L_1} + \frac{\ln\left(\frac{D_{sur}}{D_o}\right)}{\pi \cdot k_{al} \cdot L_1} + \frac{1}{h_{water} \cdot \pi \cdot D_{sur} \cdot L_1}} \quad (1)$$

To determine the heat transfer due to free convection, the cylinder is modeled as a vertical flat plate ignoring edge effects. For laminar free convection on a vertical surface using a numerical solution obtained by Ostrach [5], the average Nusselt number is expressed as

$$Nu_L = \frac{4}{3} \cdot \left(\frac{Gr_L}{4}\right)^{\frac{1}{4}} \cdot g(Pr) \quad (2)$$

where the dimensionless temperature gradient (g(Pr)) at the surface is a function of the Prandtl number

$$g(Pr) = \frac{0.75\sqrt{Pr}}{\left(0.609 + 1.221\sqrt{Pr} + 1.238\,Pr\right)^{\frac{1}{4}}} \tag{3}$$

With a heat load of 200W in 1.7°C water, it became clear that natural convection was insufficient and ice would form on the surface of the evaporator. With a surface temperature of -1.9 °C, the heat transfer coefficient is only 7.9 W/K. A model was developed to calculate ice growth and the effect on performance of the smooth cylinder evaporator. The model, detailed in Appendix A, takes into account the latent heat gained from freezing the water, the thermal conductivity of the ice as well as free convection on the growing surface of the ice. For 200W, the thickness of ice as a function of time is shown for still (natural convection) 1.7°C water in Figure 12. Testing was performed and verified the model was sufficient in predicting ice growth. With the heat load maintained, after half an hour from the initial ice formation, 12 mm of ice had formed. The test setup and evaporator under testing is shown in Figure 13.

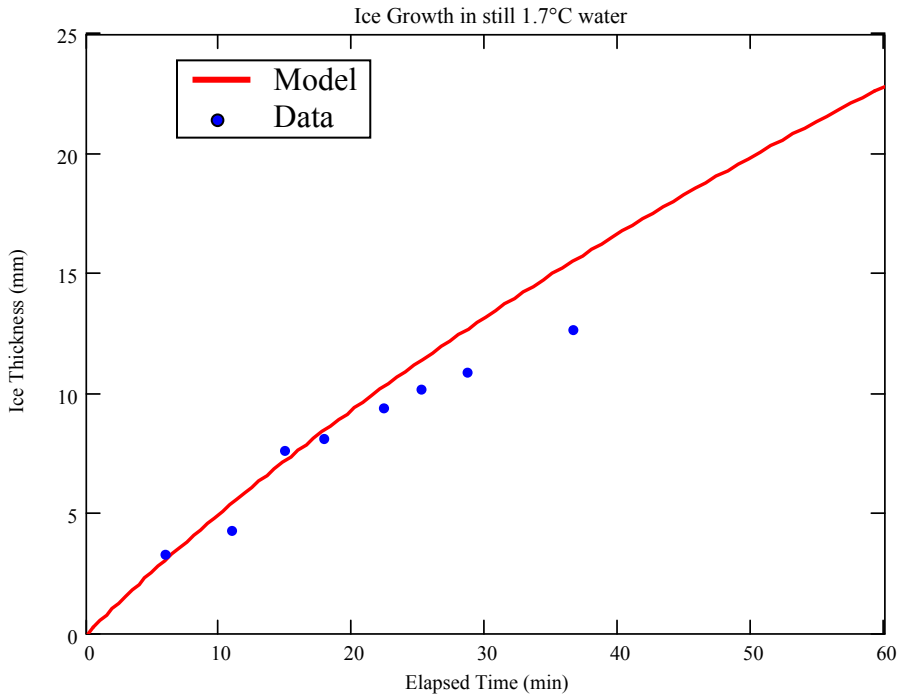

Figure 12: Ice build up in still 1.7°C water

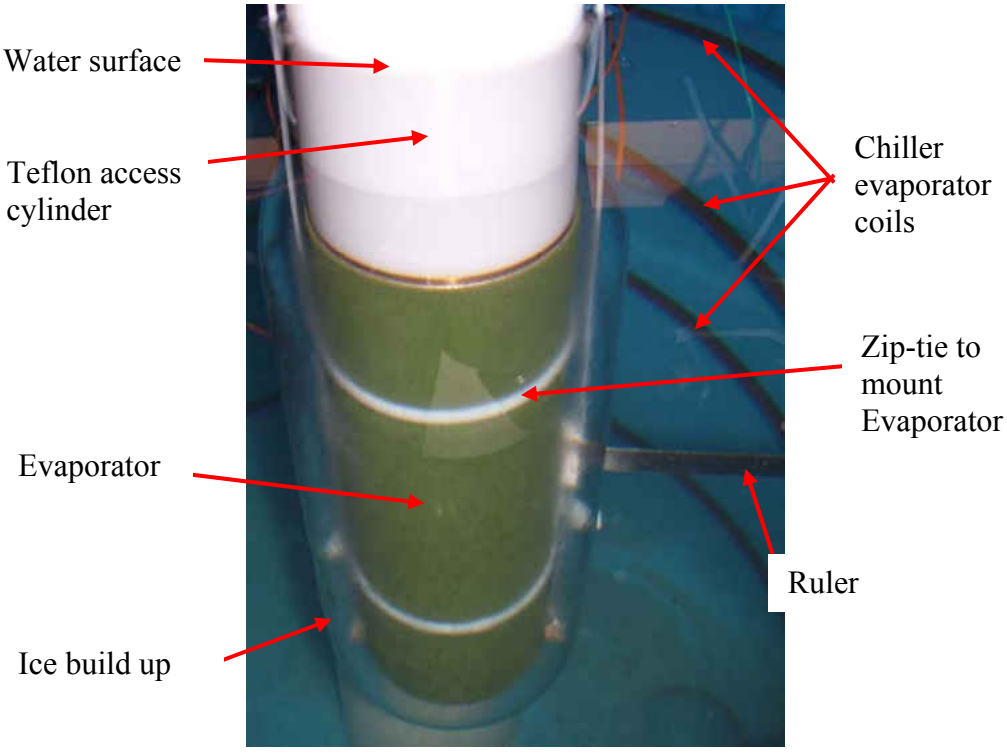

Figure 13: Evaporator with ruler to measure ice thickness

As the ice thickness becomes greater, the thermal resistance between the refrigerant and water increases. This increase in resistance requires a much lower evaporator saturation temperature to maintain the desired heat load as shown in Figure 14. This is undesirable because it increases the lift required of the compressor. The growth of the ice continues and lowers the saturation temperature throughout the 12 hour required run time. This decreases the efficiency of the compressor and increases the power dramatically throughout the required duration. Thus enhancements will be required to increase the performance of the evaporator to prevent ice formation.

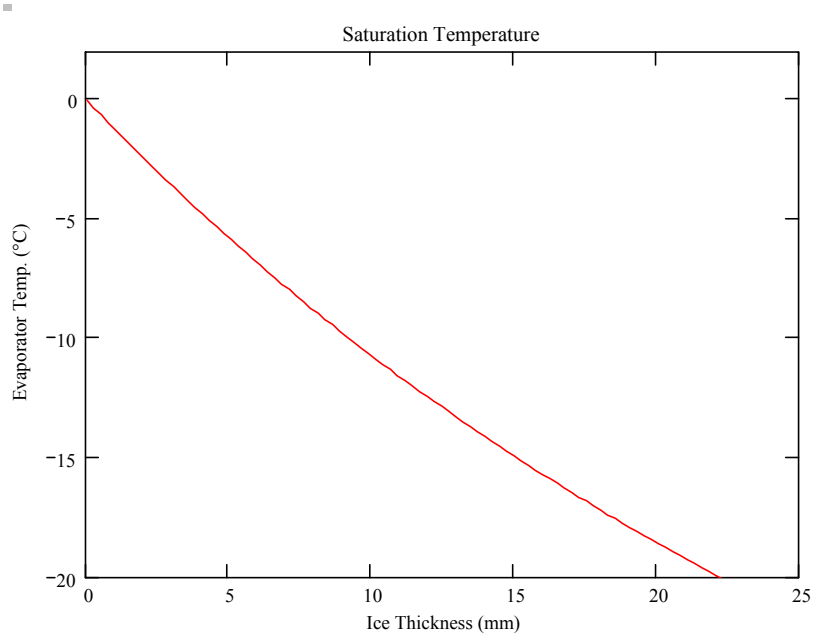

Figure 14: Evaporator temperature as a function of ice thickness

Ducted Evaporator

To enhance the heat transfer between the water and evaporator surface, forced convection is investigated. This will require a duct and a method to provide the flow. To meet the Navy's contaminated water diver requirement, particles up to 3 mm must be

able to pass through the evaporator. Using a low solidity impeller to provide the flow will allow large particles to flow through the evaporator ducting without becoming clogged. In addition to ducting flow over the evaporator surface, it is desirable to add fins to reducing the flow work required by the impeller. It is also desirable to keep the flow low such that no noticeable thrust is generated by the impeller.

In addition to particulate matter, the fins must be thick enough to provide rigid support for the duct and meet the environmental requirements. Fin height and thickness will be determined through analytical analysis. With the additional design constraint of preventing ice formation, a simple calculation is performed to determine the minimum required flow rate of 28 cc/s.

$$\frac{Q_{des}}{\rho_{water} \cdot C_{p\ water} \cdot \left(T_{amb\ min} - T_{ice}\right)} = 28 \frac{cm^3}{s} \tag{4}$$

A layout of the evaporator is shown in Figure 3.

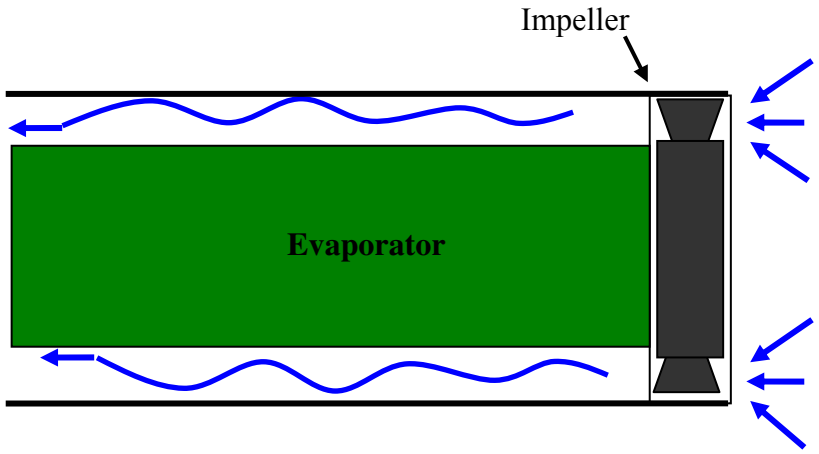

Figure 15: Evaporator with impeller

CHAPTER THREE: MODELING

Heat Transfer

To model the evaporator, the approximate conditions of the evaporator within the system must first be determined. Since the system conditions are dependent upon the evaporator performance, an initial estimation is sufficient and iterations can be performed to determine system performance more accurately. The thermodynamic cycle, shown in Figure 16, presents required performance of the evaporator to prevent freezing. From this analysis, the saturation temperature and heat load of the evaporator can be used for detailed modeling of the evaporator.

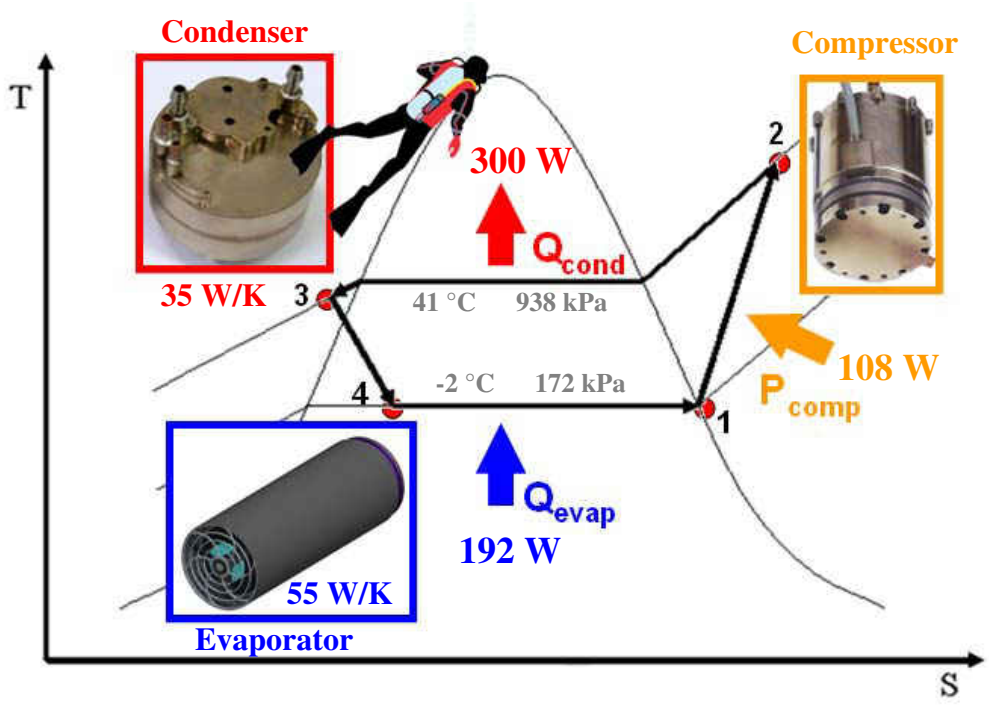

Figure 16: T-s diagram of thermodynamic cycle

A numerical method is required for determining the saturation temperature of the refrigerant based on the heat load, ambient water temperature, and geometry. From this

analysis, the thermal resistance of the evaporator is determined allowing for the evaporator outlet pressure to be determined. With the evaporator outlet pressure known, the performance of the compressor can be determined and the thermodynamic model can more accurately predict the system performance. Then the heat absorbed through the evaporator can be updated and re-analyzed.

First the performance of the water side is determined. A logistic regression, shown in Figure 17 is applied to a table developed by Kays [6] relating the duct aspect ratio to the Nusselt number (Equation 5) and friction factors for fully developed laminar flow.

$$Nu_D = \frac{h \cdot D_h}{k} \tag{5}$$

This takes into account the increase in heat transfer due to the aspect ratio. This will allow for a more accurate representation of the data presented in the table than a simple linear interpolation model.

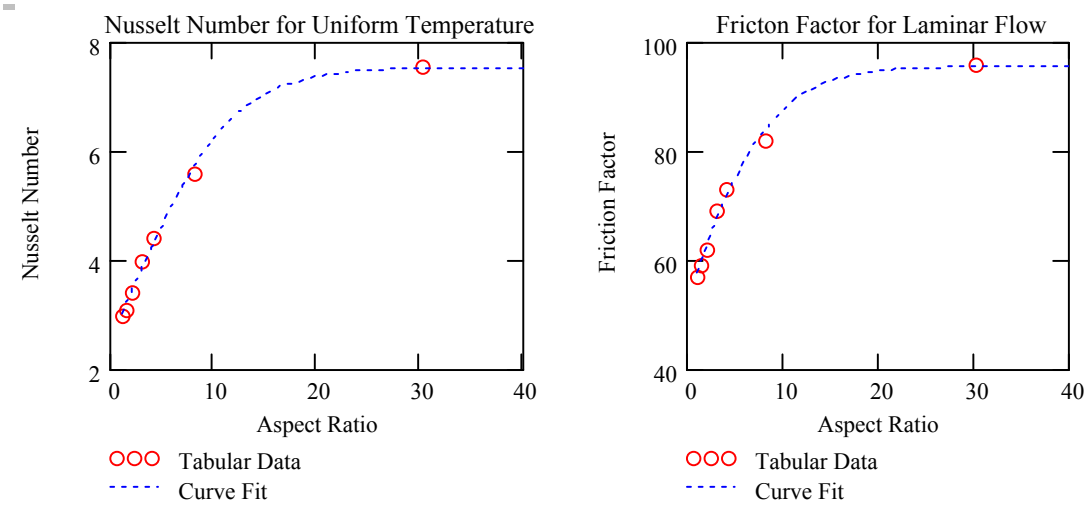

Figure 17: Logistic regression for aspect ratio effect in laminar flow heat transfer

Next, based on the impeller flow and motor characteristics, the fin geometry can be selected such that the power required of the impeller is optimized. A simple algorithm runs combinations of number and thickness of fins. If the impeller performance is known across the range of resulting pressures, the fin combination that results in the lowest impeller power and highest heat transfer can be selected. With the selection of the number and thickness of fins, the water side heat transfer is known and can be used in the numerical analysis.

To determine the pressure drop, a two-phase relation is needed to model the evaporation pressure drop. Then a vapor relation is needed to model the superheat vapor heat transfer. For the two-phase pressure drop the Lockhart and Martinelli correlation for round tubes [7] is used. The Martinelli parameter is defined as a function of mass flow rate, quality, refrigerant channel geometry and saturation temperature.

$$X = \left[\frac{B_f \cdot Re_f^{-n_f} \cdot (1-x)^2 \cdot \rho_g}{B_g \cdot Re_g^{-n_g} \cdot x^2 \cdot \rho_f} \right]^{\frac{1}{2}} \tag{6}$$

The two phase multipliers φ_f and φ_g are then defined [8].

$$\phi_f = \sqrt{1 + \frac{C}{X} + \frac{1}{X^2}} \qquad \phi_g = \sqrt{1 + C \cdot X + X^2} \tag{7a-7b}$$

The constant C varies depending on the flow regime as shown in Table 6.

Table 6: Turbulent-Viscous constant

Liquid	Gas	C
Turbulent	Turbulent	20
Laminar	Turbulent	12
Turbulent	Laminar	10
Laminar	Laminar	5

Thus the two-phase head loss is defined in equation 8 where F_{ReAR} is the aspect ratio factor for laminar flow.

$$H_{L2\phi} = \phi_f^2 \cdot \frac{2 \cdot \frac{B_f}{\left[\frac{G \cdot (1-x) \cdot D_h}{\mu_f}\right]^{n_f}} \cdot [G \cdot (1-x)]^2}{\rho_f D_h} \cdot F_{ReAR} \tag{8}$$

The vapor head loss is defined as

$$H_{Lg} = 2 \cdot f_{gO} \cdot \frac{G^2}{D_h \cdot \rho_g} \cdot F_{ReAR} \tag{9}$$

The superheated vapor heat transfer is determined as a function of mass flow rate, refrigerant spiral geometry and saturation temperature.

$$h_g = \frac{k_g}{D_h} \cdot Nu_g \tag{10}$$

To determine the Nusselt number, a relation defined by Grielinski [9] is used for good agreement with small Reynolds numbers. It is valid for smooth tubes and Prandtl numbers between 0.5 and 2000.

$$Nu_g = 0.023 \cdot Re_g^{0.8} \cdot Pr_g^{0.4} \tag{11}$$

The friction factor is defined in equation 12. Typically a *Moody diagram* is used to determine the friction factor but this is inconvenient for numerical analysis thus a single correlation for a large range of Reynolds numbers developed by Petukhov [10] is used for turbulent flow.

$$f = \left(0.790 \ln\left(Re_g\right) - 1.64\right)^{-2} \tag{12}$$

The two-phase evaporation heat transfer is calculated using the Chen correlation [11] which determines the heat transfer coefficient as a summation of the microscopic (nucleate boiling) and macroscopic (bulk convection) heat transfer.

$$h_{2p} = h_{mac} + h_{mic} \tag{13}$$

The bulk macroscopic heat transfer [12] is defined as

$$h_{mac} = h_f \cdot F_{Xtt} \cdot Pr_f^{0.296} \tag{14}$$

where the liquid component is calculated using the Dittus-Boelter equation

$$h_f = 0.023\left(\frac{k_f}{D_h}\right) Re_f^{0.8} \cdot Pr_f^{0.4} \tag{15}$$

and an empirical correlation developed by Collier [13] is used that is a function of the turbulent-turbulent Lockhart Martinelli parameter [14].

$$F_{Xtt} = 2.35\left(0.213 + \frac{1}{X_{tt}}\right)^{0.736} \tag{16}$$

$$X_{tt} = \left(\frac{\rho_g}{\rho_f}\right)^{0.5} \cdot \left(\frac{\mu_f}{\mu_g}\right)^{0.1} \cdot \left(\frac{1-x}{x}\right)^{0.9} \tag{17}$$

The microscopic contribution is determined by applying a correction factor S that suppresses the nucleate boiling prediction developed by Forster and Zuber [15]. The suppression factor [16] takes into account that as macroscopic convection increases in strength, nucleate boiling is suppressed.

$$h_{mic} = S \cdot 0.00122 \left(\frac{k_f^{0.79} \cdot Cp_f^{0.45} \cdot \rho_f^{0.49}}{\sigma_{sat}^{0.5} \cdot \mu_f^{0.29} \cdot h_{fg}^{0.24} \cdot \rho_g^{0.24}} \right) \cdot \left(T_{wall} - T_{sat}\right)^{0.24} \cdot \left(P_{sat}\left(T_{wall}\right) - P_l\right)^{0.75} \quad (18)$$

where the suppression factor is

$$S = \frac{1 - \exp\left(-F_{Xtt} \cdot h_f \frac{X_o}{k_f}\right)}{F_{Xtt} \cdot h_f \frac{X_o}{k_f}} \quad (19)$$

where

$$X_o = 0.041 \left[\frac{\sigma_{sat}}{g \cdot \left(\rho_f - \rho_g\right)} \right]^{0.5} \quad (20)$$

Thus the two-phase heat transfer coefficient as a function of quality is as illustrated in Figure 18.

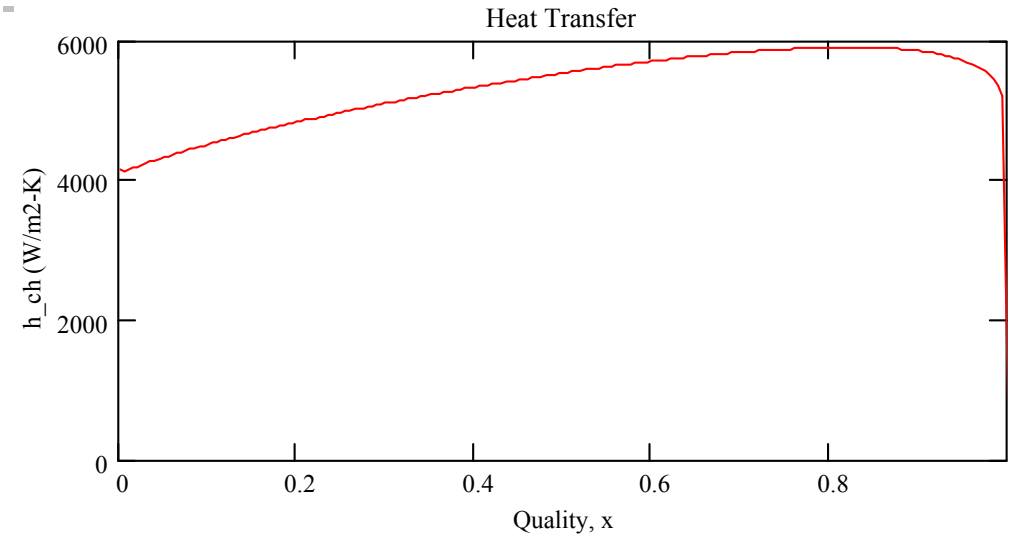

Figure 18: Heat transfer coefficient as a function of quality

With the two-phase and vapor heat transfer, and pressure drop relations determined, a numerical method can be applied to determine the heat transfer of the evaporator.

The model starts with an initial saturation temperature estimate. With the initial saturation temperature, the model steps through at very small increments and determines the amount of heat absorbed by the refrigerant. At the final length, the total heat transferred is known for the initial saturation temperature. Newton iteration, equation 21, is then applied to update the initial saturation temperature

$$T_{n+1} = T_n - \frac{f(T_n)}{\left(\frac{d}{dT} f(T_n)\right)} \tag{21}$$

where the overall thermal resistance of the evaporator is held constant and the initial temperature is updated base on the log mean temperature difference (LMTD).

$$LMTD = \frac{\left(T_{sea_0} - T_{sat_0}\right) - \left(T_{sea_{nn}} - T_{sat_{nn}}\right)}{\ln\left[\frac{\left(T_{sea_0} - T_{sat_0}\right)}{\left(T_{sea_{nn}} - T_{sat_{nn}}\right)}\right]} \tag{22}$$

This iteration method converges on the solution quickly as shown in Figure 19 even with a poor initial saturation temperature guess. A better initial saturation temperature results in convergence within a few iterations.

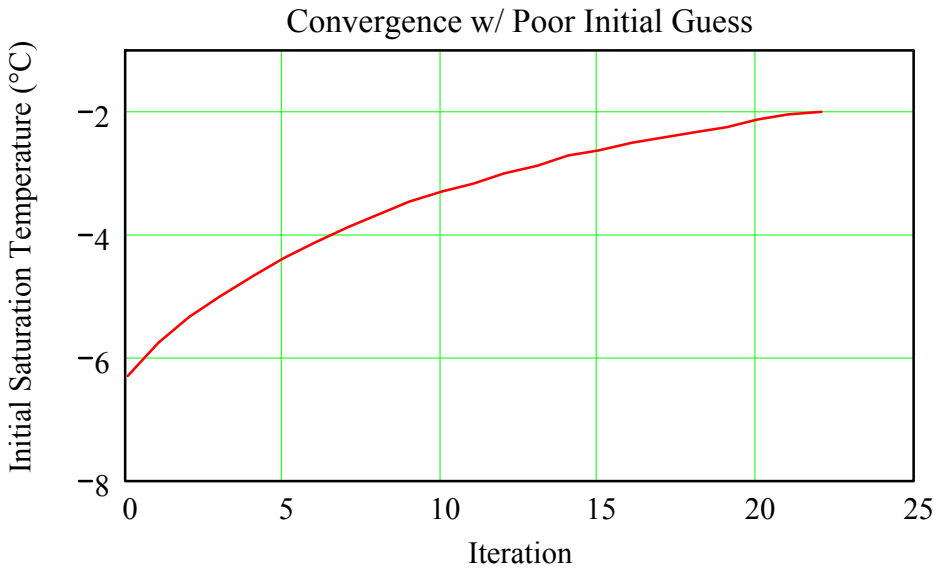

Figure 19: Model convergence with poor initial guess

The performance (Equation 23) is modeled for a range of flows and different superheats in Figure 20. With a large amount of superheat, a greater portion of the channel length is required to super heat the vapor.

$$\text{Performance} = \frac{Q_{evap}}{T_{in} - T_{sat\_avg}} \tag{23}$$

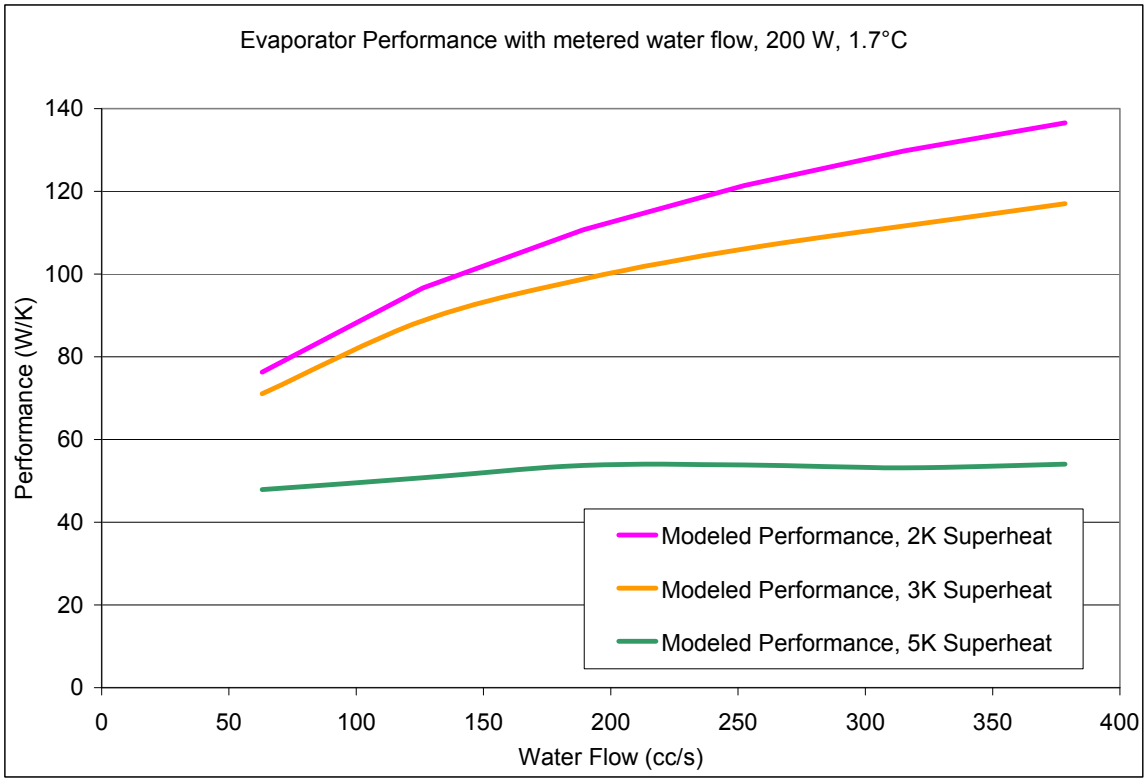

Figure 20: Modeled performance different superheats and water flow rates

The thermal resistance of the water and refrigerant is shown in Figure 21. Initially the water has the higher thermal resistance (inverse of overall convection coefficient) until the refrigerant is completely evaporated. The heat transfer of the superheated refrigerant vapor is then the highest resistance. This plot also shows the large spiral distance that is required to achieve 5 K of superheat at the outlet.

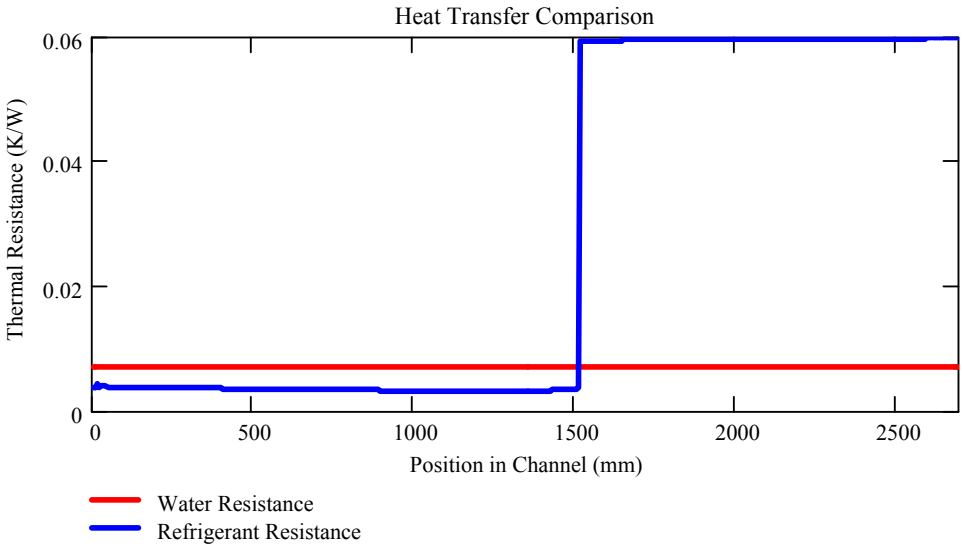

Figure 21: Thermal resistance of water and refrigerant

The temperature distribution along the channel length is shown in Figure 22. The heat flux on the outer wall of the refrigerant channel is shown in Figure 23. The point of complete evaporation is again easily noticeable in both.

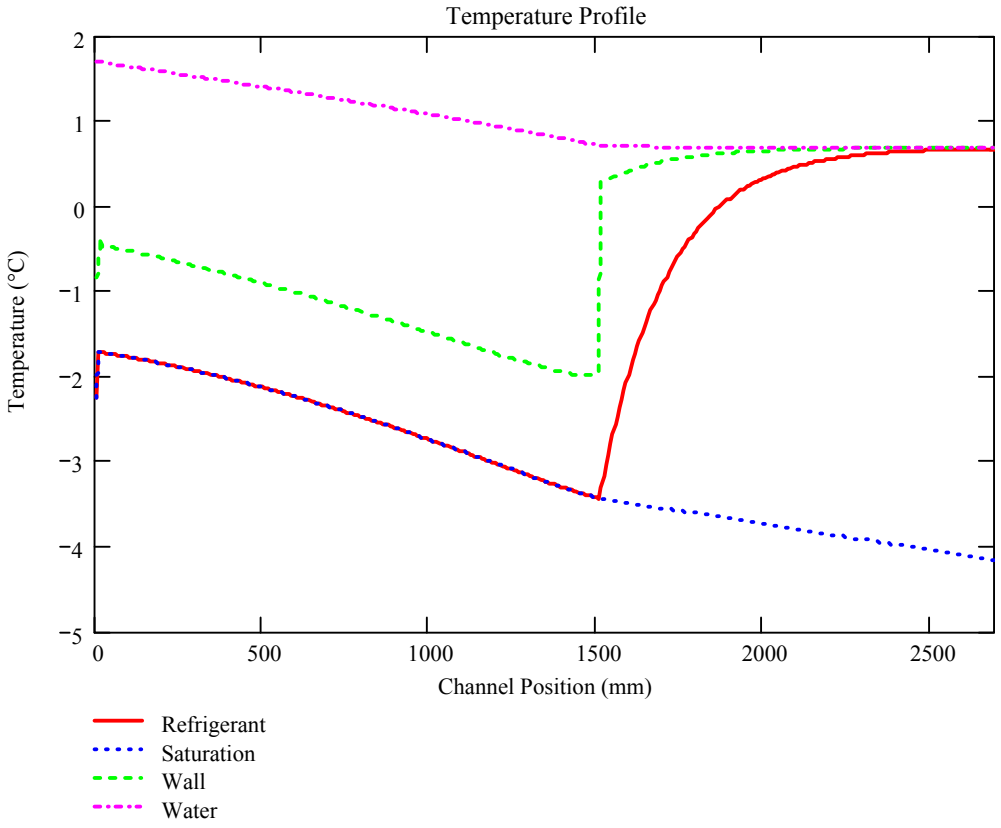

Figure 22: Temperature distribution along channel

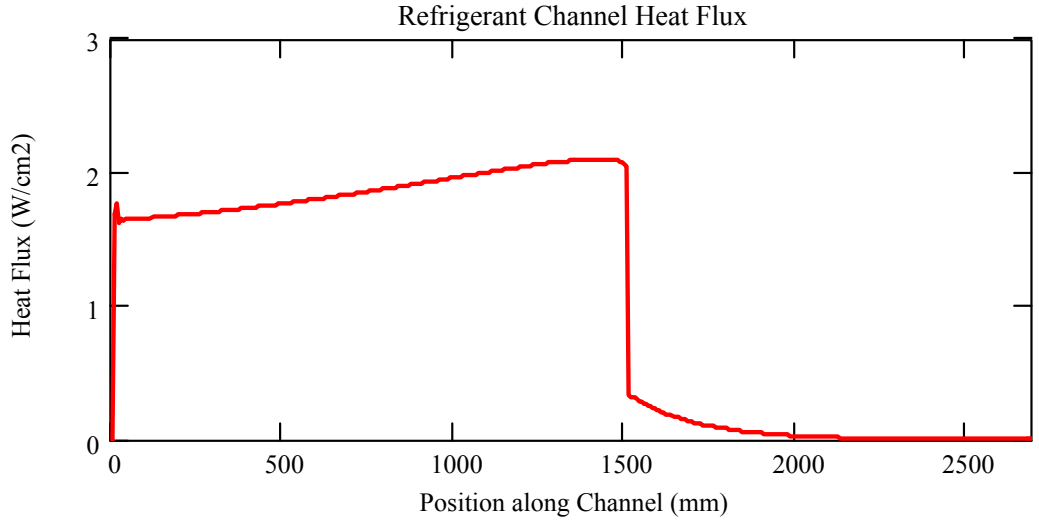

Figure 23: Refrigerant channel heat flux

Evaporator Depth Analysis

Evaporator Cylinder

Analysis of the evaporator at depth required a mixture of analytical and Finite Element Analysis (FEA) to prepare for depth qualification testing at 91 MSW. The evaporator cylinder is complex composite structure, illustrated in Figure 24. For simplicity, just the inner cylinder was analyzed where the complete structure will provide additional support and safety margin. Calculations and verification where applicable are provided in Appendix C.

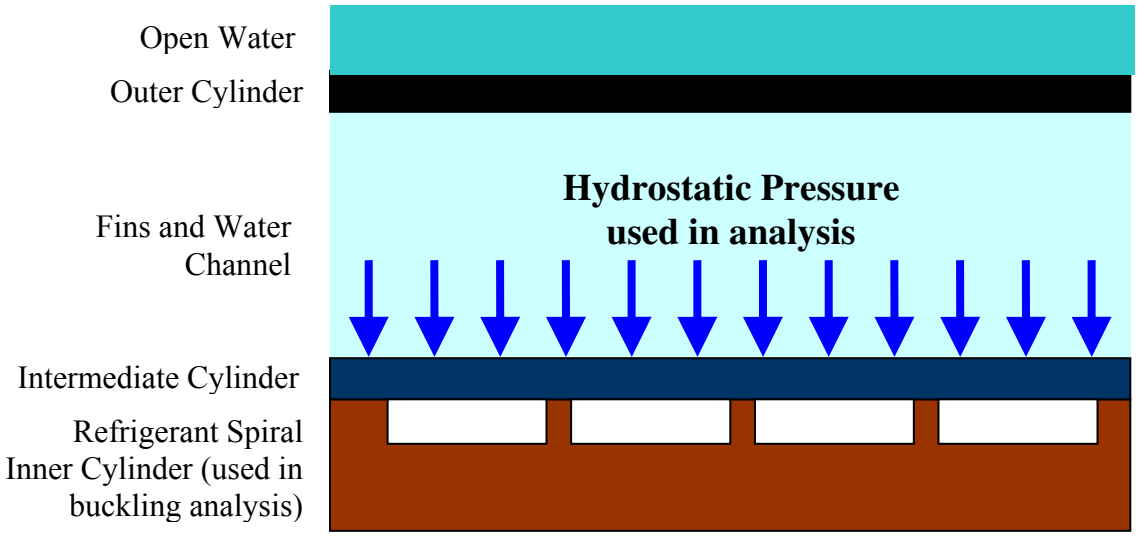

Figure 24: Cross section of evaporator

Two mechanisms of failure are possible for the cylinder: buckling and yielding. For the depth and cylinder of interest, the minimum cylinder thickness allowable [17] is 0.13 mm to prevent yielding (Equation 24).

$$t_{yield} = d_o \cdot \frac{1}{2} \cdot \left(1 - \sqrt{1 - \frac{2 \cdot P_{ext}}{\sigma_{yp}}} \right) \tag{24}$$

This is far thinner than what can be reasonably machined for a cylinder of this size (0.8 mm minimum) thus buckling will be the primary mode of failure. Initial calculations were performed using Euler's buckling equation for ideal slender rods (Equation 25) which yielded a extremely high factor of safety (>>100).

$$F_{cr\_Euler} = \frac{\pi^2 \cdot E_{al} \cdot \left[\left(\frac{d_o}{2}\right)^4 - \left(\frac{d_i}{2}\right)^4\right] \cdot \frac{\pi}{4}}{(2 \cdot L)^2} \tag{25}$$

For an infinitely long cylinder [18] the minimum thickness for buckling, shown in Equation 266, yielded a minimum thickness of 1.5 mm however a relation for a short cylinder was desired.

$$t_{bcl} = \left(P_{ext} \cdot \frac{1 - \nu^2}{2 \cdot E_{al}}\right)^{\frac{1}{3}} \cdot d_o \tag{26}$$

Further study found a method for calculating the buckling for a well machined short cylinder. This design process developed by Ross [19], a leading researcher in stress analysis on submarine pressure hulls. Theoretical calculations and experimental test data are taken into account with this method. The process starts with Equation 27 [20] to determine the theoretical critical load. Then a thinness ratio is calculated in Equation 28.

$$P_{cr\_DTMB} = \frac{2.42 \cdot E_{al} \cdot \left(\frac{t_s}{d_{avg}}\right)^{\frac{5}{2}}}{\left(1 - \nu^2\right)^{\frac{3}{4}} \cdot \left[\left(\frac{l_s}{2 \cdot r_{avg}}\right) - 0.447 \cdot \left(\frac{t_s}{2 \cdot r_{avg}}\right)^{\frac{1}{2}}\right]} \tag{27}$$

$$\lambda = \left[\frac{\left(\frac{l_s}{d_{avg}} \right)^2}{\left(\frac{t_s}{d_{avg}} \right)^3} \right]^{\frac{1}{4}} \cdot \sqrt{\frac{\sigma_{yp}}{E_{al}}} \tag{28}$$

From the inverse of the thinness ratio, a plastic reduction factor (PKD) is selected in Figure 25. This reduction factor takes into account experimental data and reduces the critical load the cylinder can withstand. For the evaporator shell the PKD was 1.2. From this process a thickness of 2.4 mm was arrived at to achieve a factor of safety of 11.3. The factor of safety is large for buckling because the calculations rely on a well machined cylinder with minimal flaws and defects. The actual machining of the cylinder may vary.

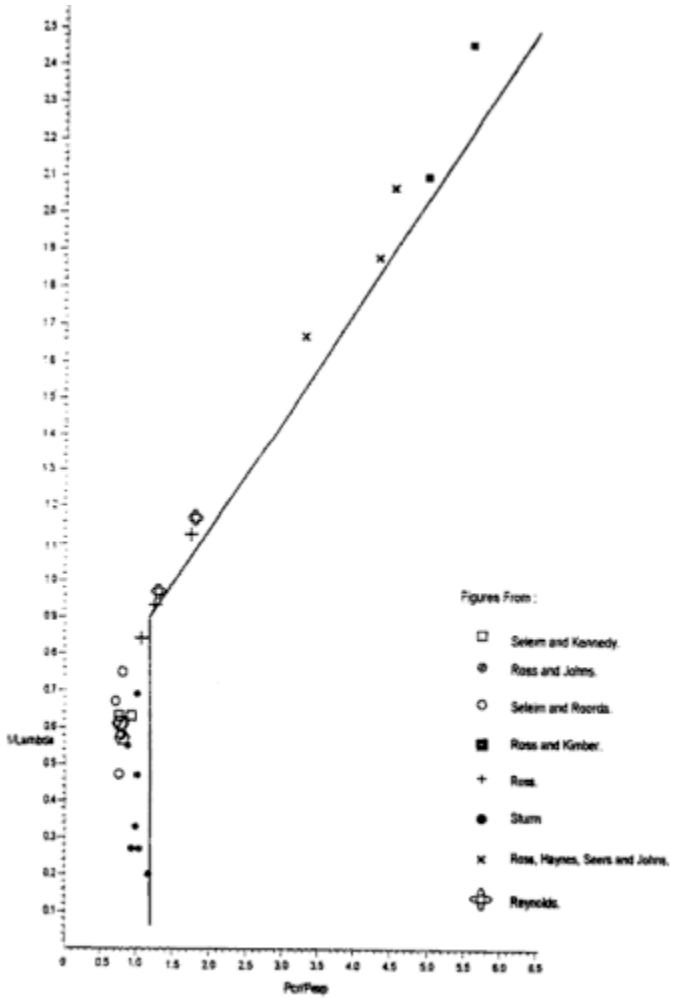

Figure 3.4 Design chart for the shell instability of machined circular cylinders.

Figure 25: Selection of PKD based on inverse of thinness ratio

Von Mises [21] also derived an equation for a simple supported cylinder that calculates the critical pressure based on the number of lobes (n_b) of the failure mode. This equation results in a critical pressure 27% higher than the Ross method for three lobes. Three lobes produced the lowest critical buckling pressure. The lower critical pressure determined from the Ross method was used in determining the thickness of the cylinder to have confidence in the margin of safety.

$$P_{cr\_VM} = \frac{E_{al}\cdot\left(\frac{t_s}{r_{avg}}\right)}{n_b^2 - 1 + 0.5\cdot\left(\pi\cdot\frac{r_{avg}}{l_s}\right)^2}\cdot\left[\frac{1}{\left[n_b^2\cdot\left(\frac{l_s}{\pi\cdot r_{avg}}\right)^2 + 1\right]^2} + \frac{t_s^2}{12\cdot r_{avg}^2\cdot\left(1-\nu^2\right)}\cdot\left[\left(n_b^2\right) - 1 + \left(\frac{\pi\cdot r_{avg}}{l_s}\right)^2\right]^2\right] \quad (29)$$

The methods investigated for buckling are summarized below for the final wall thickness.

Table 7: Summary of buckling calculations for final design

Method:	Safety Factor:
Ideal Cylinder (Euler)	478
Infinitely Long Cylinder (Bryan)	4
David Taylor Model Basin	14
Plastic Reduction Factor (Ross Method)	**11**
Simple Supported Cylinder (Von Mises)	14

Impeller Stator Housing

The initial design utilized a thin aluminum impeller housing to save weight however it was not satisfactory to meet the depth requirement. The minimum thickness of the end cap was calculated (2 mm) using the following equation from an engineering handbook [22].

$$t_{min} = d_{stator}\cdot\frac{1}{2}\cdot\sqrt{\frac{3\cdot\left(\frac{3}{\nu}+1\right)\cdot P_{ext}}{\frac{8}{\nu}\cdot\sigma_{yp}}} \quad (30)$$

Due to the unusual geometry of the end cap, finite element analysis was performed to analysis the stress and displacement of the stator housing end cap. FEA determined that although the safety factor was adequate, the displacement of the impeller shaft was too large. The pocket under one side of the stator for wiring shown in Figure 26 caused the shaft to tilt away from the pocket under pressure by 0.5 mm. This displacement, shown in Figure 27, would cause the motor rotor to contact the stator. To

reduce the displacement, the end cap was re-analyzed with a vapor charge equal to half the pressure of the full depth rating. As shown in Figure 28, the displacement was reduced but is still greater than desired. Finally, the bottom of the stator housing was thickened and a large radius was added to the outer edge to minimize both the axial and radial displacement. The new design, shown in Figure 29, displaces 0.005 mm in the radial direction and 0.1 mm axially at 91 m.

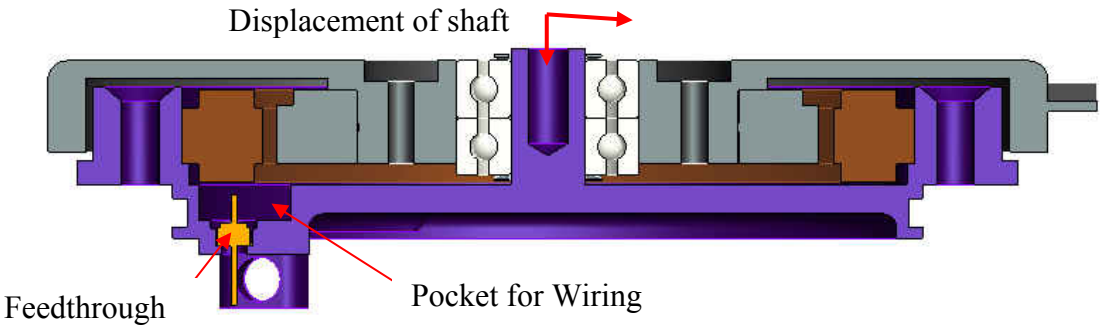

Figure 26: Impeller stator housing

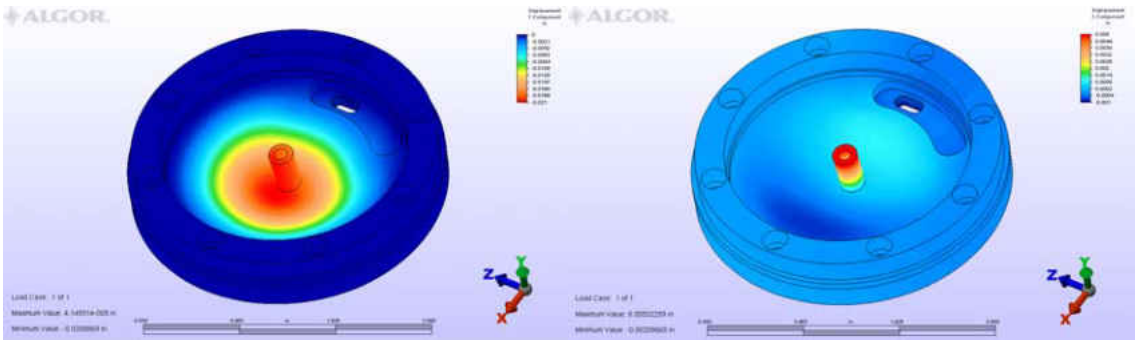

Figure 27: Displacement with out charge at 91 m

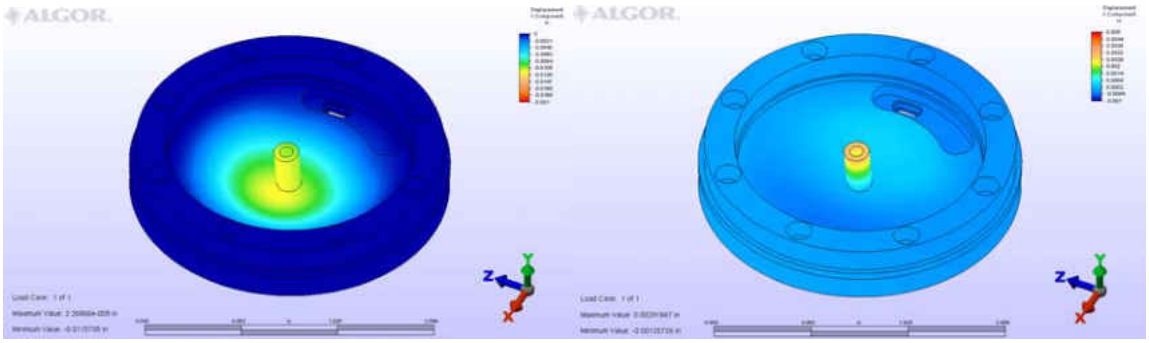

Figure 28: Displacement with charge at 91 m

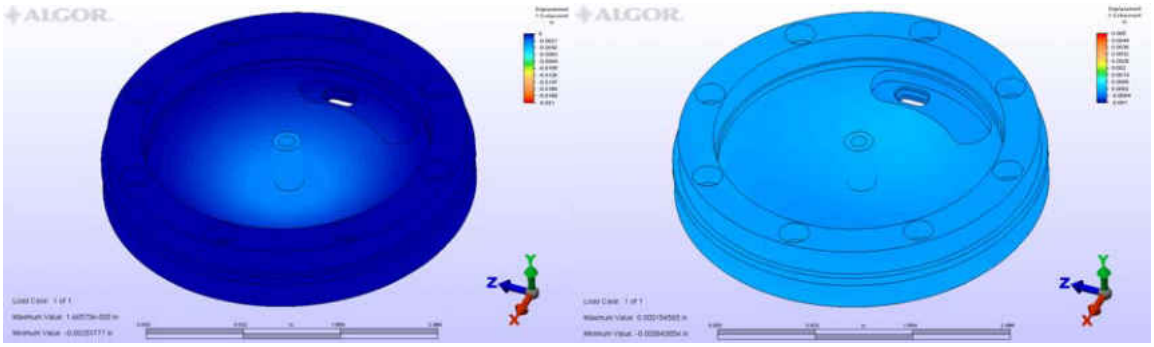

Figure 29: Displacement of reinforced bottom with charge at 91 m

Large End Cover

The end cap on the opposite end has the power connections and hot water hose barbs as shown in Figure 30. On this end, both the maximum stress and heat leak from the hose barbs are important. The heat leak from the hose barbs must be minimized such that the unit will provide the full 300 W of heat to the diver. Heat lost to the ambient water and evaporator must be compensated for and will reduce the efficiency of system. Plastics offer the best thermal insulation, but their strength may not be sufficient. If metals are to be used, candidates would have high strength, low thermal conductivity, and low galvanic potential. The first step was to perform a stress analysis to determine adequate material thickness for each material type, and then the heat leak was analyzed on the determined geometry.

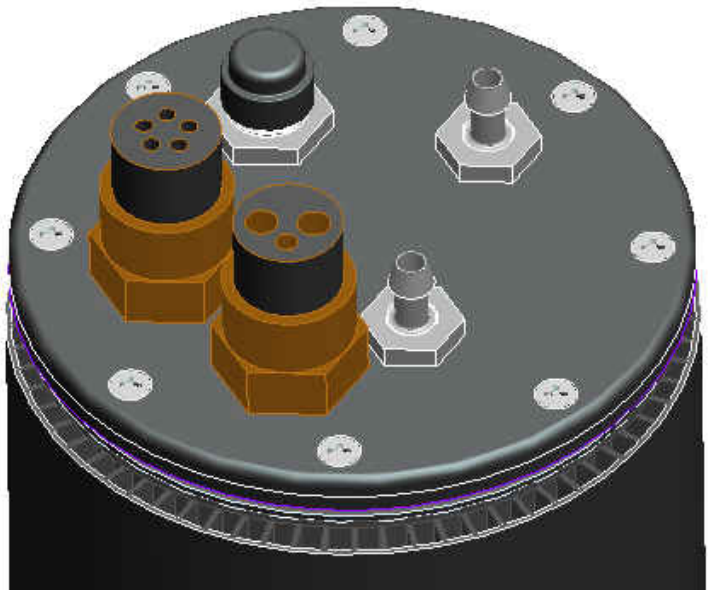

Figure 30: End cap to be analyzed with hose barbs and electrical connections

To minimize the heat loss from the hose barbs, an Acrylonitrile Butadiene Styrene (ABS) plastic end cap would be the most desirable however the structural integrity at depth was questionable. Using Equation 30, the minimum thickness for ABS plastic end cap without any hole is 7.6 mm. The holes for the electrical connections and hose barbs will cause stress concentrations requiring an even greater thickness, thus it is not feasible with a reasonable safety factor, thus a different material must be investigated.

Of the metals investigated, titanium grade 2 and 316 stainless steel were the lowest thermal conductivity and highest strength. 316 Stainless steel was chosen for lower galvanic potential and cost. Although the thermal conductivity of stainless steel is 100 times greater than ABS plastic, geometric changes such as lengthening the thermal path and reducing the thickness of the plate will limit heat loss. The stress analysis, shown in Figure 31 was performed and yielded a maximum stress of 120 MPa which provides a safety factor of 2.9. Verification was performed through mesh refinement and

by calculating the stress of a simple supported end cap and accounting for a circular stress concentration of 3. Displacement in the Y-direction was constrained at the locations of the flat head screws. Rotation was constrained by pinning translation on one screw and constraining translation in the X-direction on screw opposite the pinned screw.

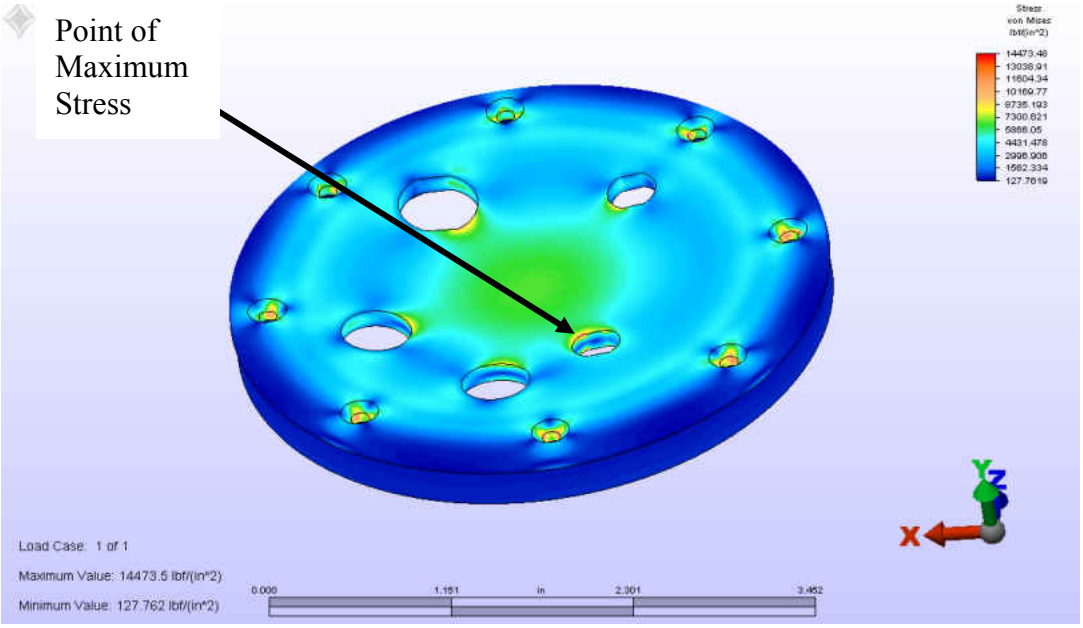

Figure 31: Stress on thin stainless steel lid at 91 MSW

With the material and thickness of the end cap determined, the heat loss was analyzed. A thermal FEA was performed and determined that 9 W will be lost from the hot panel mount hose barbs to the ambient. This will require the condenser, internal to the unit, to produce 309 W of heat to get 300 W to the diver. The temperature distribution on the stainless steel lid is shown in Figure 32. Verification was performed through mesh refinement. Simplified electrical connections and hose barbs were modeled to capture the effect of the high thermal conductivity electrical connections. Convection was applied to the inner surface of the stainless steel hose barbs to model the hot water flow to and from the diver. Convection was added to the exterior surface of the

end cap and electrical connections to simulate a moderate swim velocity. Additionally, a heat flux was applied to the location of contact with the evaporator. The heat flux was incremented until the temperature at the location of contact with the evaporator was the refrigerant saturation temperature. This would model the worst case scenario determining a maximum heat loss of 9 W.

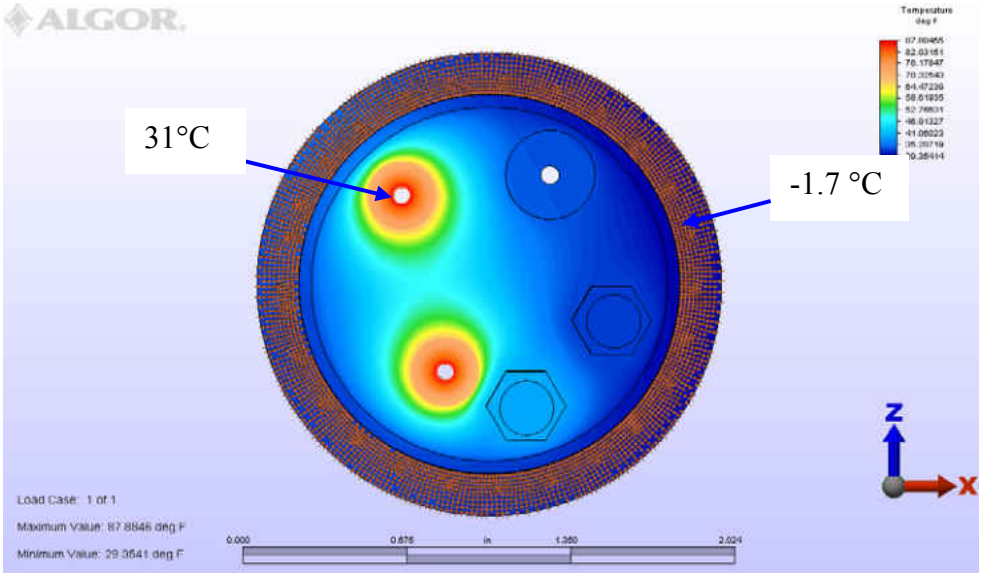

Figure 32: Temperature distribution on stainless steel lid

CHAPTER FOUR: FABRICATION

With the layout and heat transfer mechanism determined, the materials and assembly technique must be selected. The fabrication of the evaporator put limits on the geometry of the evaporator fins and refrigerant channel spirals. Aluminum (6061-T6) was selected as the working material due to its high thermal conductivity, low weight, ease of machining, moderate tensile strength, and ability to be welded and brazed. Some draw backs to aluminum are difficulty in creating low profile aluminum to copper transition joints for soldering and protecting the aluminum from corrosion. Traditionally, threaded, nickel plating, or large compression fittings are used.

The corrosion protection can be accomplished a number of ways. Applicable barrier coatings [23] include hard-coat anodizing, electroless nickel-phosphorus plating, nickel-chrome plating and painting with a polyurethane based marine coating are effect method. Cathodic (sacrificial) protection is also commonly used in marine applications. A zinc cathode could easily be attached to the exterior of the unit to provide additional protection over a barrier coating. Many of these techniques are common for recreational dive equipment.

Fins can be manufactured in a variety of ways illustrated in Figure 33. In high quantity production, it would be desirable to have a custom cylindrical extrusion containing the fins but this would be cost prohibitive in low quantities and prototypes. Clad aluminum fin stock, shown in Figure 34, allows for simple dip brazing of the fins between two shells. This process requires intricate fixtures and trial-and-error to fully

braze all fins without deforming them during the dip brazing process due to the temperature being very close to the melting point. Weight is also added due to the short sections connecting the fins as illustrated in Figure 33. Several fin variations are available such as straight, ruffled, herringbone, and lanced. This method would be a reasonable method for low to moderate quantity production. Another method is to weld fins onto a smooth cylinder however this greatly limits the fin spacing and is a labor intensive process. A more feasible option for prototyping is milling the fins into a solid cylinder of aluminum. This will ensure an accurate geometry at the lowest cost.

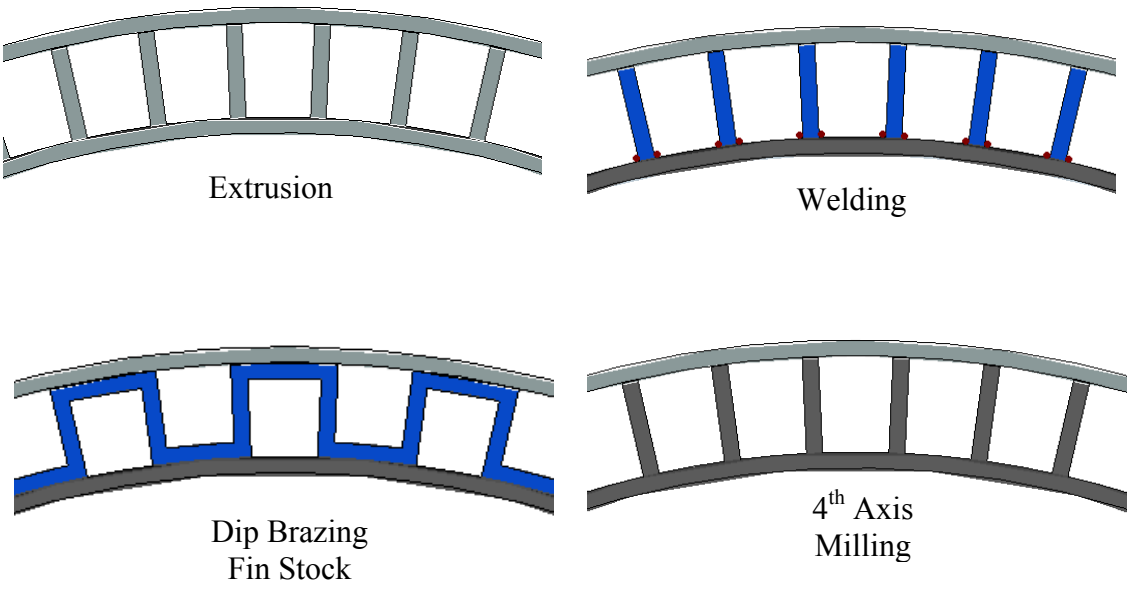

Figure 33: Manufacturing of aluminum fins

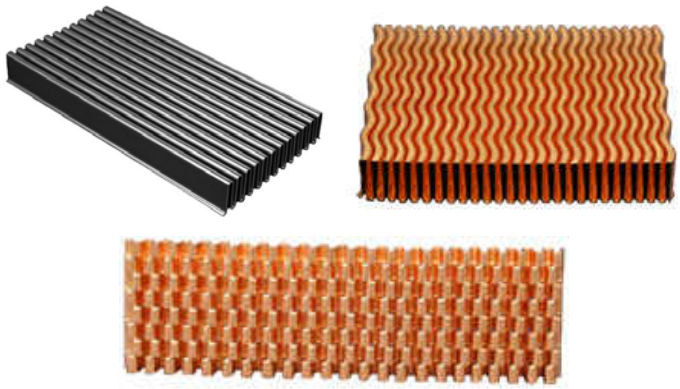

Figure 34: Clad fin stock

The refrigerant spiral can be created several ways. In high quantities, casting then turning would be an appropriate method but would require a thicker inner wall possibly increasing the diameter of the evaporator. All calculations have been done using high tensile strength 6061-T6 aluminum however only low strength alloys can be cast. For low quantities, milling on a fourth axis computer numerical controlled (CNC) mill is also a possibility however it is very time consuming and produces a rough milled finish that could change the flow characteristics of the refrigerant. A quicker method is to use a CNC turning center with a square edge ACME threading tool. This produces accurate smooth refrigerant channels however the pitch of the channels is limited to roughly 25 mm per revolution depending upon the depth of the channel. With too high of a pitch instead of cutting the aluminum, the side of the tool scrapes at the cylinder axially creating high forces on the cylinder and lathe. A picture of a spiral produced on a CNC turning center is shown in Figure 35.

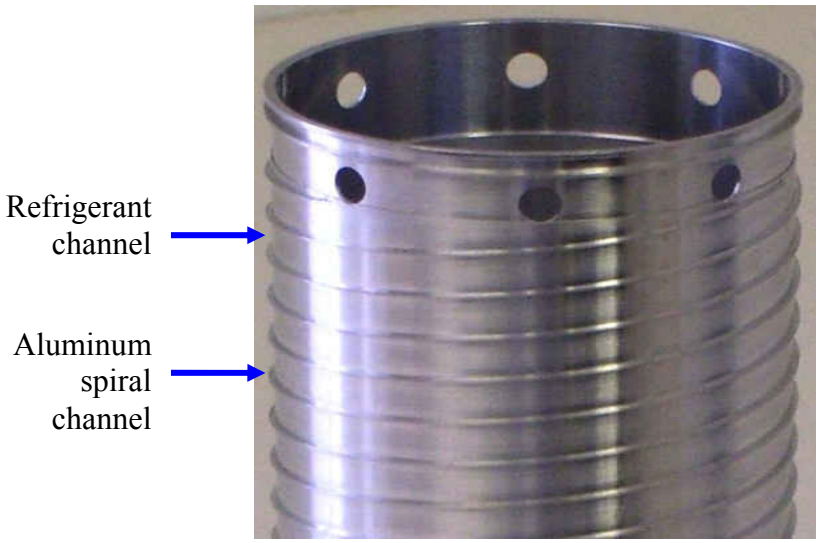

Figure 35: Refrigerant spiral produced on a CNC lathe

In addition to functioning as an evaporator, the cylinder encloses the "core" refrigeration components and electronics. Therefore it must be sealed from the surrounding water and pressure. A clever combination of brazing and welding seals the refrigerant spiral and allows for the ends to be sealed with O-ring end caps. O-rings around the screws and perimeter of the cover seal the core. A redundant back-up O-ring was added to further insure that no water leaks into the unit. This sealing configuration not only provides redundancy but prevents water from corroding the screws and threads. This will ensure the proper screw tension is maintained and make disassembly easier. Both ends of the unit use this sealing technique.

The "core" is assembled outside of the evaporator then once completed, it is assembled into the evaporator, and a solder connection is made on both ends connecting the "core" to the evaporator. The unit is then charged and the final assembly is completed.

CHAPTER FIVE: TESTING AND RESULTS

Required Measurements And Instrumentation

To determine the performance of the evaporator and verify the model, there are three measurements that are need. The first is the ambient inlet water temperature and the second is the saturation temperature of the evaporator. The third is the rate of heat exchange between the water and refrigerant. These three measurements are used to calculate the performance in Equation 31. The units of performance are Watts per Kelvin (W/K).

$$\text{Performance} = \frac{Q}{T_{sat\_avg} - T_{amb}} \tag{31}$$

Measuring the inlet water temperature is simply done with several Type-T thermocouples placed in the inlet water. The average saturation temperature is determined by measuring the inlet and outlet pressures. The saturation temperatures for those pressures are then determined using a table generated by EES and averaged assuming a linear pressure drop.

The heat rate was measured several ways for comparison to reduce measurement error and increase accuracy. To determine the heat rate based on the refrigerant, the mass flow rate and enthalpy change across the evaporator must be known. A volumetric flow meter is used to measure the refrigerant volumetric flow rate. The pressure and temperature are measured at the outlet of the flow meter to calculate the density and thus mass flow rate. The enthalpy before the expansion valve is calculated from the pressure

and temperature (subcooling) using double interpolation. Assuming isenthalpic expansion, the evaporator inlet enthalpy is known. The evaporator outlet enthalpy is calculated in a similar manner, the pressure and temperature are measured and a table is used to determine the enthalpy. The calculation is shown in Equation 32.

$$\dot{Q}_{R134a} = \dot{V}_{dot\_R134a} \cdot \rho_{fm} \cdot (h_{sc} - h_{sh}) \tag{32}$$

The heat rate can also be measured from the water. A volumetric flow meter and the inlet and outlet water temperatures allow for the heat rate to be determined. The specific heat and density of the water are determined from a table generated in EES. In Equation 33, the heat rate calculation is shown..

$$\dot{Q}_{water} = \dot{V}_{dot\_water} \cdot \rho_{water\_in} \cdot C_{p\_water} \cdot (T_{in} - T_{out}) \tag{33}$$

Refrigeration Setup

The test setup is divided into two parts for simplicity of explanation, the refrigerant loop and water tank. The refrigerant loop, shown in Figure 36 allows for variation of flow rate, condensing pressure, subcool, and superheat. A picture of the refrigerant loop is shown in Figure 37.

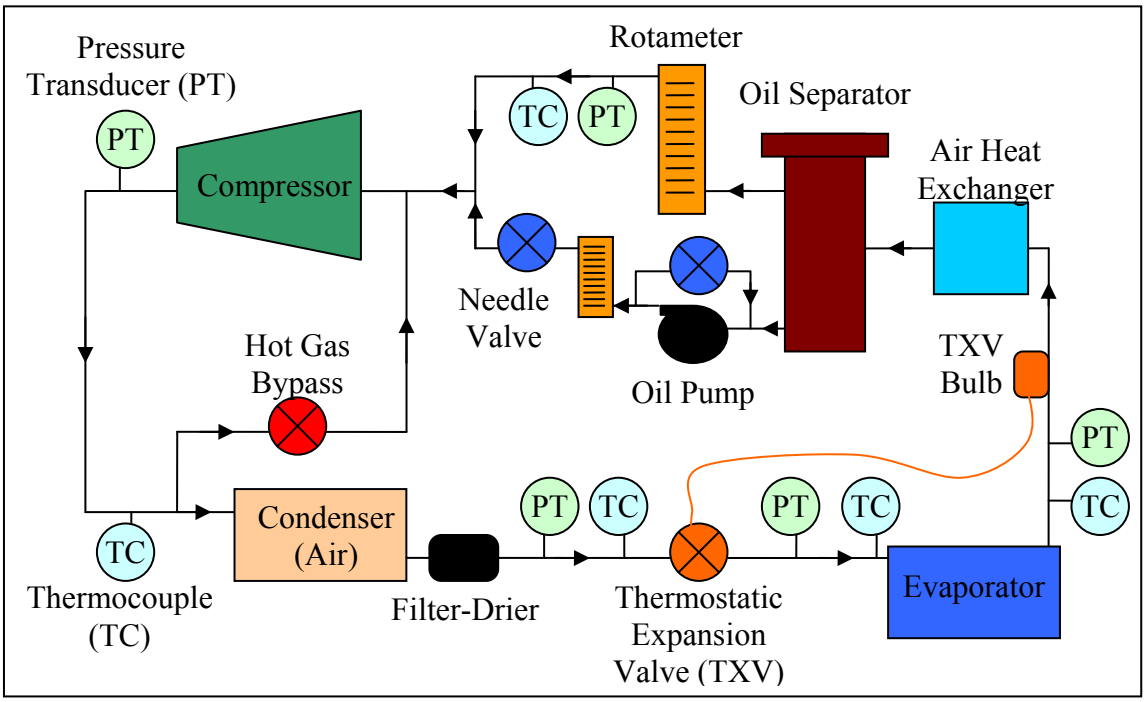

Figure 36: Refrigerant test loop diagram

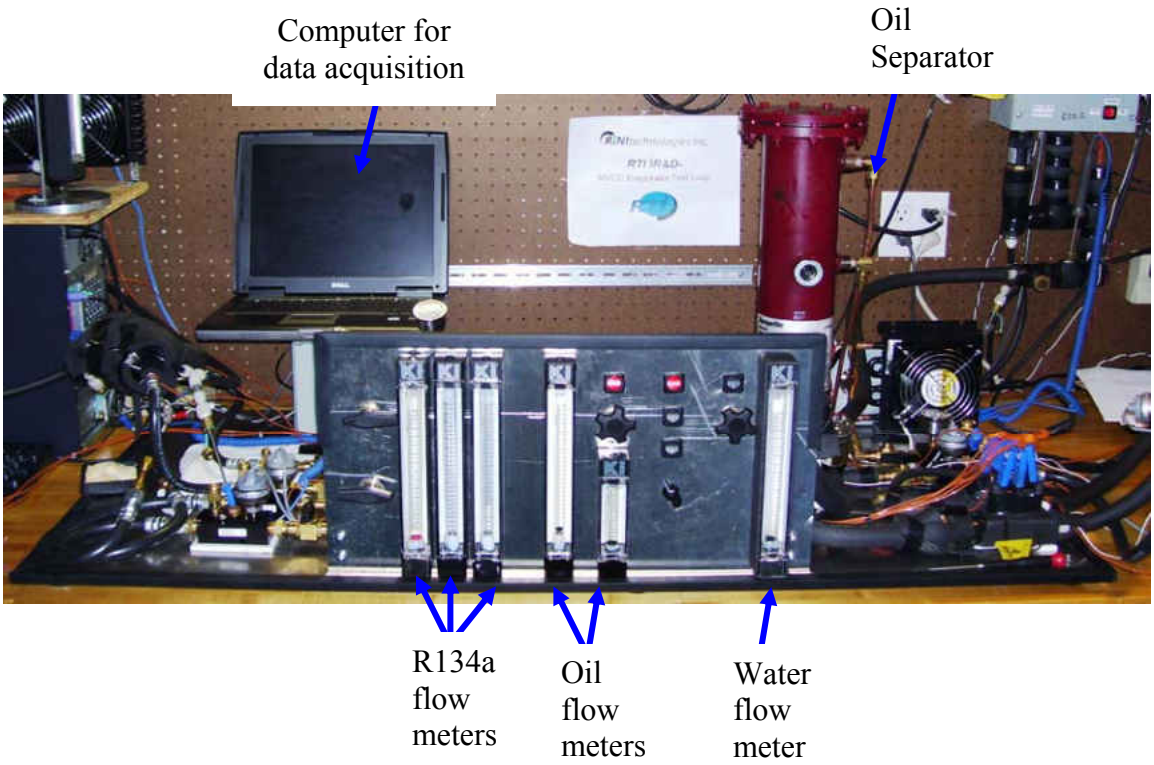

Figure 37: Refrigerant test loop

Thermocouples were calibrated at 0.0°C using an Omega TRCIII Icepoint and also at 390.0°C to within 0.1°C. The pressure transducers were calibrated using an Ashcroft 0-200 psi gauge to within 0.5 psi.

Data is recorded using a USB data acquisition system (OMB-DAQ-56) and expansion module (OMB-PDQ2) from Omega Engineering, Inc. The data is then manipulated and displayed live using a custom program created in National Instruments LabView 7.1. The program was developed to graphically display important parameters and calculations for adjustment of the test stand to achieve the desired test conditions. Data is taken every 2 seconds and recorded. The reported data utilizes an average function activated by the user that averages 45 points. This eliminates small high frequency variations to improve precision. A screen shot of the program Graphical User Interface (GUI) is shown in Figure 38. Further information on the test stand equipment, data acquisition, and program is presented in Appendix D.

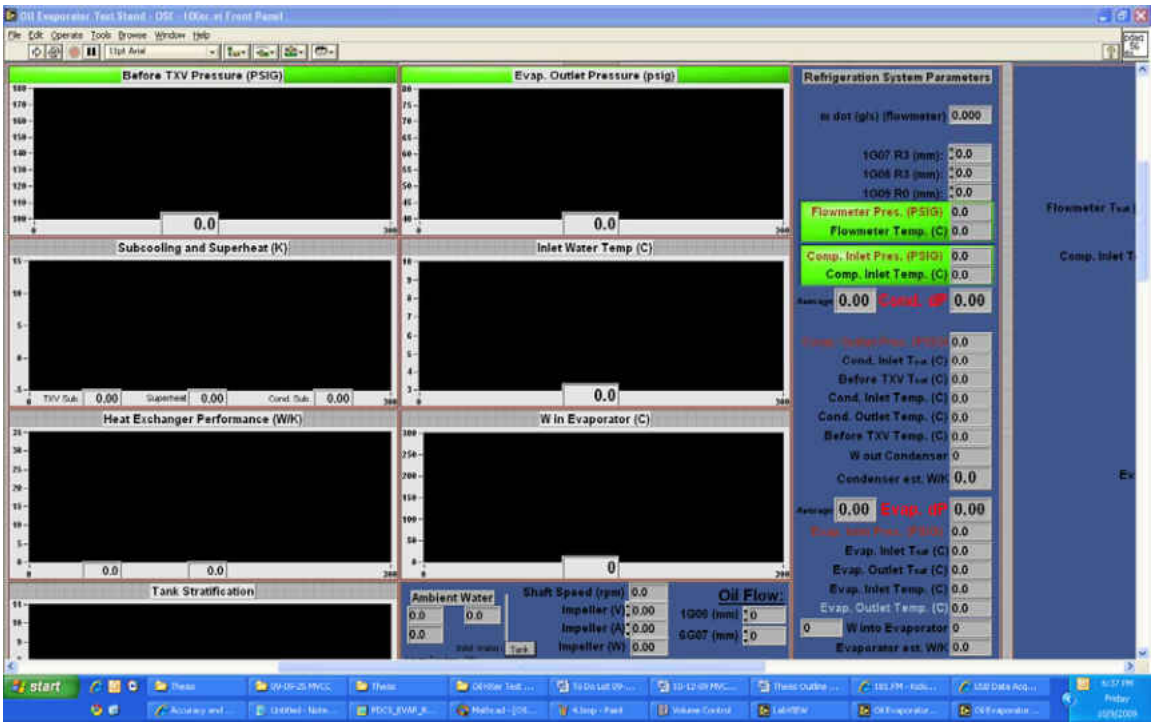

Figure 38: LabView program for evaporator characterization

Tank Setup

Two in tank variations were required for complete characterization of the evaporator. The first test stand, illustrated in Figure 39, uses a centrifugal water pump to create the water flow. The pump allows for a volumetric flow meter to be used to calculate the heat rate from the water as well as verify the water flow rate required. This will determine if the modeling was accurate.

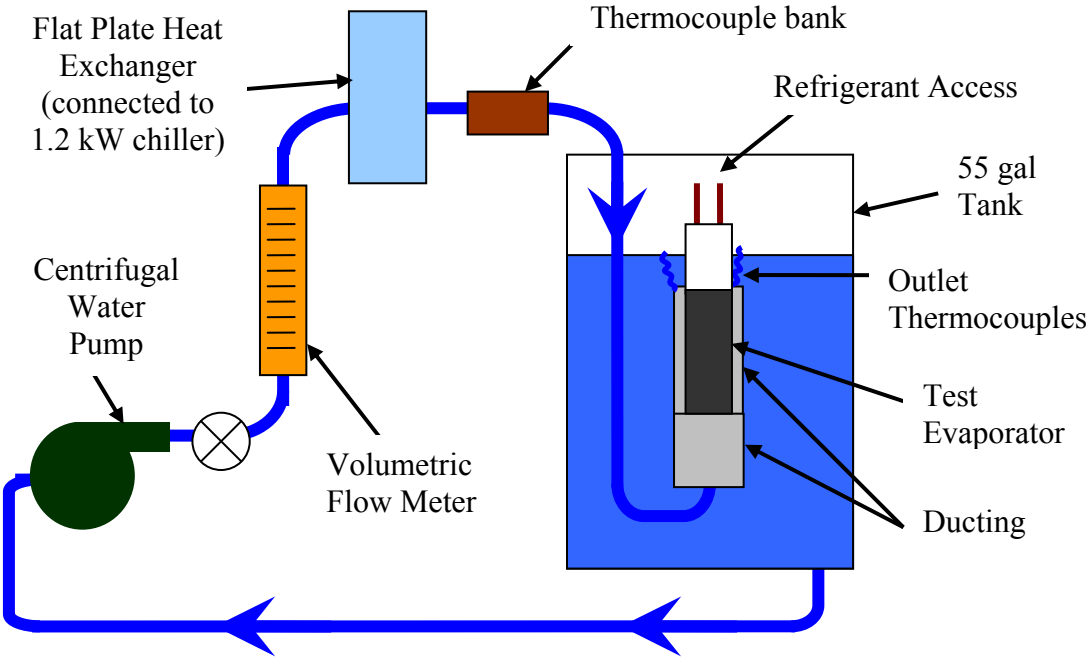

Figure 39: Diagram of water flow loop

The second test tank variation was to evaluate the impeller performance. The flow rate of the water with the impeller was not measured due to the restriction caused by the mechanical measurement devices that were within budget. The restrictions on paddle and turbine flow meters were greater than the resistance of the evaporator and would affect the flow of the impeller. The diagram of the evaporator layout and test is shown in Figure 40.

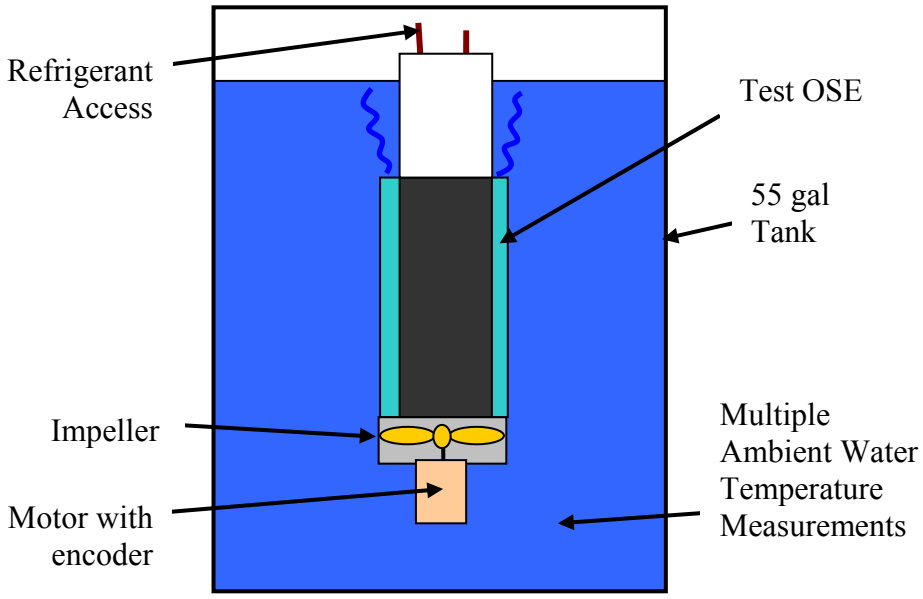

Figure 40 Evaluation of evaporator with impeller

Evaporator Test Results

Testing was focused on determining the water velocity to prevent ice formation on the smooth, open fin, and ducted fin outer spiral evaporator. The duct, shown in Figure 41 without the shroud, has a radial gap to align with the fins, forcing the metered flow down the channels, simulating an impeller.

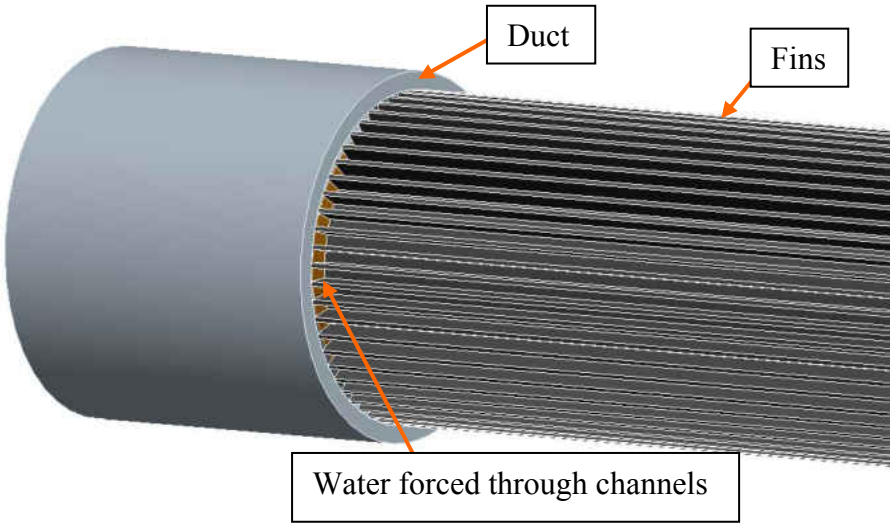

Figure 41: Duct with open fin OSE (outer duct not shown)

The goal performance to prevent ice formation as discussed previously is 55 W/K. The performance was tested with the duct across a variety of flows to determine the appropriate conditions for the impeller. The heat rate (200 W) and inlet water temperature (1.7°C) were held constant while the water flow rate was varied. The results are presented in Figure 42 along with the predicted performance from the analytical model. The model matches well at lower water flow rates but over predicts by 20% at the highest water flow rates. There is a large variation for the test data performance number but recall the performance equation (32). A small variation in either temperature measurement causes a significant swing in the performance. Error analysis is performed in Appendix E.

$$\text{Performance} = \frac{Q_{evap}}{T_{in} - T_{sat\_avg}} \tag{34}$$

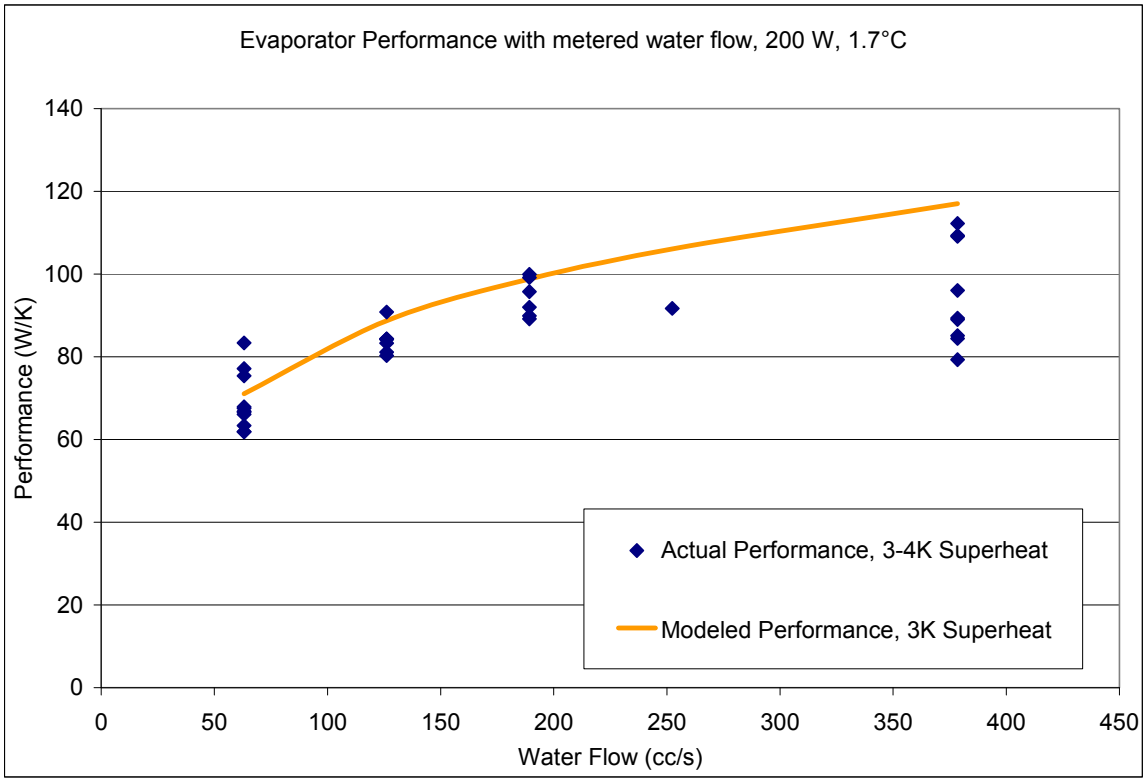

Figure 42: Performance of evaporator with variable forced convection

While collecting data at very low temperatures, difficulty was encountered due to pressure fluctuations, as seen in Figure 43, from an improperly sized thermostatic expansion valve and high oil flow rate. At warmer temperatures, the oil viscosity is much lower and the valve controls the pressure well as seen in Figure 44. These fluctuations however were corrected with a change in the valve size and oil flow rate.

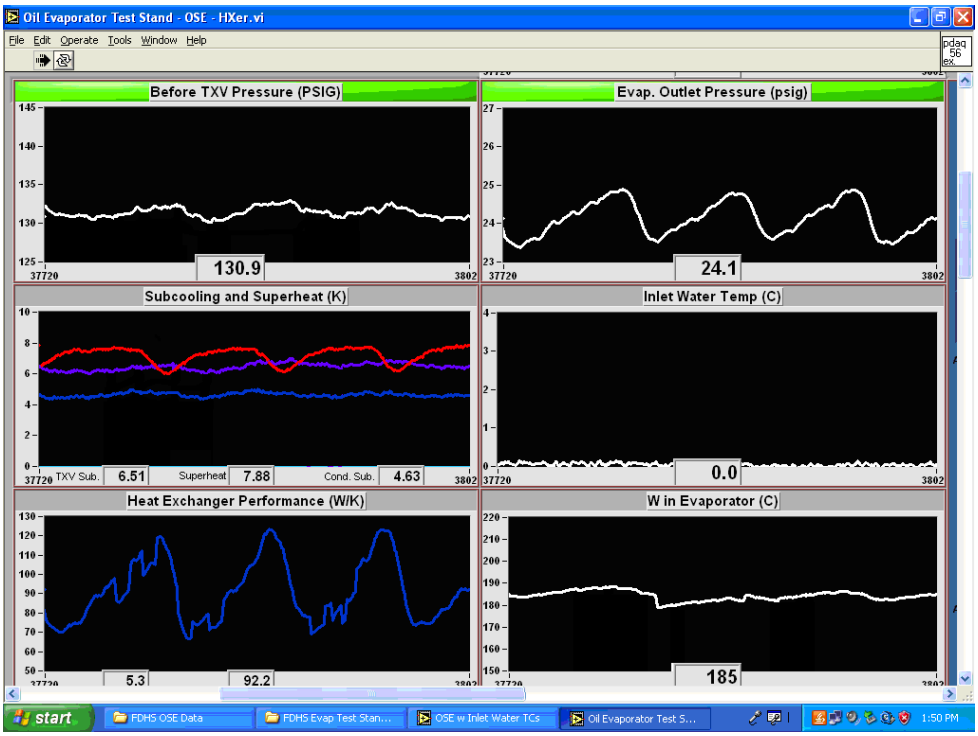

Figure 43: Low temperature oscillation

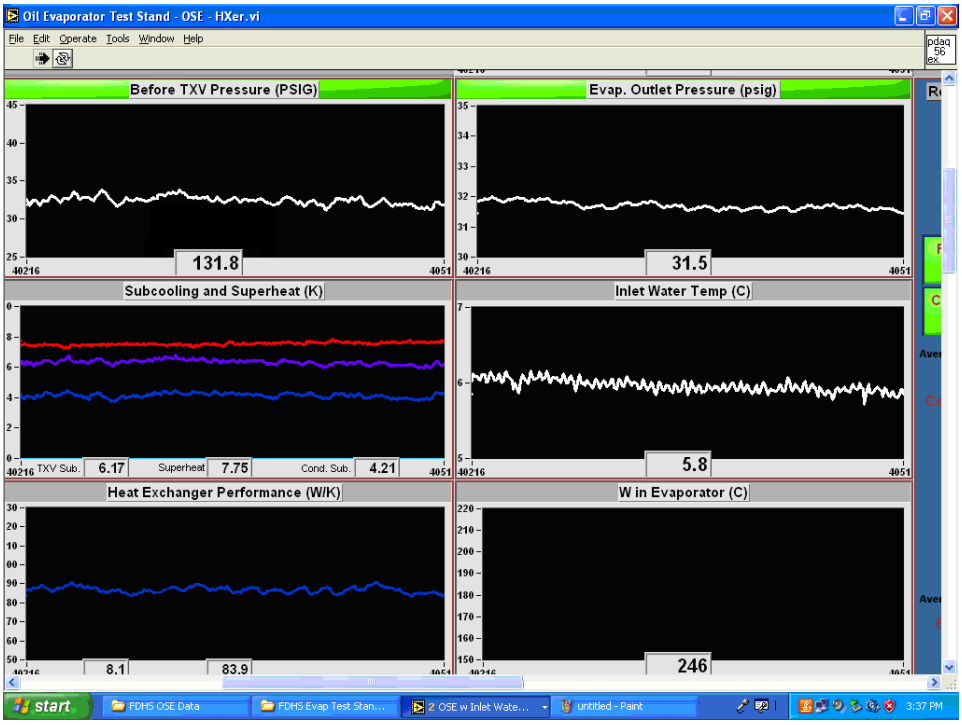

Figure 44: Steady operation

An attempt was made to freeze the evaporator to determine the effects of ice formation. With the centrifugal pump providing 126 cc/s and the inlet water thermocouples reading -0.1°C to 0.0°C, no ice formation was noticeable on the evaporator. The temperature was not lowered further to prevent the risk of damage to the large stainless steel plate heat exchanger used to chill the tank. Not forming ice implies a temperature error of at least 0.38 K, a flow rate error, or a freezing point below 0°C from using tap water. Error analysis is performed in Appendix E.

Impeller Testing

Achieving the minimum required flow at the lowest possible power is the goal of the impeller. To achieve the lowest power, the resistance of the evaporator must be low and the characteristics of the impeller must be favorable for the motor. In general, BrushLess Direct Current (BLDC) motors prefer higher speed and lower torques for maximum efficiency. Of the impellers to be investigated, the Lightnin A-310 shown in Figure 45 has the highest shaft speed due to the low blade pitch and solidity (2D projection of blades looking down axially). Thus less water is moved per revolution of the impeller. This is beneficial to the motor because the shaft speed required to achieve the flow will be higher and torque less, allowing for the motor to run at a higher efficiency.

Figure 45: Lightnin A-310 impeller

The motor used to test the impeller was characterized on a steady state dynamometer. This allowed for the torque to be determined based on the shaft speed and motor current, both of which can be measured during submerged evaporator testing. With the torque, shaft speed, and evaporator performance, the impellers can be compared and contrasted to determine the lowest power configuration. The torque and shaft speed required to achieve the desired evaporator performance will also be used with the system voltage to select an appropriate motor winding for integration into the system.

The impeller was then attached to the characterized test motor in addition to an optical encoder for an accurate shaft speed measurement. The motor/impeller assembly was then attached to the evaporator shroud and submerged performance was evaluated. The results shown in Table 8 present two shaft speeds tested. Evaporator performance at the lowest speed (67 W/K) exceeded the minimum required 55 W/K. Due to the limitations of the evaluation motor and controller, a lower shaft speed could not be evaluated.

Table 8: Lightnin A-310 impeller performance

Shaft Speed (RPM)	Impeller Motor Power (W)	Evaporator Performance (W/K)
582	4.2	67

Since the performance is more than necessary, system analysis was performed and deemed it necessary to reduce the flow rate to decrease system power. The decrease in impeller motor power would decrease the saturation pressure slightly causing the compressor to do more work. Since the compressor is more efficient, it is desirable to transfer more of the load to the compressor. To reduce the flow rate and simultaneously increase the shaft speed, a custom hub was created to cover the center of the impeller shown in Figure 46. The decrease in motor power for the same evaporator performance is shown in Table 9. The increase in shaft speed as well as reduction in torque from the hub is shown in Table 10.

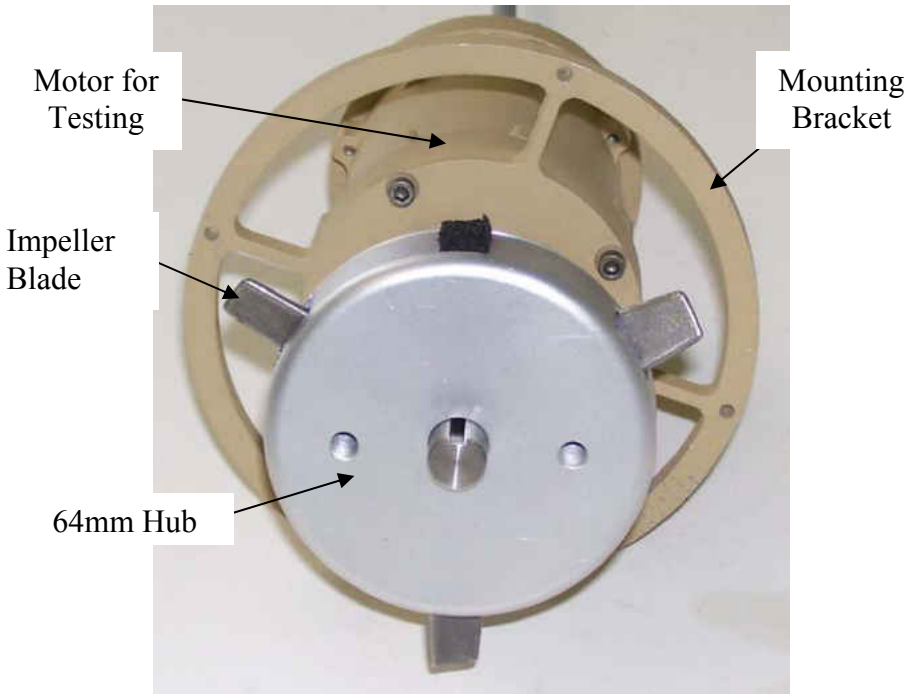

Figure 46: Impeller evaluation assembly with 2.5" hub

Table 9: Impeller hub motor power reduction

Full Impeller		64 mm Hub	
Impeller Motor Power (W)	Evap. Performance (W/K)	Impeller Motor Power (W)	Evap. Performance (W/K)
4.2	67	3.4	67

Table 10: Impeller conditions for 67 W/K evaporator

	Shaft Speed	Torque	Shaft Work
Impeller	rpm	oz-in	W
full	582	4.7	2.0
64 mm hub	590	4.3	1.9

The effect of the hub on impeller speed was satisfactory as shown in Figure 47. The shaft speed was increased while overall reducing the amount of shaft work done allowing for a better motor efficiency to be achieved.

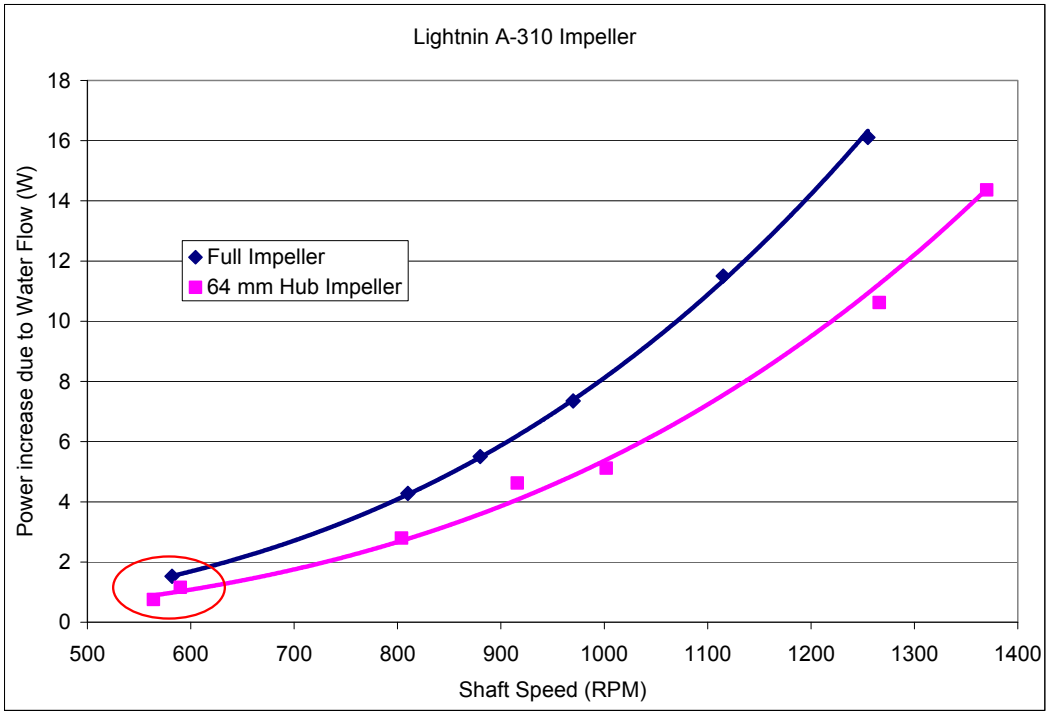

Figure 47: Effect of 64 mm hub on shaft speed

In addition to making the operation point of the motor more efficient, the hub will create a more compact design. Without the hub, the motor would have to be integrated

with the motor axially away from the impeller with a shaft connecting the two components, thus increasing the length of the unit. With the large hub, the motor can be placed in the same lateral plane as the impeller, minimizing the volume of the system. This is illustrated in Figure 48.

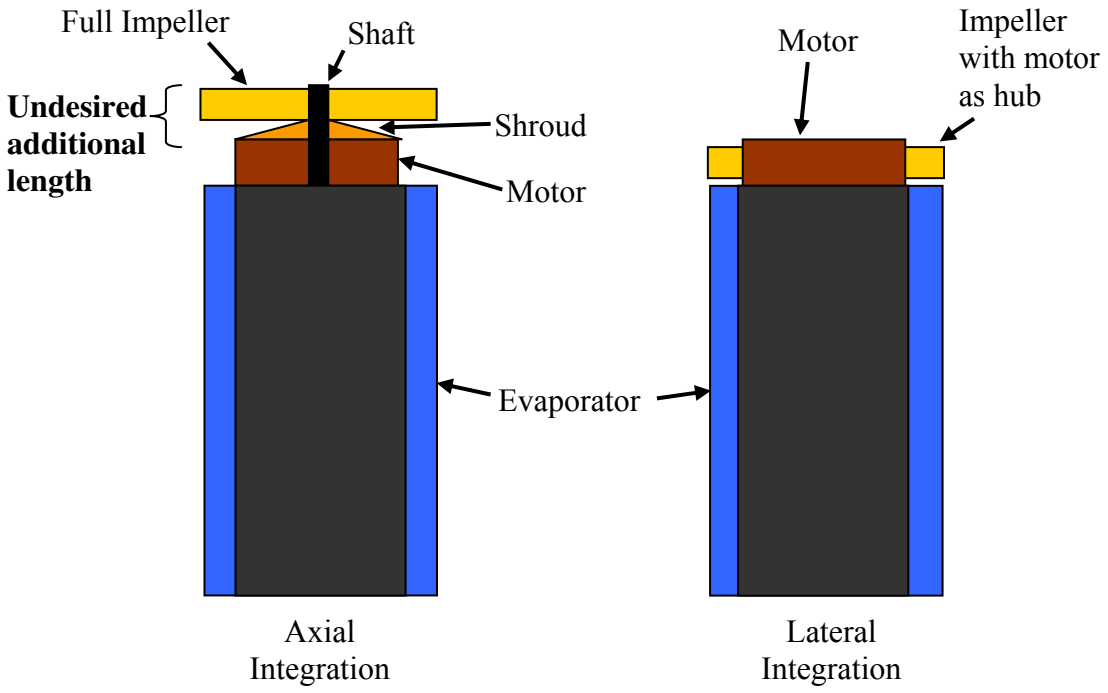

Figure 48: Volume savings with hub.

Impeller Motor

With the satisfactory performance of the impeller, motors for integration were investigated using the more desirable 64 mm hub operation point shown in Table 11.

Table 11: Impeller motor operation conditions

Impeller	Shaft Speed (RPM)	Torque (oz-in)	Shaft Work (W)
64 mm Hub	590	4.3	1.9

Over a dozen brushless motors were investigated to find the optimal balance of size and efficiency for integration. The calculations used to determine the motor efficiency from information provided by the manufacturer are presented in Appendix F. The combination of high torque, low speed, and short length make selecting a motor difficult. Over a dozen possible motors and were compared and the Applimotion UTH-62 was selected for the low axial length, weight, and high efficiency.

The impeller motor shown in Figure 49 was tested to determine the motor efficiency at steady state operation. At the conditions of interest, the total electrical power was measured to be 6 W, 3 W higher than calculated. The manufacturer attributed this discrepancy to the high winding resistance causing the BLDC sensor-less motor controller to be inefficient. With a senor-less controller tuned to this motor or a Hall-sensor controller, the efficiency would improve greatly.

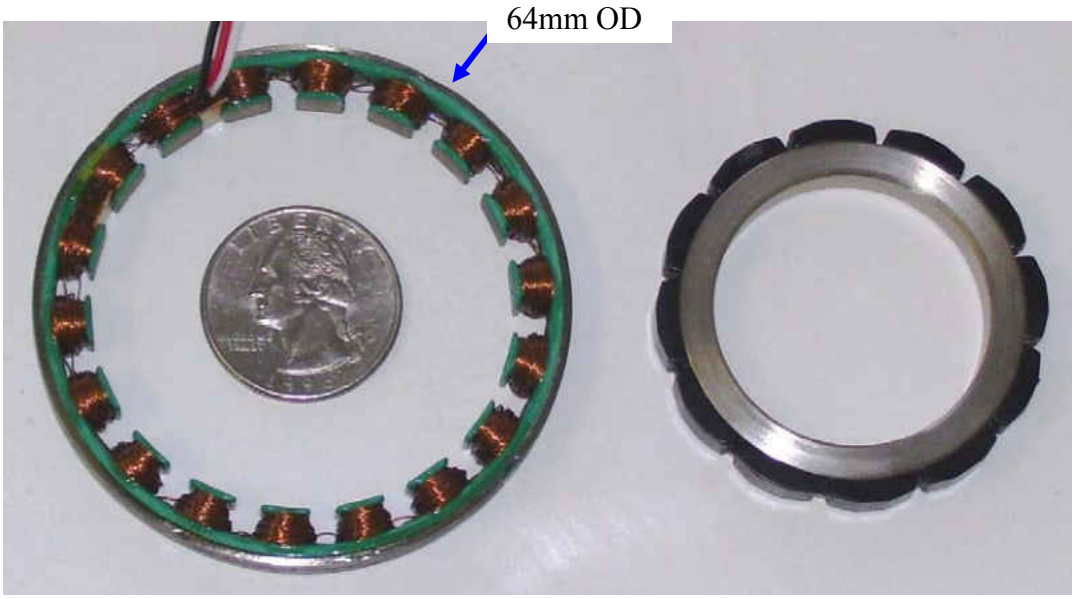

Figure 49: Impeller motor stator (left) and rotor (right)

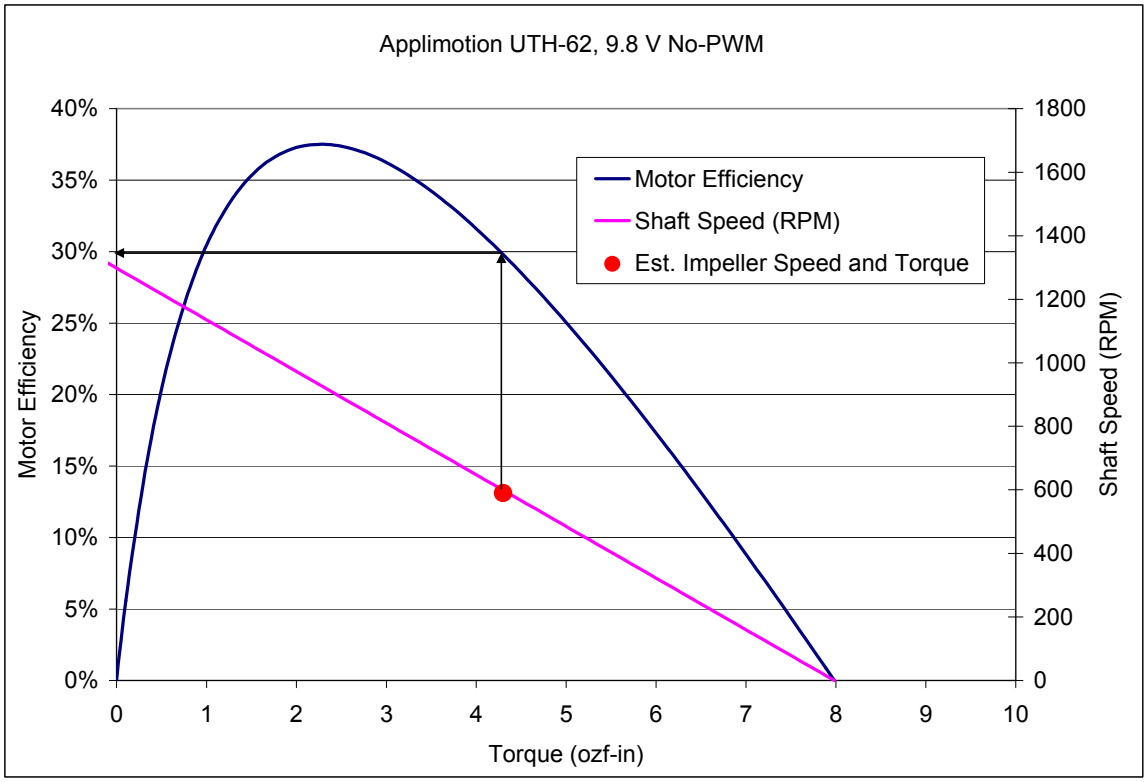

Figure 50: Motor efficiency at impeller operating conditions

CHAPTER SIX: CONCLUSION

An evaporator design capable of operation in very cold (1.7 °C) sea water was successfully developed. Traditional heat transfer calculations were applied to a numerical model to determine the appropriate geometry and performance. An investigation was then performed into the possible manufacturing methods and a prototype was created. Test apparatus was then assembled and the performance of the prototype was evaluated. Using a pump and flow meter, the correlation developed to predict the performance of the evaporator was evaluated and found to be within 20% of experimental data. An investigation into impellers to provide the desired flow and pressure was performed and a capable impeller was found. The impeller was then characterized and tested with the evaporator. To reduce the power draw, a hub was attached to the center of the impeller with favorable results. The shaft speed was increased and torque reduced, resulting in more favorable motor conditions. An investigation into a motor was performed and the selected motor was tested. The final design meets all of the critical design criteria and was integrated with the existing components.

CHAPTER SEVEN: RECOMMENDATIONS FOR FUTURE WORK

Though the correlation model and initial evaporator design are satisfactory, they can be improved with additional testing. Corrosion testing of a variety of fin thicknesses with a salt fog test would determine a minimum fin width. With the minimum fin width, likely smaller than used here, the performance of the evaporator could be further improved.

A complete finite element analysis of the evaporator at depth would be beneficial. Complete analysis may allow for the thickness of the cylinder wall to be reduced thus saving weight.

The impeller power could be reduced by optimizing the impeller design for the motor. Analysis of the number, solidity and pitch of the impeller fins could arrive at a design that optimizes the motor while providing the necessary flow through the evaporator.

APPENDIX A: MODELING WITH ICE

Water Properties from Engineering Equation Solver, Commercial V7.078 (04/05/04)

$kJ := 1000 \cdot J \qquad kPa := 1000 \cdot Pa \qquad °C := K \qquad T_{s1} := -4K$

$Q_{h2} := 200W$

Pure Water at 101kPa from Engineering Equation Solver 8-17°C by 1°C:

temperature thermal conductivity viscosity

$$T_W := \begin{pmatrix} 1.7 \\ 2 \\ 3 \\ 4 \\ 5 \\ 6 \\ 7 \\ 8 \\ 9 \\ 10 \\ 11 \\ 12 \\ 13 \\ 14 \\ 15 \\ 16 \\ 17 \end{pmatrix} \cdot K \qquad k_W := \begin{pmatrix} 0.551 \\ 0.5516 \\ 0.5536 \\ 0.5556 \\ 0.5576 \\ 0.5596 \\ 0.5616 \\ 0.5635 \\ 0.5655 \\ 0.5674 \\ 0.5694 \\ 0.5713 \\ 0.5732 \\ 0.5751 \\ 0.577 \\ 0.5788 \\ 0.5806 \end{pmatrix} \frac{W}{m \cdot K} \qquad \mu_W := \begin{pmatrix} 0.001691 \\ 0.001674 \\ 0.00162 \\ 0.001568 \\ 0.001519 \\ 0.001472 \\ 0.001428 \\ 0.001385 \\ 0.001345 \\ 0.001307 \\ 0.00127 \\ 0.001235 \\ 0.001201 \\ 0.001169 \\ 0.001138 \\ 0.001109 \\ 0.00108 \end{pmatrix} \frac{kg}{m \cdot s}$$

density

$$\rho_w := \begin{pmatrix} 1000 \\ 1000 \\ 1000 \\ 1000 \\ 1000 \\ 1000 \\ 1000 \\ 1000 \\ 999.7 \\ 999.6 \\ 999.5 \\ 999.4 \\ 999.3 \\ 999.1 \\ 999 \\ 998.8 \\ 998.7 \end{pmatrix} \cdot \frac{kg}{m^3}$$

Prandtl number

$$Pr_w := \begin{pmatrix} 12.94 \\ 12.79 \\ 12.31 \\ 11.86 \\ 11.44 \\ 11.04 \\ 10.66 \\ 10.3 \\ 9.964 \\ 9.642 \\ 9.336 \\ 9.045 \\ 8.769 \\ 8.505 \\ 8.253 \\ 8.013 \\ 7.783 \end{pmatrix}$$

volumetric expansion coefficient

$$\beta_w := \begin{pmatrix} -0.000047 \\ -0.00004137 \\ -0.00002311 \\ -0.000005551 \\ 0.00001135 \\ 0.00002764 \\ 0.00004336 \\ 0.00005855 \\ 0.00007323 \\ 0.00008744 \\ 0.0001012 \\ 0.0001146 \\ 0.0001275 \\ 0.0001401 \\ 0.0001523 \\ 0.0001643 \\ 0.0001759 \end{pmatrix} \cdot \frac{1}{K}$$

$ii := 0$

$T_{amb} := T_{w_{ii}}$ $\beta_{water} := \beta_{w_{ii}}$

$k_{water} := k_{w_{ii}}$ $\rho_{water} := \rho_{w_{ii}}$

$\mu_{water} := \mu_{w_{ii}}$ $Pr_{water} := Pr_{w_{ii}}$

$$\nu_{water} := \frac{\mu_{water}}{\rho_{water}} \qquad \nu_{water} = 1.691 \times 10^{-6} \frac{m^2}{s}$$

kinematic viscosity=viscous force/inertia force (density)

salt water freezing temperature:

p (bar abs)
s (ppm)

Ranges:
t = 0<20C temperature
s=0-40% salinity
p=1-1000bar abs pressure

$T_{il}(S_w, P_d) := \left(-0.02831 - 0.0499 S_w - 0.000112 S_w^{\,2} - 0.00759 P_d\right) \cdot K$ Fujino et al. (1974)

$S_w := 0$ $P_d := 1$ $T_{il}(S_w, P_d) = -0.036K$ $T_{il}(35, 1) = -1.92K$

Properties of ice

thermal conductivity heat of sublimation density

$k_{ice} := 2.22 \frac{W}{m \cdot K}$ $L_{water} := 334 \frac{J}{gm}$ $\rho_{ice} := 0.9167 \frac{gm}{cm^3}$

Geometric Constraints and Properties

single geometry to be evaluated

$t_{c2} := .030 \cdot in$ Channnel depth

$w2 := .275 \cdot in$ Channel width

$n_{c2} := 3$ Number of Channels

set minimum wall width to 0.015in

$$t_w(t_c) := \begin{cases} 0.015 \cdot in & \text{if } \frac{t_c}{3} < .015 \cdot in \\ \frac{t_c}{3} & \text{otherwise} \end{cases}$$ Channel wall width

$t_w(t_{c2}) = 0.015in$

$d_i := 3.35 \cdot in$ inside diameter of shell

$L_e := 7.27in$ .length of evaporator (accounting for non-usable ends)

$t_{shell} := 0.050in$ thickness of shell

$k_{shell} := 167 \frac{W}{m \cdot K}$ thermal conductivity of shell (6061-T6 aluminum)

$$R_{shell} := \frac{\ln\left(\frac{d_i + 2t_{shell}}{d_i}\right)}{2\cdot\pi\cdot k_{shell}\cdot L_e} \qquad R_{shell} = 1.518\times 10^{-4}\,\frac{K}{W}$$ resistance of shell

$$A_{evap} := \pi\cdot\left(d_i + 2\cdot t_{shell}\right)\cdot L_e \qquad A_{evap} = 78.8in^2$$ heat exchange area of shell

$$A_{conv}\left(t_{ice}\right) := \pi\cdot\left(d_i + 2\cdot t_{shell} + 2\cdot t_{ice}\right)\cdot L_e \qquad A_{conv}(1in) = 124.5in^2$$ external heat exchange area of ice

$$R_{ice}\left(t_{ice}\right) := \frac{\ln\left(\frac{d_i + 2t_{shell} + 2\cdot t_{ice}}{d_i + 2t_{shell}}\right)}{2\cdot\pi\cdot k_{ice}\cdot L_e} \qquad R_{ice}(1in) = 0.178\frac{K}{W}$$ thermal resistance of ice

$$t_{ice2} := 0in, 0.01in .. 12in$$

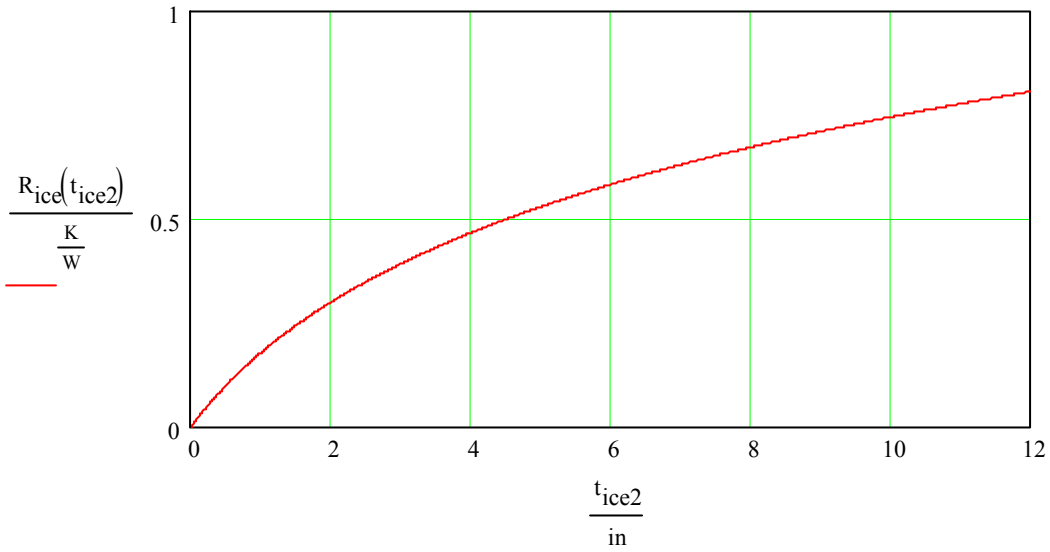

$$\theta\left(w, t_c, n_c\right) := \operatorname{acos}\left[\frac{n_c\cdot\left(w + t_w\left(t_c\right)\right)}{\pi\cdot d_i}\right] \qquad \theta\left(w2, t_{c2}, n_{c2}\right) = 85.3deg$$ pitch angle

$$N_s\left(w, t_c, n_c\right) := \frac{L_e\cdot\sin\left(\theta\left(w, t_c, n_c\right)\right)}{n_c\cdot\left(w + t_w\left(t_c\right)\right)} \qquad N_s\left(w2, t_{c2}, n_{c2}\right) = 8.3$$ number of sections (swirls)

$$Pitch\left(w, t_c, n_c\right) := \frac{L_e}{N_s\left(w, t_c, n_c\right)} \qquad Pitch\left(w2, t_{c2}, n_{c2}\right) = 0.873in$$ must be 1in or less to be turned

$$L_{ch}\left(w, t_c, n_c\right) := \frac{\pi\cdot d_i}{\sin\left(\theta\left(w, t_c, n_c\right)\right)}\cdot N_s\left(w, t_c, n_c\right) \qquad L_{ch}\left(w2, t_{c2}, n_{c2}\right) = 87.945in$$ length of a channel

$$D_h(w, t_c) := \frac{4 \cdot t_c \cdot w}{2 \cdot t_c + 2 \cdot w}$$ Hydraulic Diameter $D_{h2} := D_h(w2, t_{c2})$ $D_h(w2, t_{c2}) = 0.054\text{in}$

$$ar(w, t_c) := \frac{w}{t_c}$$ Aspect Ratio $ar_2 := ar(w2, t_{c2})$ $ar(w2, t_{c2}) = 9.167$

"aspect ratio factor" for increased heat transfer and pressure drop in high aspect ratio ducts (fully deveoloped LAMINAR flow)

aspect ratio | Nusselt number (Uniform Surface Temperature | friction factor $xx := 1, 2 .. 40$

$$LAM_{Dh} := \begin{pmatrix} 1 & 2.976 & 57 \\ 1.4 & 3.1 & 59 \\ 2 & 3.4 & 62 \\ 3 & 4.0 & 69 \\ 4 & 4.4 & 73 \\ 8 & 5.6 & 82 \\ 30 & 7.541 & 96 \end{pmatrix}$$

logistic curve fit

$$\begin{pmatrix} a2 \\ b2 \\ c2 \end{pmatrix} := lgsfit\left[LAM_{Dh}^{\langle 0 \rangle}, LAM_{Dh}^{\langle 1 \rangle}, \begin{pmatrix} 7.54 \\ 0.8 \\ 0.2 \end{pmatrix}\right]$$

$$\begin{pmatrix} a3 \\ b3 \\ c3 \end{pmatrix} := lgsfit\left[LAM_{Dh}^{\langle 0 \rangle}, LAM_{Dh}^{\langle 2 \rangle}, \begin{pmatrix} 96 \\ 0.8 \\ 0.2 \end{pmatrix}\right]$$

$$Y_{Nu}(xx) := \frac{a2}{1 + b2 \cdot e^{-c2 \cdot xx}}$$

$$Y_{Re}(xx) := \frac{a3}{1 + b3 \cdot e^{-c3 \cdot xx}}$$

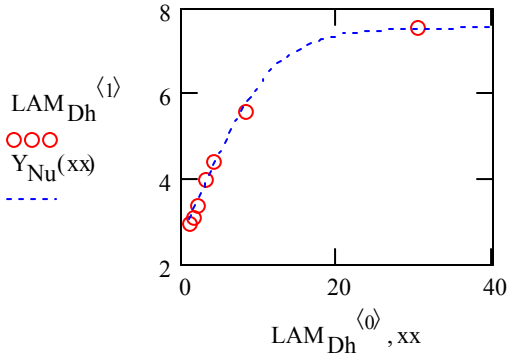

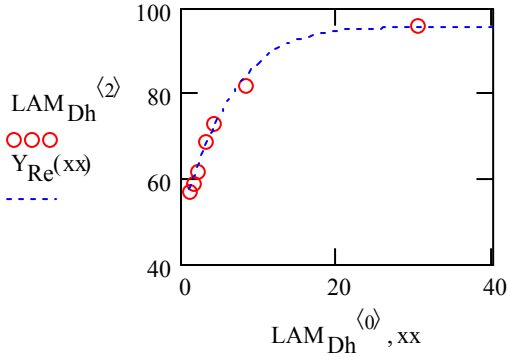

$$F_{NuAR}(w, t_c) := \frac{Y_{Nu}(ar(w, t_c))}{3.66}$$

$$F_{NuAR}(w2, t_{c2}) = 1.653$$

$$F_{ReAR}(w, t_c) := \frac{Y_{Re}(ar(w, t_c))}{64}$$

$$F_{ReAR}(w2, t_{c2}) = 1.349$$

Water Side Heat Transfer

Vertical Cylinder in quiesant water:

$$\text{free\_dir} := \begin{cases} 1 & \text{if } \beta_{water} < 0 \quad \text{rising flow} \\ 0 & \text{if } \beta_{water} = 0 \quad \text{neutral} \\ -1 & \text{otherwise} \quad \text{sinking flow} \end{cases}$$

$$Gr_L(T_s) := \frac{g \cdot |\beta_{water}| \cdot (T_{amb} - T_s) \cdot L_e^{\,3}}{(\nu_{water})^2} \qquad Gr_L(T_{il}(S_w, P_d)) = 1.762 \times 10^6$$

Newton and Fourier with g(Pr) estimation (pg504 DeWitt):

$$g_{Pr} := \frac{0.75 \cdot \sqrt{Pr_{water}}}{\left(0.609 + 1.221 \cdot \sqrt{Pr_{water}} + 1.238 \cdot Pr_{water}\right)^{\frac{1}{4}}} \qquad g_{Pr} = 1.26$$

$$Nu_L(T_s) := \frac{4}{3} \cdot \left(\frac{Gr_L(T_s)}{4}\right)^{\frac{1}{4}} \cdot g_{Pr} \qquad Nu_L(T_{il}(S_w, P_d)) = 43.279$$

$$h_L(T_s) := \frac{Nu_L(T_s) \cdot k_{water}}{L_e} \qquad h_L(T_{il}(S_w, P_d)) = 129 \frac{W}{m^2 K}$$

$$Q(T_s, t_{ice}) := h_L(T_s) \cdot \pi \cdot (d_i + 2 \cdot t_{shell} + 2 \cdot t_{ice}) \cdot L_e \cdot (T_{amb} - T_s) \qquad Q(T_{il}(S_w, P_d), 0in) = 11\,W$$

$$Ra_L(T_s) := Gr_L(T_s) \cdot Pr_{water} \qquad Ra_L(T_{s1}) = 7.486 \times 10^7$$

$$Nu_L(T_s) := \begin{cases} 0.68 + \dfrac{0.670\,Ra_L(T_s)^{\frac{1}{4}}}{\left[1 + \left(\dfrac{0.492}{Pr_{water}}\right)^{\frac{9}{16}}\right]^{\frac{4}{9}}} & \text{if } Ra_L(T_s) \le 10^9 \\ \left[0.825 + \dfrac{0.387 \cdot Ra_L(T_s)^{\frac{1}{6}}}{\left[1 + \left(\dfrac{0.492}{Pr_{water}}\right)^{\frac{9}{16}}\right]^{\frac{8}{27}}}\right]^2 & \text{otherwise} \end{cases}$$

$$Nu_L(T_{il}(S_w, P_d)) = 44.039$$

$$h_L(T_s) := \frac{Nu_L(T_s) \cdot k_{water}}{L_e}$$

$$h_L(T_{il}(S_w, P_d)) = 129.141 \frac{W}{m^2 K}$$

$$Q(T_s, t_{ice}) := h_L(T_s) \cdot \pi \cdot (d_i + 2 \cdot t_{shell} + 2 \cdot t_{ice}) \cdot L_e \cdot (T_{amb} - T_s)$$

$$Q(T_{il}(S_w, P_d), 0in) = 11.596W$$

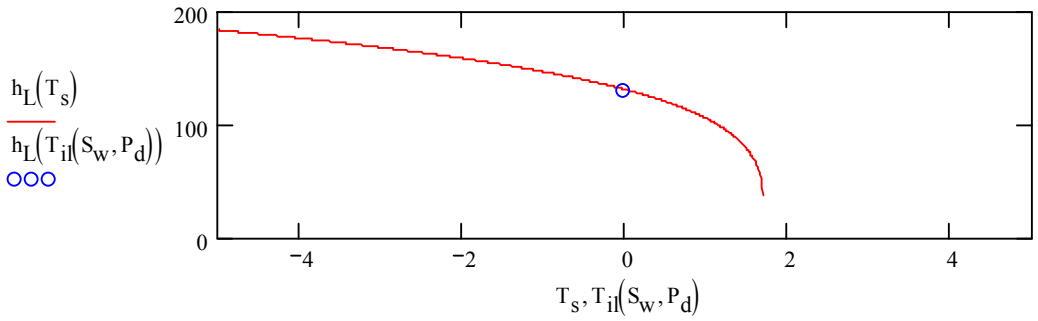

Forced Convection Vertical:

pg371-373 DeWitt

$V_{swim2} := 0.1\frac{ft}{s}$ $V_{swim2} = 1.2\frac{in}{s}$ $V_{swim2} = 0.068\frac{mi}{hr}$

direction of swimming:
-1 sinking
0 transverse
1 rising

$swim\_dir := 0$

Thrust:v*dm/dt

$$\rho_{water}\cdot\left[\left(d_i + 2\cdot t_{shell} + 0.5\cdot in\right)^2 - \left(d_i + 2\cdot t_{shell}\right)^2\right]\cdot\frac{\pi}{4}\cdot V_{swim2}{}^2 = 3.916\times 10^{-4}\,lbf$$

$$Re_L(V_{swim}) := \frac{V_{swim}\cdot L_e}{\nu_{water}} \qquad Re_L(V_{swim2}) = 3328$$

$Pr_{water} = 12.94$

for 0.6<Pr<60

$$Nu_{L\_f}(V_{swim}) := \begin{cases} 0.664\,Re_L(V_{swim})^{\frac{1}{2}}\cdot Pr_{water}^{\frac{1}{3}} & \text{if } Re_L(V_{swim}) < 5\cdot 10^5 \\ \left(0.037\cdot Re_L(V_{swim})^{\frac{4}{5}} - 871\right)Pr_{water}^{\frac{1}{3}} & \text{if } 5\cdot 10^5 < Re_L(V_{swim}) \le 10^8 \\ 0.0296\,Re_L(V_{swim})^{\frac{4}{5}}\cdot Pr_{water}^{\frac{1}{3}} & \text{otherwise} \end{cases}$$

$$h_{fv}(V_{swim}) := \frac{Nu_{L\_f}(V_{swim})\cdot k_{water}}{L_e} \qquad Nu_{L\_f}(V_{swim2}) = 89.936 \qquad h_{fv}(V_{swim2}) = 268\frac{W}{m^2\cdot K}$$

$V_{swim} := 0.01\frac{ft}{s}, 0.02\frac{ft}{s} .. 40\frac{ft}{s}$

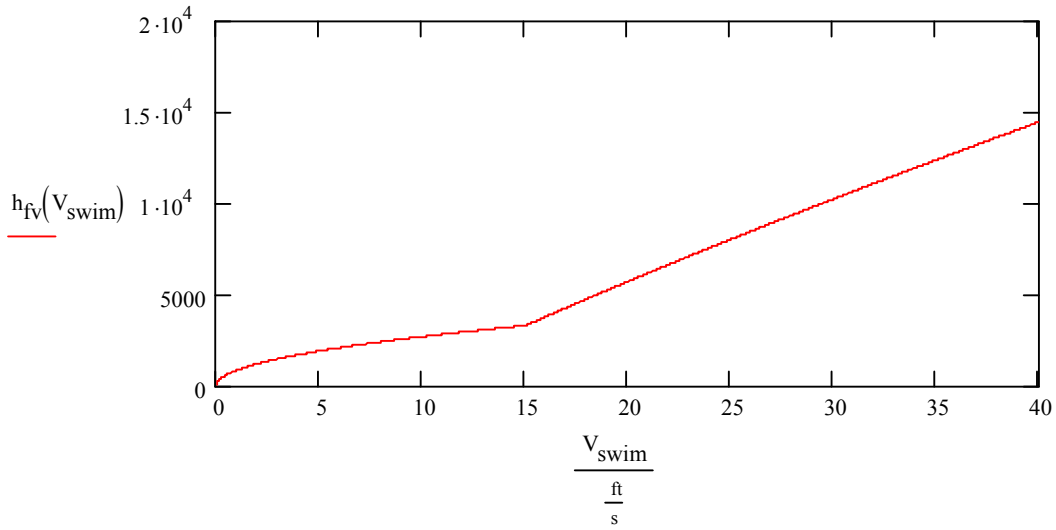

$Q_{fv}(T_s, V_{swim}, t_{ice}) := h_{fv}(V_{swim}) \cdot 1 \cdot \pi \cdot (d_i + 2 \cdot t_{shell} + 2 \cdot t_{ice}) \cdot L_e \cdot (T_{amb} - T_s)$

$Q_{fv}(T_{il}(S_w, P_d), V_{swim2}, 0in) = 24\,W$

Approximate combination of forced and free convection for cylinder:

add for assisting and transverse, subtract for opposing

$n_{cyl} := 4$

$$Nu_{mix\_ass}(T_s, V_{swim}) := \left(\left| Nu_L(T_s)^{n_{cyl}} + Nu_{L\_f}(V_{swim})^{n_{cyl}} \right| \right)^{\frac{1}{n_{cyl}}} - Nu_L(T_s)$$

$Nu_{mix\_ass}(T_{il}(S_w, P_d), V_{swim2}) = 47.163$

$$Nu_{mix\_opp}(T_s, V_{swim}) := \left(\left| Nu_L(T_s)^{n_{cyl}} - Nu_{L\_f}(V_{swim})^{n_{cyl}} \right| \right)^{\frac{1}{n_{cyl}}} - Nu_L(T_s)$$

$Nu_{mix\_opp}(T_{il}(S_w, P_d), V_{swim2}) = 44.576$

based on water temperature (free convection flow) and swim direction, determine mixed

$$Nu_{mix}(T_s, V_{swim}) := \begin{cases} Nu_{mix\_ass}(T_s, V_{swim}) & \text{if } |free\_dir + swim\_dir| \le 1 \wedge free\_dir \neq 0 \quad \text{assiting} \\ Nu_{mix\_opp}(T_s, V_{swim}) & \text{if } |free\_dir + swim\_dir| > 1 \quad \text{oppositing} \\ Nu_{L\_f}(V_{swim}) & \text{if } free\_dir = 0 \quad \text{no free conv.} \\ 0 & \text{otherwise} \quad \text{error} \end{cases}$$

$$Nu_{mix}(T_{il}(S_w, P_d), V_{swim2}) = 47.163$$

convection

$$h_{mix}(T_s, t_{ice}, V_{swim}) := \frac{Nu_{mix}(T_s, V_{swim}) \cdot k_{water}}{d_i + 2 \cdot t_{shell} + 2 t_{ice}} \qquad h_{mix}(T_{il}(S_w, P_d), 0in, V_{swim2}) = 296.551 \frac{W}{m^2 \cdot K}$$

$$\frac{Gr_L(T_{il}(S_w, P_d))}{Re_L(V_{swim2})^2} = 0.159$$

if << 1, free convection negligible
if >> 1, force convection negligible
if ~1, use approx. combination for cylinders

$$h_w(T_s, t_{ice}, V_{swim}) := \begin{cases} h_{fv}(V_{swim}) & \text{if } \frac{Gr_L(T_{s1})}{Re_L(V_{swim})^2} < 0.5 \\ h_L(T_s) & \text{if } \frac{Gr_L(T_{s1})}{Re_L(V_{swim})^2} > 2 \\ h_{mix}(T_s, t_{ice}, V_{swim}) & \text{otherwise} \end{cases}$$

$$h_w(T_{il}(S_w, P_d), 0in, V_{swim2}) = 296.551 \frac{W}{m^2 \cdot K}$$

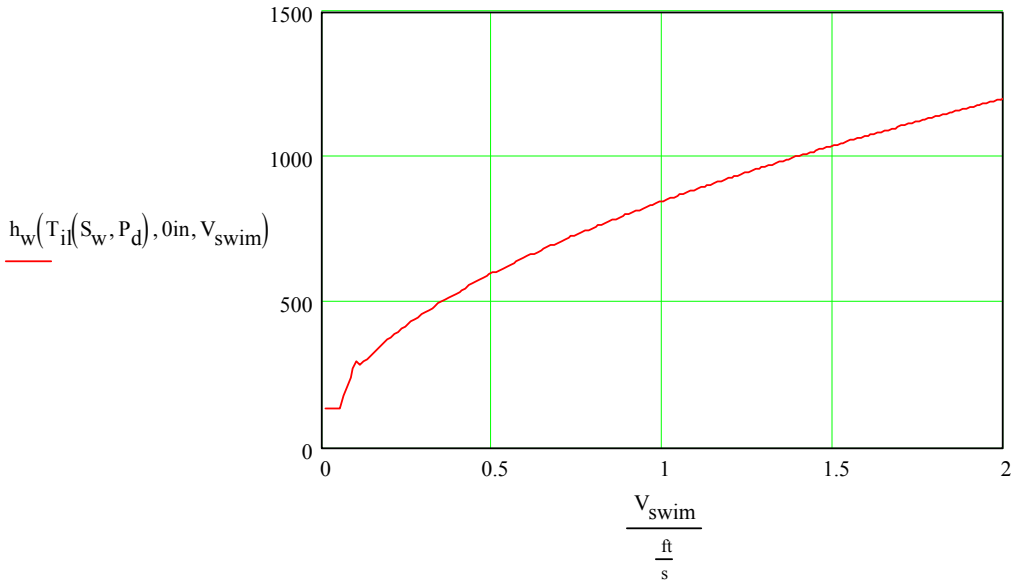

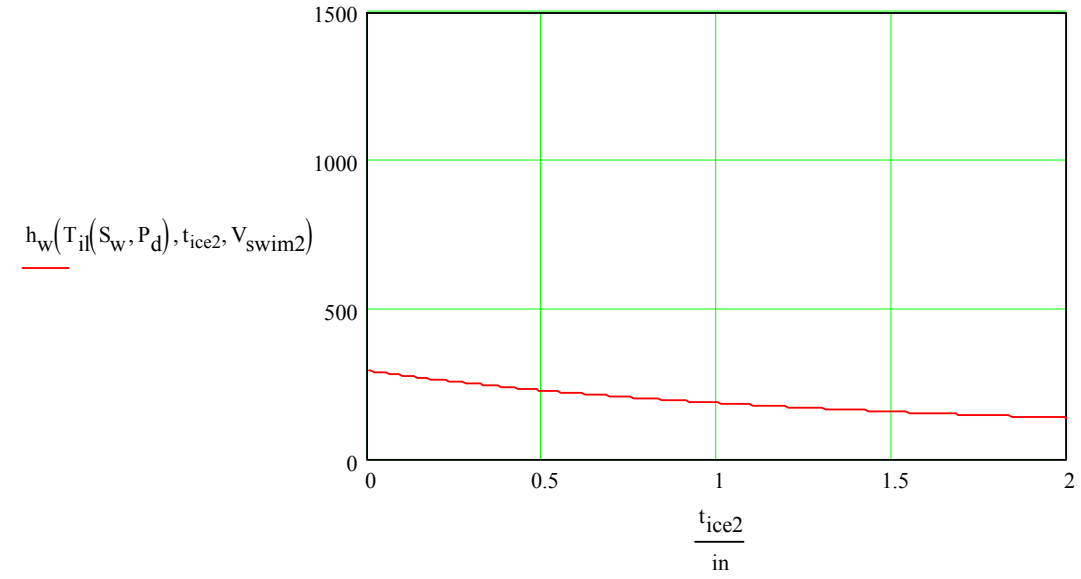

$$Q_w(T_s, V_{swim}, t_{ice}) := h_w(T_s, t_{ice}, V_{swim}) \cdot A_{conv}(t_{ice}) \cdot (T_{amb} - T_s)$$

$$Q_w(T_{il}(S_w, P_d), V_{swim2}, 0in) = 26\,W$$

$$A_{conv}(0in) \cdot h_w(T_{il}(S_w, P_d), 0in, V_{swim2}) = 15.075 \frac{W}{K}$$

Ice Buildup:

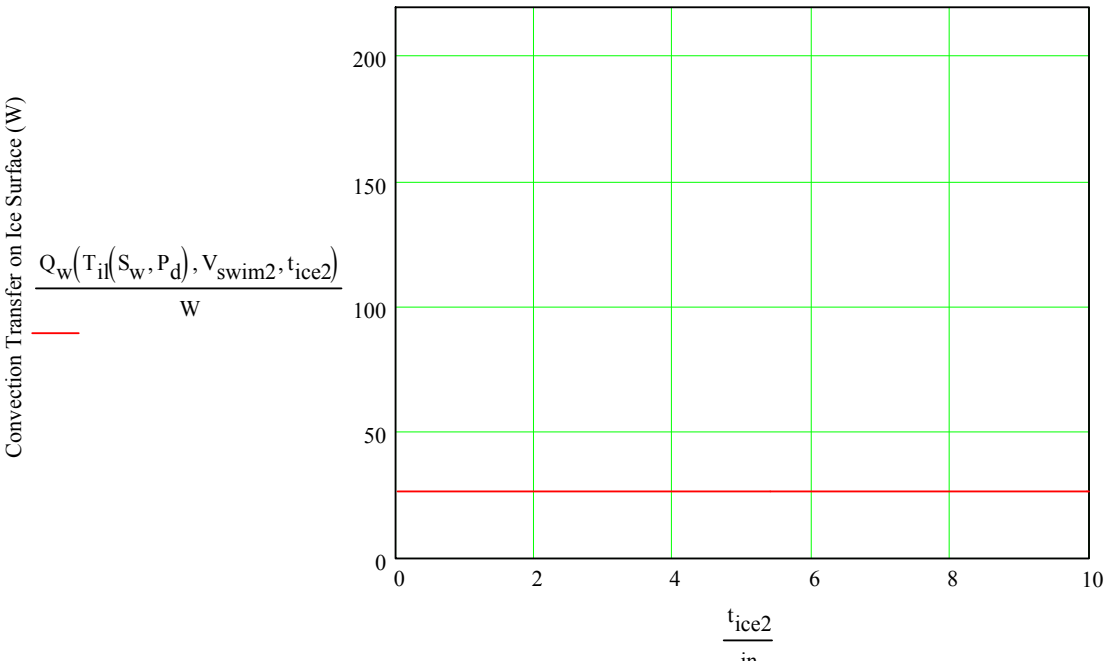

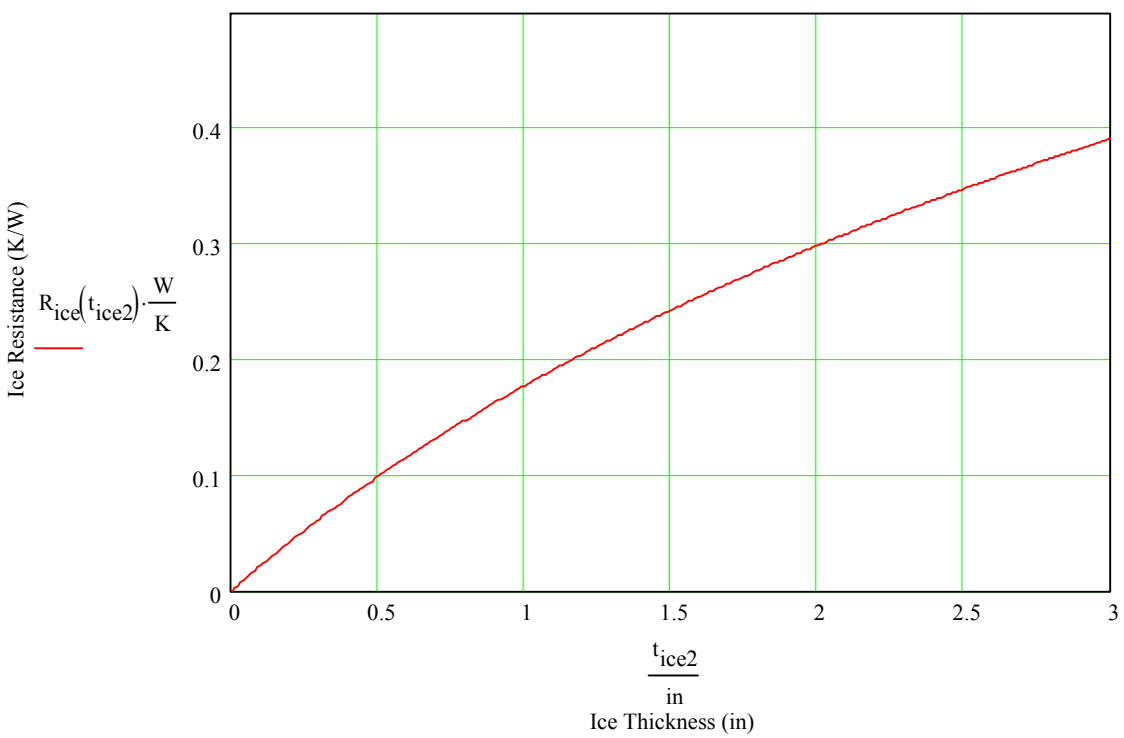

$$T_{evap}(t_{ice}) := T_{il}(S_w, P_d) - \left(Q_{h2} - Q_w(T_{il}(S_w, P_d), V_{swim2}, t_{ice})\right)\cdot\left(R_{shell} + R_{ice}(t_{ice})\right)$$

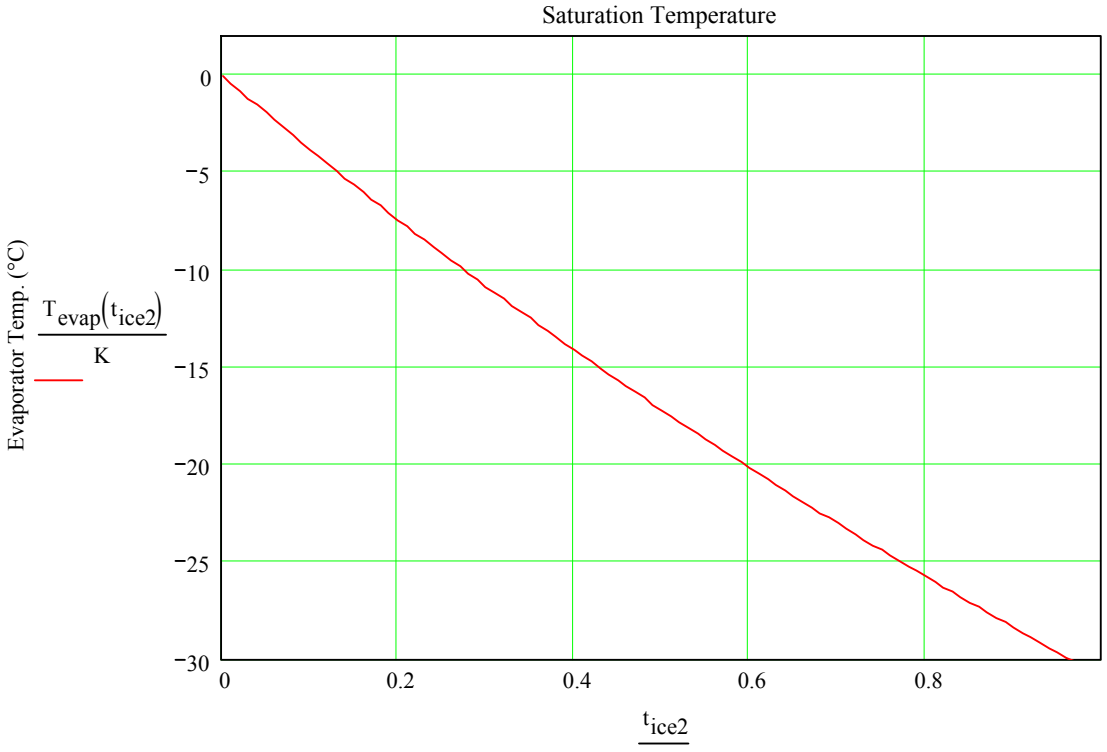

$$Time(t_{ice}) := \frac{\left[\left(d_i + 2 \cdot t_{shell} + 2 \cdot t_{ice}\right)^2 - \left(d_i + 2 \cdot t_{shell}\right)^2\right] \cdot \frac{\pi}{4} \cdot L_e \cdot L_{water} \cdot \rho_{ice}}{Q_{h2} - Q_w\left(T_{il}\left(S_w, P_d\right), V_{swim2}, t_{ice}\right)}$$

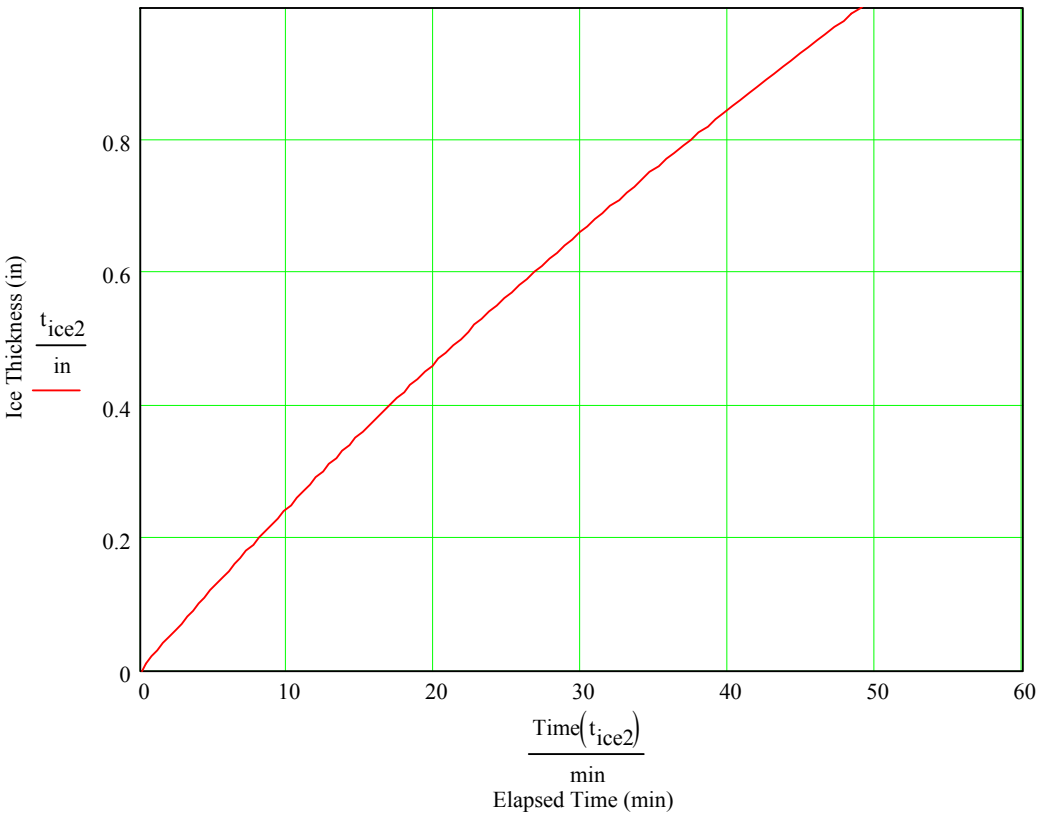

APPENDIX B: HEAT EXCHANGE MODELING

$kJ := 1000 \cdot J \qquad kPa := 1000 \cdot Pa \qquad °C := K \qquad T_{s1} := -4K$

Range of interest: 35-40°F (1.7-4.4°C)

Pure Water at 101kPa from Engineering Equation Solver 8-17°C by 1°C:

temperature thermal conductivity viscosity specific heat

$$T_w := \begin{pmatrix} 1.7 \\ 2 \\ 3 \\ 4 \\ 5 \\ 6 \\ 7 \\ 8 \\ 9 \\ 10 \\ 11 \\ 12 \\ 13 \\ 14 \\ 15 \\ 16 \\ 17 \end{pmatrix} \cdot K \qquad k_w := \begin{pmatrix} 0.551 \\ 0.5516 \\ 0.5536 \\ 0.5556 \\ 0.5576 \\ 0.5596 \\ 0.5616 \\ 0.5635 \\ 0.5655 \\ 0.5674 \\ 0.5694 \\ 0.5713 \\ 0.5732 \\ 0.5751 \\ 0.577 \\ 0.5788 \\ 0.5806 \end{pmatrix} \frac{W}{m \cdot K} \qquad \mu_w := \begin{pmatrix} 0.001691 \\ 0.001674 \\ 0.00162 \\ 0.001568 \\ 0.001519 \\ 0.001472 \\ 0.001428 \\ 0.001385 \\ 0.001345 \\ 0.001307 \\ 0.00127 \\ 0.001235 \\ 0.001201 \\ 0.001169 \\ 0.001138 \\ 0.001109 \\ 0.00108 \end{pmatrix} \frac{kg}{m \cdot s} \qquad Cp_w := \begin{pmatrix} 4.216 \\ 4.214 \\ 4.208 \\ 4.204 \\ 4.2 \\ 4.196 \\ 4.194 \\ 4.191 \\ 4.189 \\ 4.188 \\ 4.187 \\ 4.186 \\ 4.185 \\ 4.184 \\ 4.184 \\ 4.183 \\ 4.183 \end{pmatrix} \cdot \frac{J}{gm \cdot K}$$

density

$$\rho_w := \begin{pmatrix} 1000 \\ 1000 \\ 1000 \\ 1000 \\ 1000 \\ 1000 \\ 1000 \\ 1000 \\ 999.7 \\ 999.6 \\ 999.5 \\ 999.4 \\ 999.3 \\ 999.1 \\ 999 \\ 998.8 \\ 998.7 \end{pmatrix} \cdot \frac{kg}{m^3}$$

Prandtl number

$$Pr_w := \begin{pmatrix} 12.94 \\ 12.79 \\ 12.31 \\ 11.86 \\ 11.44 \\ 11.04 \\ 10.66 \\ 10.3 \\ 9.964 \\ 9.642 \\ 9.336 \\ 9.045 \\ 8.769 \\ 8.505 \\ 8.253 \\ 8.013 \\ 7.783 \end{pmatrix}$$

volumetric expansion coefficient

$$\beta_w := \begin{pmatrix} -0.000047 \\ -0.00004137 \\ -0.00002311 \\ -0.000005551 \\ 0.00001135 \\ 0.00002764 \\ 0.00004336 \\ 0.00005855 \\ 0.00007323 \\ 0.00008744 \\ 0.0001012 \\ 0.0001146 \\ 0.0001275 \\ 0.0001401 \\ 0.0001523 \\ 0.0001643 \\ 0.0001759 \end{pmatrix} \cdot \frac{1}{K}$$

$ii := 0$

$T_{amb} := T_{w_{ii}}$ $\beta_{water} := \beta_{w_{ii}}$ $k_{water} := k_{w_{ii}}$ $\rho_{water} := \rho_{w_{ii}}$

$\mu_{water} := \mu_{w_{ii}}$ $Pr_{water} := Pr_{w_{ii}}$ $Cp_{water} := Cp_{w_{ii}}$

$$\nu_{water} := \frac{\mu_{water}}{\rho_{water}} \qquad \nu_{water} = 1.691 \times 10^{-6} \frac{m^2}{s}$$

kinematic viscosity=viscous force/inertia force (density)

salt water freezing temperature:

p (bar abs)
s (ppm)

Ranges:
t = 0<20C temperature
s=0-40% salinity
p=1-1000bar abs pressure

$$T_{il}(S_w, P_d) := \left(-0.02831 - 0.0499 S_w - 0.000112 S_w^{\,2} - 0.00759 P_d\right) \cdot K$$

Fujino et al. (1974)

$S_w := 0$ $P_d := 1$ $T_{il}(S_w, P_d) = -0.036K$ $T_{il}(35,1) = -1.92K$

Properties of ice

thermal conductivity heat of sublimation density

$k_{ice} := 2.22\frac{W}{m \cdot K}$ $L_{water} := 334\frac{J}{gm}$ $\rho_{ice} := 0.9167\frac{gm}{cm^3}$

Geometric Constraints and Properties

single geometry to be evaluated

$t_{c2} := .030 \cdot in$ Channnel depth

$w2 := .275 \cdot in$ Channel width

$n_{c2} := 3$ Number of Channels

set minimum wall width to 0.015in

$$t_w(t_c) := \begin{cases} 0.015 \cdot in & \text{if } \frac{t_c}{3} < .015 \cdot in \\ \frac{t_c}{3} & \text{otherwise} \end{cases}$$ Channel wall width

$t_w(t_{c2}) = 0.015in$

$d_i := 3 \cdot in$ inside diameter of shell

$L_e := 9.79in$ .length of evaporator (accounting for non-usable ends)

$\theta(w, t_c, n_c) := \operatorname{acos}\left[\frac{n_c \cdot (w + t_w(t_c))}{\pi \cdot d_i}\right]$ $\theta(w2, t_{c2}, n_{c2}) = 84.7deg$ pitch angle

$N_s(w, t_c, n_c) := \frac{L_e \cdot \sin(\theta(w, t_c, n_c))}{n_c \cdot (w + t_w(t_c))}$ $N_s(w2, t_{c2}, n_{c2}) = 11.2$ number of sections (swirls)

$Pitch(w, t_c, n_c) := \frac{L_e}{N_s(w, t_c, n_c)}$ $Pitch(w2, t_{c2}, n_{c2}) = 0.874in$ must be 1in or less to be turned

$L_{ch}(w, t_c, n_c) := \frac{\pi \cdot d_i}{\sin(\theta(w, t_c, n_c))} \cdot N_s(w, t_c, n_c)$ $L_{ch}(w2, t_{c2}, n_{c2}) = 106.056in$ length of a channel

shell

$t_{shell} := 0.050in$ thickness of shell

$k_{al} := 167\frac{W}{m \cdot K}$ thermal conductivity of shell (6061-T6 aluminum)

$k_{shell} := k_{al}$

$$R_{shell} := \frac{\ln\left(\frac{d_i + 2t_{shell}}{d_i}\right)}{2\cdot\pi\cdot k_{shell}\cdot L_e} \qquad R_{shell} = 1.257\times 10^{-4}\,\frac{K}{W}$$ resistance of shell

ns

$N_{n2} := 57$ # of fins

$t_2 := .05in$ fin thickness

$Q2 := 45\frac{gal}{hr}$ $Q2 = 0.75\frac{gal}{min}$

$L_c := 9.79in$ length of fins

$L_f := .25in$ radial length of fins

$d_{fi} := d_i + 2t_{shell}$ inside diameter (base of fins) $d_{fi} = 3.1\,in$

$d_{fo} := d_i + 2t_{shell} + 2L_f$ outside diameter (tip of fins) $d_{fo} = 3.6in$

$\theta_f(N_n) := \frac{2\cdot\pi}{N_n}$ .angle from one fin to the next $\theta_f(N_{n2}) = 6.316deg$

$d_{ave} := \frac{d_{fo} + d_{fi}}{2}$ .average diameter

$$w_c(N_n, d, t) := \frac{d}{\tan\left(\frac{\pi - \theta_f(N_n)}{2}\right)} - t$$ distance from one fin to the next at the diameter specified $w_c(N_{n2}, d_{fi}, t_2) = 0.12$

$w(N_n, t) := w_c(N_n, d_{ave}, t)$ distance from one fin to the next at the average diameter $w(N_{n2}, t_2) = 0.135in$

$ar_f(N_n, t) := \frac{L_f}{w_c(N_n, d_{ave}, t)}$ aspect ratio of rectangular ducts $ar_f(N_{n2}, t_2) = 1.854$

$A_{flow}(N_n, t) := \frac{\pi}{4}\cdot\left(d_{fo}^{\,2} - d_{fi}^{\,2}\right) - N_n\cdot t\cdot L_f$ flow area, all ducts $A_{flow}(N_{n2}, t_2) = 1.919in^2$

Hydraulic Diameter and Aspect Ratio Effects (laminar only)

$D_h(w, t_c) := \frac{4\cdot t_c\cdot w}{2\cdot t_c + 2\cdot w}$ Hydraulic Diameter $D_{h2} := D_h(w2, t_{c2})$ $D_h(w2, t_{c2}) = 0.054$

$ar(w, t_c) := \frac{w}{t_c}$ Aspect Ratio $ar_2 := ar(w2, t_{c2})$ $ar(w2, t_{c2}) = 9.167$

aspect ratio factor for increased heat transfer and pressure drop in high aspect ratio ducts (fully deveoloped LAMINAR flow)

aspect ratio | Nusselt number (Uniform Surface Temperature | friction factor $xx := 1, 2.. 4$

$$LAM_{Dh} := \begin{pmatrix} 1 & 2.976 & 57 \\ 1.4 & 3.1 & 59 \\ 2 & 3.4 & 62 \\ 3 & 4.0 & 69 \\ 4 & 4.4 & 73 \\ 8 & 5.6 & 82 \\ 30 & 7.541 & 96 \end{pmatrix}$$

logistic curve fit

$$\begin{pmatrix} a2 \\ b2 \\ c2 \end{pmatrix} := lgsfit\left[LAM_{Dh}^{\langle 0 \rangle}, LAM_{Dh}^{\langle 1 \rangle}, \begin{pmatrix} 7.54 \\ 0.8 \\ 0.2 \end{pmatrix}\right] \qquad \begin{pmatrix} a3 \\ b3 \\ c3 \end{pmatrix} := lgsfit\left[LAM_{Dh}^{\langle 0 \rangle}, LAM_{Dh}^{\langle 2 \rangle}, \begin{pmatrix} 96 \\ 0.8 \\ 0.2 \end{pmatrix}\right]$$

$$Y_{Nu}(xx) := \frac{a2}{1 + b2 \cdot e^{-c2 \cdot xx}} \qquad Y_{Re}(xx) := \frac{a3}{1 + b3 \cdot e^{-c3 \cdot xx}}$$

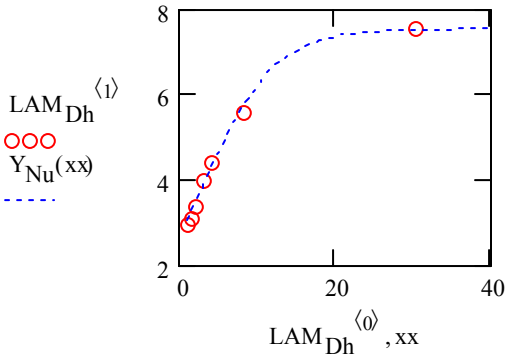

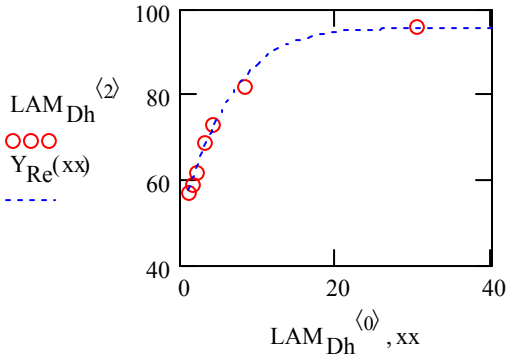

$$F_{NuAR}(w, t_c) := \frac{Y_{Nu}(ar(w, t_c))}{3.66} \qquad F_{ReAR}(w, t_c) := \frac{Y_{Re}(ar(w, t_c))}{64}$$

$F_{NuAR}(w2, t_{c2}) = 1.653$ $F_{ReAR}(w2, t_{c2}) = 1.349$

Fin channels:

$$D_{hf}(N_n, t) := \frac{4 \cdot 0.5 \cdot (w_c(N_n, d_{fi}, t) + w_c(N_n, d_{fo}, t)) \cdot L_f}{w_c(N_n, d_{fi}, t) + w_c(N_n, d_{fo}, t) + 2 \cdot L_f}$$ hydraulic diameter $D_{hf}(N_{n2}, t_2) = 0.1752in$

$$LD(N_n, t) := \frac{L_c}{D_{hf}(N_n, t)}$$ Ratio of length to diameter > 100 is "fully developed" $LD(N_{n2}, t_2) = 55.886$

$$u_{flow}(Q_f, N_n, t) := \frac{Q_f}{A_{flow}(N_n, t)}$$ flow velocity through the fins $u_{flow}(Q2, N_{n2}, t_2) = 0.0382 \frac{m}{s}$

aspect ratio factor for increased heat transfer and pressure drop in high aspect ratio ducts (fully deveoloped LAMINAR flow)

$$Nu(N_n, t) := Y_{Nu}(ar_f(N_n, t))$$ $$F_{Re}(N_n, t) := Y_{Re}(ar_f(N_n, t))$$

$Nu(N_{n2}, t_2) = 3.381$ $F_{Re}(N_{n2}, t_2) = 61.911$

$$Re(Q_f, N_n, t) := \frac{\rho_{water} \cdot u_{flow}(Q_f, N_n, t) \cdot D_{hf}(N_n, t)}{\mu_{water}}$$ Reynolds number $Re(Q2, N_{n2}, t_2) = 101$

Now account for entrance effects (again assumes laminar flow)

$$\frac{L_{ef}(5\%)}{D} \cong 0.05\,\mathrm{Re}_D \quad Mills(4.48)$$

$$\frac{L_{eh}(5\%)}{D} \cong 0.017\,\mathrm{Re}_D\,\mathrm{Pr} \quad Mills(4.49)$$

$$\overline{Nu}_D = 3.66 + \frac{0.065\frac{D}{L}\mathrm{Re}_D\,\mathrm{Pr}}{1 + 0.04\left[\frac{D}{L}\mathrm{Re}_D\,\mathrm{Pr}\right]^{\frac{2}{3}}} \quad \mathrm{Re}_D \le 2300 \quad Mills(4.50)$$

$$\frac{\bar{f}}{f} = 1 + \frac{0.0533\frac{D}{L}\mathrm{Re}_D}{1 + 0.083\left[\frac{D}{L}\mathrm{Re}_D\right]^{\frac{2}{3}}} \quad \mathrm{Re}_D \le 2300 \quad Estimated$$

$$\Delta P(Q_f, N_n, t) := F_f(Q_f, N_n, t) \cdot \frac{F_{Re}(N_n, t)}{Re(Q_f, N_n, t)} \cdot \rho_{water} \cdot \frac{u_{flow}(Q_f, N_n, t)^2}{2} \cdot \frac{L_c}{D_{hf}(N_n, t)}$$

pressure drop through the duct (laminar)

$\Delta P(Q2, N_{n2}, t_2) = 26\,Pa$

$\Delta P(Q2, N_{n2}, t_2) = 0.004\,psi$

dummy impeller curve:

$$P_{pr1}(Q_f) := \left(900 - 2 \cdot Q_f \frac{hr}{gal}\right) \cdot Pa$$

Guess $Q_f := 1 \cdot \frac{gal}{hr}$ laminar velocity, using complete fan curve $ff_2 :=$

Given $P_{pr1}(Q_f) = \Delta P(Q_f, N_n, t)$ $QQ(N_n, t, ff) := Find(Q_f)$

$QQ(N_{n2}, t_2, ff_2) = 5.485 \frac{gal}{min}$ $\frac{1}{64} = 0.016$

$QQ(N_n, t, ff) := 4 \frac{gal}{min}$

$Re(QQ(N_{n2}, t_2, ff_2), N_{n2}, t_2) = 536$

$\Delta P_L(N_n, t, ff) := \Delta P(QQ(N_n, t, ff), N_n, t)$ $\Delta P_L(N_{n2}, t_2, ff_2) = 164.928 Pa$

$h(N_n, t, ff) := \frac{F_{Nu}(QQ(N_n, t, ff), N_n, t) \cdot Nu(N_n, t) \cdot k_{water}}{D_{hf}(N_n, t)}$ heat transfer coefficient $h(N_{n2}, t_2, ff_2) = 1.563 \times 10^3$

$m_a(N_n, t, ff) := \sqrt{\frac{2 \cdot h(N_n, t, ff)}{k_{al} \cdot t}}$ fin efficiency coefficient

$\eta_{fin}(N_n, t, ff) := \frac{\tanh[m_a(N_n, t, ff) \cdot (L_f + 0.5 \cdot t)]}{m_a(N_n, t, ff) \cdot (L_f + 0.5 \cdot t)}$ fin efficiency (function is for h applied to all sides of fin, but not end tip area

$\eta_{fin}(N_{n2}, t_2, ff_2) = 0.814$

$A_{Ht}(N_n, t, ff) := (d_i \cdot \pi - t \cdot N_n) \cdot L_e + 2 \cdot (L_f \cdot L_e) \cdot N_n \cdot \eta_{fin}(N_n, t, ff)$ total heat transfer area

$hA(N_n, t, ff) := h(N_n, t, ff) \cdot A_{Ht}(N_n, t, ff)$ $hA(N_{n2}, t_2, ff_2) = 293.782 \frac{W}{K}$

$WK(N_n, t, ff) := \rho_{water} \cdot Cp_{water} \cdot QQ(N_n, t, ff) \cdot \left(1 - e^{\frac{-hA(N_n, t, ff)}{\rho_{water} \cdot Cp_{water} \cdot QQ(N_n, t, ff)}}\right)$

Watts per K (Laminar)

$1.7K \cdot WK(N_{n2}, t_2, ff_2) = 436.409 W$ $WK(N_{n2}, t_2, ff_2) = 256.711 \frac{W}{K}$

Now optimize the design based on number of fins for impeller

$$NN := \begin{pmatrix} 10 \\ 15 \\ 20 \\ 25 \\ 30 \\ 35 \\ 40 \\ 50 \\ 60 \\ 70 \\ 80 \\ 90 \\ 100 \end{pmatrix} \qquad tt := \begin{pmatrix} .006 \\ .010 \\ .020 \\ .030 \\ .040 \\ .050 \\ .060 \\ .070 \end{pmatrix} \cdot in \qquad NN := \begin{pmatrix} 142 \\ 144 \\ 146 \\ 148 \\ 152 \\ 154 \\ 156 \\ 158 \end{pmatrix}$$

$OUTPUT :=$ for $ii \in 0..rows(NN) - 1$

for $jj \in 0..rows(tt) - 1$

$k \leftarrow ii \cdot rows(tt) + jj$

$QQQ \leftarrow QQ\left(NN_{ii}, tt_{jj}, ff_2\right)$

$DP \leftarrow \Delta P\left(QQQ, NN_{ii}, tt_{jj}\right)$

$RE \leftarrow Re\left(QQQ, NN_{ii}, tt_{jj}\right)$

$$hh \leftarrow \frac{F_{Nu}\left(QQQ, NN_{ii}, tt_{jj}\right) \cdot Nu\left(NN_{ii}, tt_{jj}\right) \cdot k_{water}}{D_{hf}\left(NN_{ii}, tt_{jj}\right)}$$

$$\theta f \leftarrow \frac{2\pi}{NN_{ii}}$$

$$df \leftarrow \tan(\theta f) \cdot \frac{d_{ave}}{2} - tt_{jj}$$

$$z \leftarrow \sqrt{\frac{2 \cdot hh}{k_{al} \cdot tt_{jj}}}$$

$$\eta_f \leftarrow \frac{\tanh\left[z \cdot \left(L_f + 0.5 \cdot tt_{jj}\right)\right]}{z \cdot \left(L_f + 0.5 \cdot tt_{jj}\right)}$$

$$hhA \leftarrow hh \cdot \left[\left(d_{fi} \cdot \pi - tt_{jj} \cdot NN_{ii}\right) \cdot L_c + 2 \cdot \left(L_f \cdot L_c\right) \cdot NN_{ii} \cdot \eta_f\right]$$

$$WWK \leftarrow \rho_{water} \cdot Cp_{water} \cdot QQQ \cdot \left(1 - e^{\frac{-hhA}{\rho_{water} \cdot Cp_{water} \cdot QQQ}}\right)$$

$FW \leftarrow DP \cdot QQQ$

$ANS_{k,0} \leftarrow \frac{d_{fi}}{in}$

$ANS_{k,1} \leftarrow \frac{d_{fo}}{in}$

$ANS_{k,2} \leftarrow \frac{L_c}{in}$

$ANS_{k,3} \leftarrow \frac{tt_{jj}}{in}$

$ANS_{k,4} \leftarrow NN_{ii}$

$ANS_{k,5} \leftarrow \frac{L_f}{in}$

$ANS_{k,6} \leftarrow \frac{DP}{Pa}$

$ANS_{k,7} \leftarrow QQQ \cdot \frac{hr}{gal}$

$ANS_{k,8} \leftarrow RE$

$ANS_{k,9} \leftarrow \eta_f$

$ANS_{k,10} \leftarrow hhA \cdot \frac{K}{W}$

$ANS_{k,11} \leftarrow WWK \cdot \frac{K}{W}$

$ANS_{k,12} \leftarrow \frac{FW}{W}$

$ANS_{k,13} \leftarrow \frac{df}{in}$

ANS

R-134a properties (pressure is absolute)

$P_{sat\_evap} := 26psi + 1atm$ $P_{sat\_evap} = 280.589kPa$ evap inlet pressure (guess)

$P_{cr} := 4059 \cdot kPa$

Curve fits from data in EES:

Reference:W:\Archive\Reference\R134a.mcd

R134a good from 130 to 330kPa abs

$$T_{satf}(P_{sat}) := \left[-0.0002\left(\frac{P_{sat}}{kPa}\right)^2 + 0.2115\frac{P_{sat}}{kPa} - 44.237\right]\cdot K \qquad T_{satf}(P_{sat\_evap}) = -0.638K$$

R134a Equations good for Tsat from -10 to 14C

evaporator outlet enthalpy:

$$h_{SH}(P_{evap\_out}, SH) := \left[\left(-1.3244310^{-6}\cdot\frac{SH}{K} - 0.000168105\right)\cdot\left(\frac{P_{evap\_out}}{kPa}\right)^2 + \left(0.000732491\frac{SH}{K} + 0.\right.\right.$$

$$h_{SH}(200kPa, 5K) = 248.736\frac{kJ}{kg}$$

condenser outlet enthalpy:

$$h_{SC}(P_{cond}, SC) := \left[\left(-0.000176829\frac{SC}{K} + 0.059394193\right)\cdot\frac{P_{cond}}{kPa} + \left(-1.279660755\frac{SC}{K} + 47.80158682\right)\right]\cdot\frac{1}{k}$$

$$h_{SC}(800kPa, 1K) = 93.896\frac{kJ}{kg}$$

$$P_{sat}(T) := \left[0.16250\left(\frac{T}{K}\right)^2 + 10.56214\frac{T}{K} + 293.01429\right]\cdot kPa$$ saturation pressure

$$Cp_f(T_{sat}) := \left(0.0028\frac{T_{sat}}{K} + 1.342\right)\cdot\frac{kJ}{kg\cdot K}$$ saturated liquid specific heat

$$Cp_g(T_{sat}) := \left(0.0046\frac{T_{sat}}{K} + 0.897\right)\cdot\frac{kJ}{kg\cdot K}$$ saturated vapor specific heat

$$k_f(T_{sat}) := \left(-0.000433\frac{T_{sat}}{K} + 0.094565\right)\cdot\frac{W}{m\cdot K}$$ saturated liquid thermal conductivity

$$k_g(T_{sat}) := \left(0.000098\frac{T_{sat}}{K} + 0.012099\right)\cdot\frac{W}{m\cdot K}$$ saturated vapor thermal conductivity

$$h_f(T_{sat}) := \left(1.3496\frac{T_{sat}}{K} + 51.926\right)\cdot\frac{kJ}{kg}$$ saturated liquid enthalpy

$$h_g(T_{sat}) := \left(0.5791\cdot\frac{T_{sat}}{K} + 250.4\right)\cdot\frac{kJ}{kg}$$ saturated vapor enthalpy

$$h_{fg}(T_{sat}) := \left(-0.7736\frac{T_{sat}}{K} + 198.46\right)\cdot\frac{kJ}{kg}$$ enthalpy of vaporization

$$\mu_f(T_{sat}) := \left(-3.30810^{-6}\cdot\frac{T_{sat}}{K} + 0.000266885\right)\cdot\frac{kg}{m\cdot s}$$ saturated liquid viscosity

$\mu_g := EES("viscosity", "P", P_{sat\_evap}, "X", 1)$ saturated vapor viscosity

$Pr_f(T_{sat}) := -0.0224 \frac{T_{sat}}{K} + 3.7769$ saturated liquid Prandtl number

$Pr_g(T_{sat}) := 0.0007 \frac{T_{sat}}{K} + 0.8099$ saturated vapor Prandtl number

$\rho_f(T_{sat}) := \left(-3.3324 \frac{T_{sat}}{K} + 1294.4\right) \cdot \frac{kg}{m^3}$ saturated liquid density

$\rho_g(T_{sat}) := \left(0.5385 \frac{T_{sat}}{K} + 14.812\right) \cdot \frac{kg}{m^3}$ saturated vapor density

$\nu_f(T_{sat}) := \frac{1}{\rho_f(T_{sat})}$ saturated liquid specific volume

$\nu_g(T_{sat}) := \frac{1}{\rho_g(T_{sat})}$ saturated vapor specific volume

$\sigma_{sat}(T_{sat}) := \left(-0.000143 \frac{T_{sat}}{K} + 0.011571\right) \cdot \frac{N}{m}$ saturated liquid surface tension

Evaporator Heat Load requirements and Condensing Pressure

$Q_{h2} := 200W$

$Super := 2 \cdot K$ superheat of evaporator outlet gas

$Subcool := 4 \cdot K$ subcooling of liquid coming out of condenser

$P_{cond} := 125psi + 1atm$ condenser pressure

expansion valve enthalpy:

$h_{exp} := h_{SC}(P_{cond}, Subcool)$

evaporator outlet enthalpy:

$h_{evap\_out}(P_{sat}) := h_{SH}(P_{sat}, Super)$

evaporator entrance quality:

$x_{entr}(T_{sat}, P_{out}) := \frac{h_{exp} - h_f(T_{sat})}{h_{evap\_out}(P_{out}) - h_f(T_{sat})}$ $x_{entr}(0K, P_{sat}(0K)) = 0.236$

$$mdot(Q_h, P_{evap\_out}) := \frac{Q_h}{h_{evap\_out}(P_{evap\_out}) - h_{exp}}$$

$$m_{dot2} := mdot(Q_{h2}, P_{sat\_evap}) \qquad m_{dot2} = 1.311\frac{gm}{s}$$

Mass flux and velocities

$$G(m_{dot}, w, t_c, n_c) := \frac{m_{dot}}{w \cdot t_c \cdot n_c}$$ Mass flux $$G(m_{dot2}, w2, t_{c2}, n_{c2}) = 82.104\frac{kg}{m^2 s}$$

Pure Liquid and Pure Vapor Velocities

$$V_{vap}(m_{dot}, w, t_c, n_c, T_{sat}) := \frac{G(m_{dot}, w, t_c, n_c)}{\rho_g(T_{sat})} \qquad V_{liq}(m_{dot}, w, t_c, n_c, T_{sat}) := \frac{G(m_{dot}, w, t_c, n_c)}{\rho_f(T_{sat})}$$

$$V_{vap}(m_{dot2}, w2, t_{c2}, n_{c2}, T_{test}) = 5.675\frac{m}{s} \qquad V_{liq}(m_{dot2}, w2, t_{c2}, n_{c2}, T_{test}) = 0.063\frac{m}{s}$$

$$Re_f(m_{dot}, x, w, t_c, n_c, T_{sat}) := \frac{G(m_{dot}, w, t_c, n_c) \cdot (1 - x) \cdot D_h(w, t_c)}{\mu_f(T_{sat})}$$ Liquid Reynolds Number

$$Re_g(m_{dot}, x, w, t_c, n_c) := \frac{G(m_{dot}, w, t_c, n_c) \cdot x \cdot D_h(w, t_c)}{\mu_g}$$ Vapor Reynolds Number

$x := 0, 0.$

$Re_f(m_{dot2}, x, w2, t_{c2}, n_{c2}, T_{test})$

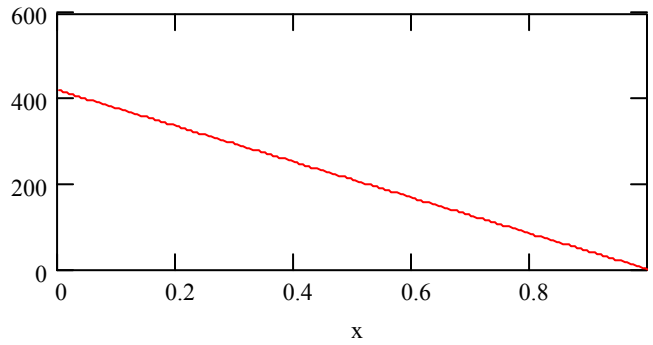

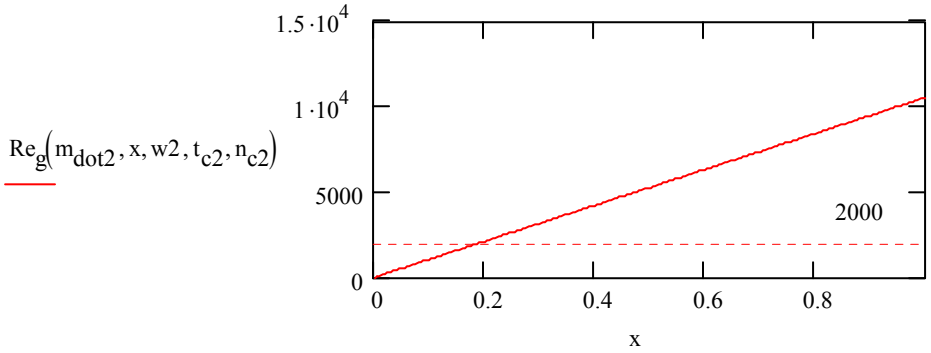

$Re_{g2} := Re_g(m_{dot2}, 1, w2, t_{c2}, n_{c2})$ $Re_{g2} = 10544$

$Re_{f2} := Re_f(m_{dot2}, 0, w2, t_{c2}, n_{c2}, T_{test})$ $Re_{f2} = 419.407$

Pressure Drop Correlation

Pressure drop correlation from Carey (pp 420-421, (403-404))

$$B_f(m_{dot}, x, w, t_c, n_c, T_{sat}) := \begin{cases} 16 & \text{if } Re_f(m_{dot}, x, w, t_c, n_c, T_{sat}) < 2000 \\ 0.079 & \text{otherwise} \end{cases}$$

$$n_f(m_{dot}, x, w, t_c, n_c, T_{sat}) := \begin{cases} 1 & \text{if } Re_f(m_{dot}, x, w, t_c, n_c, T_{sat}) < 2000 \\ 0.25 & \text{otherwise} \end{cases}$$ friction factor relationships

$$B_g(m_{dot}, x, w, t_c, n_c) := \begin{cases} 16 & \text{if } Re_g(m_{dot}, x, w, t_c, n_c) < 2000 \\ 0.079 & \text{otherwise} \end{cases}$$

$$n_g(m_{dot}, x, w, t_c, n_c) := \begin{cases} 1 & \text{if } Re_g(m_{dot}, x, w, t_c, n_c) < 2000 \\ 0.25 & \text{otherwise} \end{cases}$$

Martinelli Parameter

$$X(m_{dot}, x, w, t_c, n_c, T_{sat}) := \left[\frac{B_f(m_{dot}, x, w, t_c, n_c, T_{sat}) \cdot Re_f(m_{dot}, x, w, t_c, n_c, T_{sat})^{-n_f(m_{dot}, x, w, t_c, n_c, T}}{B_g(m_{dot}, x, w, t_c, n_c) \cdot Re_g(m_{dot}, x, w, t_c, n_c)^{-n_g(m_{dot}, x, w, t_c, n_c)}} \right.$$

pg 404

$$C(m_{dot}, x, w, t_c, n_c, T_{sat}) := \begin{cases} 20 & \text{if } \left(Re_f(m_{dot}, x, w, t_c, n_c, T_{sat}) \geq 2000 \wedge Re_g(m_{dot}, x, w, t_c, n_c) \geq 2000\right) \\ 12 & \text{if } \left(Re_f(m_{dot}, x, w, t_c, n_c, T_{sat}) < 2000 \wedge Re_g(m_{dot}, x, w, t_c, n_c) \geq 2000\right) \\ 10 & \text{if } Re_f(m_{dot}, x, w, t_c, n_c, T_{sat}) \geq 2000 \wedge Re_g(m_{dot}, x, w, t_c, n_c) < 2000 \\ 5 & \text{otherwise} \end{cases}$$

$$\phi_f(m_{dot}, x, w, t_c, n_c, T_{sat}) := \sqrt{1 + \frac{C(m_{dot}, x, w, t_c, n_c, T_{sat})}{X(m_{dot}, x, w, t_c, n_c, T_{sat})} + \frac{1}{X(m_{dot}, x, w, t_c, n_c, T_{sat})^2}}$$

$$\phi_g(m_{dot}, x, w, t_c, n_c, T_{sat}) := \sqrt{1 + C(m_{dot}, x, w, t_c, n_c, T_{sat}) \cdot X(m_{dot}, x, w, t_c, n_c, T_{sat}) + X(m_{dot}, x, w, t_c}$$

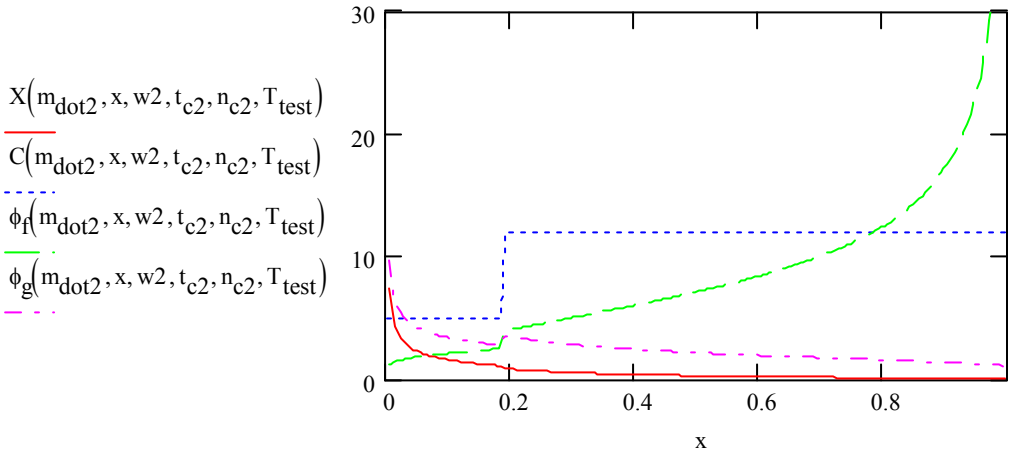

$$H_{L2\phi}(m_{dot}, x, w, t_c, n_c, T_{sat}) := \phi_f(m_{dot}, x, w, t_c, n_c, T_{sat})^2 \cdot 2 \cdot \frac{B_f(m_{dot}, x, w, t_c, n_c, T_{sat}}{\left[\frac{G(m_{dot}, w, t_c, n_c) \cdot (1 - x) \cdot D_h(w, t_c)}{\mu_f(T_{sat})}\right]^{n_f(m_{dot}, w, t_c, n_c)}} \cdot \rho_f(T_{sat}$$

$$f_{fO}(m_{dot}, w, t_c, n_c, T_{sat}) := \begin{cases} 0.046 \left(\frac{G(m_{dot}, w, t_c, n_c) \cdot D_h(w, t_c)}{\mu_f(T_{sat})}\right)^{-0.2} & \text{if } \frac{G(m_{dot}, w, t_c, n_c) \cdot D_h(w, t_c)}{\mu_f(T_{sat})} \\ \frac{16}{\frac{G(m_{dot}, w, t_c, n_c) \cdot D_h(w, t_c)}{\mu_f(T_{sat})}} \cdot F_{ReAR}(w, t_c) & \text{otherwise} \end{cases}$$

$$f_{gO}(m_{dot}, w, t_c, n_c) := \begin{cases} 0.046 \left(\frac{G(m_{dot}, w, t_c, n_c) \cdot D_h(w, t_c)}{\mu_g}\right)^{-0.2} & \text{if } \frac{G(m_{dot}, w, t_c, n_c) \cdot D_h(w, t_c)}{\mu_g} > 2(\\ \frac{16}{\frac{G(m_{dot}, w, t_c, n_c) \cdot D_h(w, t_c)}{\mu_g}} \cdot F_{ReAR}(w, t_c) & \text{otherwise} \end{cases}$$

$$H_{Lf}(m_{dot}, w, t_c, n_c, T_{sat}) := 2 \cdot f_{fO}(m_{dot}, w, t_c, n_c, T_{sat}) \cdot \frac{G(m_{dot}, w, t_c, n_c)^2}{D_h(w, t_c) \cdot \rho_f(T_{sat})} \cdot \begin{cases} F_{ReAR}(w2, t_{c2}) & \text{if } \frac{G(m_{dot}, w, t_c, n_c) \cdot D_h(w, t_c)}{\mu_f(T_{sat})} < 2000 \\ 1 & \text{otherwise} \end{cases}$$

$$H_{Lf}(m_{dot2}, w2, t_{c2}, n_{c2}, T_{test}) = 0.023 \frac{psi}{ft}$$

$$H_{Lg}(m_{dot}, w, t_c, n_c, T_{sat}) := 2 \cdot f_{gO}(m_{dot}, w, t_c, n_c) \cdot \frac{G(m_{dot}, w, t_c, n_c)^2}{D_h(w, t_c) \cdot \rho_g(T_{sat})} \cdot \begin{cases} F_{ReAR}(w2, t_{c2}) & \text{if } \frac{G(m_{dot}, w, t_c, n_c) \cdot D_h(w, t_c)}{\mu_g} < 2000 \\ 1 & \text{otherwise} \end{cases}$$

$$H_{Lg}(m_{dot2}, w2, t_{c2}, n_{c2}, T_{test}) = 0.216 \frac{psi}{ft}$$

$$H_L(m_{dot}, x, w, t_c, n_c, T_{sat}) := \begin{cases} H_{Lf}(m_{dot}, w, t_c, n_c, T_{sat}) & \text{if } x \le 0 \\ H_{Lg}(m_{dot}, w, t_c, n_c, T_{sat}) & \text{if } x \ge 1 \\ H_{L2\phi}(m_{dot}, x, w, t_c, n_c, T_{sat}) & \text{otherwise} \end{cases}$$

$$H_{Lg} = 2 \cdot f_{gO} \cdot \frac{G^2}{D_h \cdot \rho_g} \cdot \begin{cases} F_{Re} \\ 1 \quad ot \end{cases}$$

Superheated Vapor Heat Transfer:

$$f(m_{dot}, x, w, t_c, n_c) := \begin{cases} \frac{64}{Re_g(m_{dot}, x, w, t_c, n_c)} & \text{if } Re_g(m_{dot}, x, w, t_c, n_c) \le 2300 \\ (0.790 \ln(Re_g(m_{dot}, x, w, t_c, n_c)) - 1.64)^{-2} & \text{otherwise} \end{cases}$$

friction factor pg438-9

Gnielinski pg460
0.5<Pr<2000
3000<Re<5*10^6

$$f(m_{dot2}, 1, w2, t_{c2}, n_{c2}) = 0.031$$

$$Nu_g(m_{dot}, x, w, t_c, n_c, T_{sat}) := \begin{cases} 0.023 \cdot Re_g(m_{dot}, 1, w, t_c, n_c)^{0.8} \cdot Pr_g(T_{sat})^{0.4} & \text{if } Re_g(m_{dot}, 1, w, t_c, n_c) \ge 2300 \\ Y_{Nu}(ar(w, t_c)) & \text{otherwise} \end{cases}$$

$$h_{g\_conv}(m_{dot}, x, w, t_c, n_c, T_{sat}) := \frac{k_g(T_{sat})}{D_h(w, t_c)} \cdot Nu_g(m_{dot}, x, w, t_c, n_c, T_{sat})$$

2-phase Heat Transfer (Chen) pg513 Carey

Dittus - Boelter

$$h_{f\_conv}(m_{dot}, x, w, t_c, n_c, T_{sat}) := 0.023 \left(\frac{k_f(T_{sat})}{D_h(w, t_c)} \right) Re_f(m_{dot}, x, w, t_c, n_c, T_{sat})^{0.8} \cdot Pr_f(T_{sat})^{0.4}$$

turbulent-turbulent Lockhart Martinelli parameter

$$X_{tt}(x, T_{sat}) := \left(\frac{\rho_g(T_{sat})}{\rho_f(T_{sat})} \right)^{0.5} \cdot \left(\frac{\mu_f(T_{sat})}{\mu_g} \right)^{0.1} \cdot \left(\frac{1.0000001 - x}{x + 0.0000001} \right)^{0.9}$$

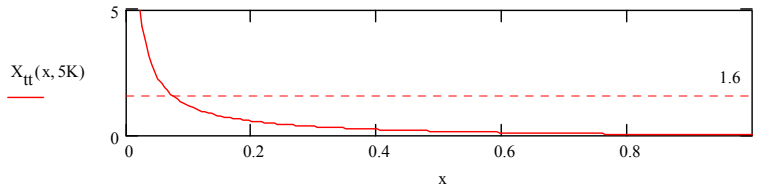

$$F_{Xtt}(x, T_{sat}) := \begin{cases} 1 & \text{if } X_{tt}(x, T_{sat})^{-1} \le 0.1 \\ 2.35 \left(0.213 + \frac{1}{X_{tt}(x, T_{sat})} \right)^{0.736} & \text{otherwise} \end{cases}$$

$$x_{test} := x_{entr}(0K, P_{sat}(0K))$$

$$F_{Xtt}(x_{test}, 5K) = 4.444$$

$$h_{mac}(m_{dot}, x, w, t_c, n_c, T_{sat}) := h_{f\_conv}(m_{dot}, x, w, t_c, n_c, T_{sat}) \cdot F_{Xtt}(x, T_{sat}) \cdot Pr_f(T_{sat})^{0.296}$$

$$h_{mac}(m_{dot2}, x_{test}, w2, t_{c2}, n_{c2}, 5K) = 1817 \frac{W}{m^2 K}$$

$$X_o(T_{sat}) := .041 \left[\frac{\sigma_{sat}(T_{sat})}{g \cdot (\rho_f(T_{sat}) - \rho_g(T_{sat}))} \right]^{0.5} \qquad X_o(T_{test}) = 3.949 \times 10^{-5} \, m$$

$$S_{hx}(m_{dot}, x, w, t_c, n_c, T_{sat}) := \frac{1 - \exp\left(-F_{Xtt}(x, T_{sat}) \cdot h_{f\_conv}(m_{dot}, x, w, t_c, n_c, T_{sat}) \cdot \frac{X_o(T_{sat})}{k_f(T_{sat})} \right)}{F_{Xtt}(x, T_{sat}) \cdot h_{f\_conv}(m_{dot}, x, w, t_c, n_c, T_{sat}) \cdot \frac{X_o(T_{sat})}{k_f(T_{sat})}}$$

$$h_{mic}(m_{dot}, x, w, t_c, n_c, T_{wall}, P_{act}, T_{sat}) := S_{hx}(m_{dot}, x, w, t_c, n_c, T_{sat}) \cdot 0.00122 \left(\frac{k_f(T_{sat})^{0.79} \cdot Cp_f(T_{sat})^{0.45} \cdot \rho_f(T_{sat})}{\sigma_{sat}(T_{sat})^{0.5} \cdot \mu_f(T_{sat})^{0.29} \cdot h_{fg}(T_{sat})^{0.24} \cdot \rho \right.$$

$$h_{2p}(m_{dot}, x, w, t_c, n_c, T_{wall}, P_{act}, T_{sat}) := h_{mac}(m_{dot}, x, w, t_c, n_c, T_{sat}) + h_{mic}(m_{dot}, x, w, t_c, n_c, T_{wall}, P_{act}, T_{sat})$$

$$h_{ch}(m_{dot}, x, w, t_c, n_c, T_{wall}, P_{act}, T_{sat}) := \begin{cases} h_{g\_conv}(m_{dot}, 1, w, t_c, n_c, T_{sat}) & \text{if } x \geq 0.999 \\ h_{2p}(m_{dot}, x, w, t_c, n_c, T_{wall}, P_{act}, T_{sat}) & \text{otherwise} \end{cases}$$

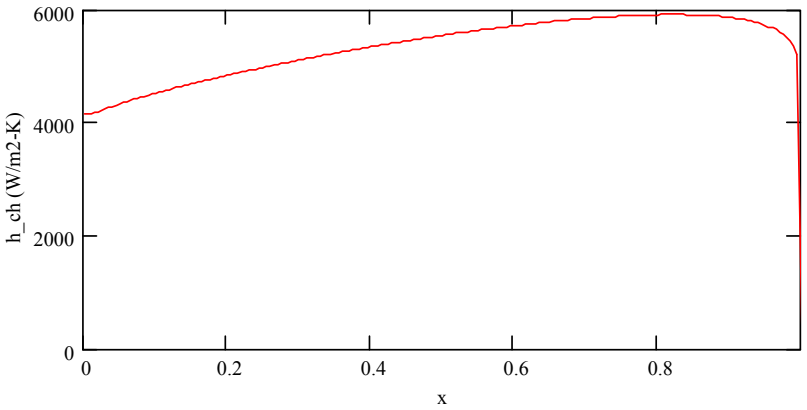

Heat Transfer:

$$q = \frac{T_{amb} - T_{ref}}{\frac{1}{h_{ref} \cdot \pi \cdot D_o \cdot L_1} + \frac{\ln\left(\frac{D_{sur}}{D_o}\right)}{\pi \cdot k_{al} \cdot L_1} + \frac{1}{h_{water} \cdot \pi \cdot D_{sur} \cdot L_1}}$$

pg107 DeWitt

$$QQ(N_{n2}, t_2, ff_2) = 4 \frac{gal}{min}$$

$nn := 400$

$$
\begin{aligned}
&OUT(w, t_c, n_c, Q_h) := \\
&\quad T_{sea_0} \leftarrow T_{amb} - \frac{Q_h}{\rho_{water} \cdot Cp_{water} \cdot QQ(N_{n2}, t_2, ff_2)} \\
&\quad T_{sat\_init_0} \leftarrow T_{sea_0} - Super - 1K \\
&\quad T_{in_0} \leftarrow T_{sat\_init_0} + Super \\
&\quad P_{in_0} \leftarrow P_{sat}\left(T_{sat\_init_0}\right) \\
&\quad \Delta Z \leftarrow \frac{L_{ch}(w, t_c, n_c)}{nn} \\
&\quad \text{for } iter \in 0..10 \\
&\qquad T_{134_0} \leftarrow T_{sat\_init_{iter}} + Super \\
&\qquad T_{sat_0} \leftarrow T_{sat\_init_{iter}} \\
&\qquad P_{sat\_init_{iter}} \leftarrow P_{sat}\left(T_{sat\_init_{iter}}\right) \\
&\qquad P_0 \leftarrow P_{sat\_init_{iter}} \\
&\qquad x_0 \leftarrow 1 \\
&\qquad m_{dot_{iter}} \leftarrow mdot\left(Q_h, P_{sat\_init_{iter}}\right) \\
&\qquad Z_0 \leftarrow 0 \cdot in \\
&\qquad \Delta P_0 \leftarrow 0 \cdot psi \\
&\qquad Q_0 \leftarrow 0 \cdot W \\
&\qquad T_{w_0} \leftarrow \frac{T_{134_0} + T_{sea_0}}{2} \\
&\qquad \text{for } j \in 1..nn \\
&\qquad\quad R_{134_j} \leftarrow \frac{1}{w \cdot L_{ch}(w, t_c, n_c) \cdot n_c \cdot h_{ch}\left(m_{dot_{iter}}, x_{j-1}, w, t_c, n_c, T_{w_{j-1}}, P_{j-1}, T_{sat_{j-1}}\right)} \\
&\qquad\quad R_{w_j} \leftarrow \frac{1}{hA(N_{n2}, t_2, ff_2)}
\end{aligned}
$$

$$T_{w_j} \leftarrow \frac{T_{sea_{j-1}} \cdot R_{134_j} + T_{sea_{j-1}} \cdot R_{shell} + T_{134_{j-1}} \cdot R_{w_j}}{R_{134_j} + R_{shell} + R_{w_j}}$$

$$\Delta Q_j \leftarrow \frac{T_{w_j} - T_{134_{j-1}}}{\frac{1}{h_{ch}\left(m_{dot_{iter}}, x_{j-1}, w, t_c, n_c, T_{w_j}, P_{j-1}, T_{sat_{j-1}}\right) \cdot w \cdot n_c \cdot \Delta Z} + \frac{\ln\left(\frac{d_i + 2 \cdot t_{shell}}{d_i}\right)}{2 \cdot \pi \cdot k_{shell} \cdot \Delta Z \cdot \cos\left(\theta\left(w, t_c, n_c\right)\right)}}$$

$$\Delta x \leftarrow \frac{\Delta Q_j}{h_{fg}\left(T_{sat_{j-1}}\right) \cdot m_{dot_{iter}}}$$

$$H_L \leftarrow H_L\left(m_{dot_{iter}}, x_{j-1}, w, t_c, n_c, T_{sat_{j-1}}\right)$$

$$\Delta P_j \leftarrow H_L \cdot \Delta Z$$

$$Z_j \leftarrow Z_{j-1} + \Delta Z$$

$$T_{sea_j} \leftarrow T_{sea_{j-1}} + \frac{\Delta Q_j}{QQ\left(N_{n2}, t_2, ff_2\right) \cdot \rho_{water} \cdot Cp_{water}}$$

$$Q_j \leftarrow Q_{j-1} + \Delta Q_j$$

$$P_j \leftarrow P_{j-1} + \Delta P_j$$

$$T_{sat_j} \leftarrow T_{satf}\left(P_j\right)$$

if $x_{j-1} \geq 1$

$$x_j \leftarrow 1$$

$$T_{134_j} \leftarrow T_{134_{j-1}} - \frac{\Delta Q_j}{m_{dot_{iter}} \cdot Cp_g\left(T_{sat_{j-1}}\right)}$$

if $T_{134_j} \leq T_{sat_j}$

$$x_j \leftarrow 0.998$$

$$T_{134_j} \leftarrow T_{sat_j}$$

$T134_j \leftarrow T_{sat_j}$

$T134_j \leftarrow T_{w_j}$ if $T134_j \geq T_{w_j}$

otherwise

$x_j \leftarrow x_{j-1} - \Delta x$

$x_j \leftarrow 0.1$ if $x_j < 0.1$

$T134_j \leftarrow T_{sat_j}$

$T134_j \leftarrow T_{w_j}$ if $T134_j \geq T_{w_j}$

$Q_{out_{iter}} \leftarrow Q_{nn}$

$P_{in_{iter+1}} \leftarrow P_{nn}$

$T_{in_{iter+1}} \leftarrow T134_j$

break if $\frac{|Q_{nn} - Q_h|}{Q_h} < 2 \cdot \% \wedge iter > 0$

$$LMTD_{iter} \leftarrow \frac{\left(T_{sea_{nn}} - T_{sat_{nn}}\right) - \left(T_{sea_0} - T_{sat_0}\right)}{\ln\left(\frac{|T_{sea_{nn}} - T_{sat_{nn}}|}{|T_{sea_0} - T_{sat_0}|}\right)}$$

$$UA_{iter} \leftarrow \frac{Q_{nn}}{LMTD_{iter}}$$

$f_1 \leftarrow Q_{nn} - Q_h$

$$df_1 \leftarrow \frac{-UA_{iter}}{\ln\left(\frac{|T_{sea_{nn}} - T_{sat_{nn}}|}{|T_{sea_0} - T_{sat_0}|}\right)} + UA_{iter} \cdot \frac{T_{sea_{nn}} - T_{sat_{nn}} - T_{sea_0} + T_{sat_0}}{\ln\left(\frac{|T_{sea_{nn}} - T_{sat_{nn}}|}{|T_{sea_0} - T_{sat_0}|}\right)^2 \cdot \left(T_{sea_{nn}} - T_{sat_{nn}}\right)}$$

$$T_{guess} \leftarrow T_{sat_0} - \frac{f_1}{df_1}$$

$$T_{guess} \leftarrow T_{sea_0} - 1 \cdot K \text{ if } T_{guess} \geq T_{sea_0} - 1K$$

$$T_{guess} \leftarrow -10 \cdot K \text{ if } T_{guess} < -10 \cdot K$$

$$T_{sat\_init_{iter+1}} \leftarrow T_{guess}$$

$$T_{w_0} \leftarrow T_{w_1}$$

$$R_{134_0} \leftarrow R_{134_1}$$

$$\begin{pmatrix} R_{134} \cdot \frac{W}{K} \\ \frac{T_{sat\_init}}{K} \\ \frac{Q_{out}}{W} \\ \frac{Z}{in} \\ x \\ \frac{\Delta P}{psi} \\ \frac{T_{134}}{K} \\ \frac{T_{sat}}{K} \\ \frac{T_{sea}}{K} \\ \frac{Q}{W} \\ \frac{T_w}{K} \end{pmatrix}$$

$$\begin{pmatrix} \frac{T_w}{K} \\ \frac{P_{sat\_init}}{psi} \\ \frac{LMTD}{K} \\ \frac{\Delta Q}{W} \\ iter \\ \frac{P_{in}}{psi} \\ m_{dot}\cdot\frac{s}{gm} \\ \frac{T_{in}}{K} \\ \frac{P}{psi} \end{pmatrix}$$

$TEST := OUT(w2, t_{c2}, n_{c2}, Q_{h2})$

$R_{134} := TEST_0 \cdot \frac{W}{K}$

$T_{sat\_init} := TEST_1 \cdot K$

$Q_{out} := TEST_2 \cdot W$

$zz := TEST_3 \cdot in$

$QQ(N_{n2}, t_2, ff_2) = 4\,\frac{gal}{min}$

$GPM := QQ(N_{n2}, t_2, ff_2)$

$w2 = 0.275\,in$

$t_{c2} = 0.03\,in$

$n_{c2} = 3$

$N_{n2} = 57$

$t_2 = 0.05\,in$

$ff_2 = 0$

$PP := TEST_5 \cdot psi$

$T134 := TEST_6 \cdot K$

$Tsat := TEST_7 \cdot K$

$Tsea := TEST_8 \cdot K$

$QQ := TEST_9 \cdot W$

$Tw := TEST_{10} \cdot K$

$P_{EVAP\_OUT} := TEST_{11} \cdot psi - 1atm$ gauge pressure

$LMTD := TEST_{12} \cdot K$

$DQ := TEST_{13} \cdot W$

$ITER := TEST_{14}$

$P_{EVAP\_IN} := TEST_{15} \cdot psi - 1atm$ gauge pressure

$M_{DOT} := TEST_{16} \cdot \frac{gm}{s}$

$T_{OUT} := TEST_{17} \cdot K$

$PP_T := TEST_{18} \cdot psi - 1atm$ gauge pressure

$TEST =$

	0
0	[401, 1]
1	[5, 1]
2	[5, 1]
3	[401, 1]
4	[401, 1]
5	[401, 1]
6	[401, 1]
7	[401, 1]
8	[401, 1]
9	[401, 1]
10	[401, 1]
11	[5, 1]
12	[4, 1]
13	[401, 1]
14	4
15	[6, 1]
16	[5, 1]
17	[6, 1]
18	[401, 1]

$$\frac{d}{dTsat0}\left[UA\cdot\frac{(Tseann - Tsatnn) - (Tsea0 - Tsat0)}{\ln\left(\frac{Tseann - Tsatnn}{Tsea0 - Tsat0}\right)} - Qdes\right] \rightarrow \frac{UA}{\ln\left(\frac{Tseann - Tsatnn}{Tsea0 - Tsat0}\right)} - UA\cdot\frac{Tseann - Tsatnn - Tsea0 + Tsat0}{\ln\left(\frac{Tseann - Tsatnn}{Tsea0 - Tsat0}\right)^2\cdot(Tsea0 - Tsat}$$

$LMTD_{ITER-1} = 1.528K$ $\quad UA := \frac{\max(QQ)}{LMTD}$ $\quad UA_{ITER-1} = 132.019\frac{W}{K}$ $\quad \max(QQ) = 201.724W$

$f_{iter} := QQ_{nn} - Q_{h2}$ $\quad f_{iter} = 1.724W$

$$df_{iter} := \frac{-UA_{ITER-1}}{\ln\left(\frac{Tsea_0 - Tsat_0}{Tsea_{nn} - Tsat_{nn}}\right)} + UA_{ITER-1}\cdot\frac{Tsea_0 - Tsat_0 - Tsea_{nn} + Tsat_{nn}}{\ln\left(\frac{Tsea_0 - Tsat_0}{Tsea_{nn} - Tsat_{nn}}\right)^2\cdot\left(Tsea_0 - Tsat_0\right)} \quad df_{iter} = -40.554\frac{W}{K}$$

$$\frac{f_{iter}}{df_{iter}} = -0.043K$$

Plot the iterative Temperature and Heat Rates: # iterations: ITER

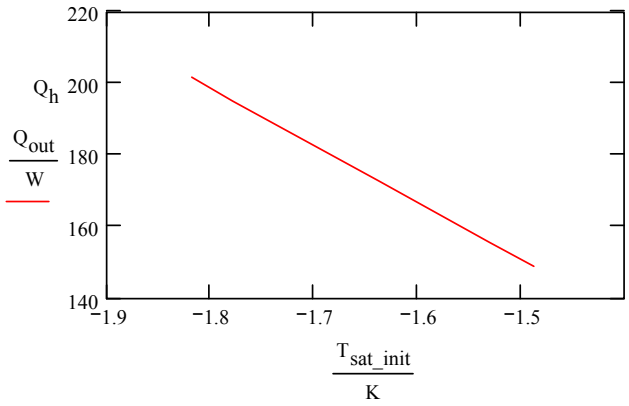

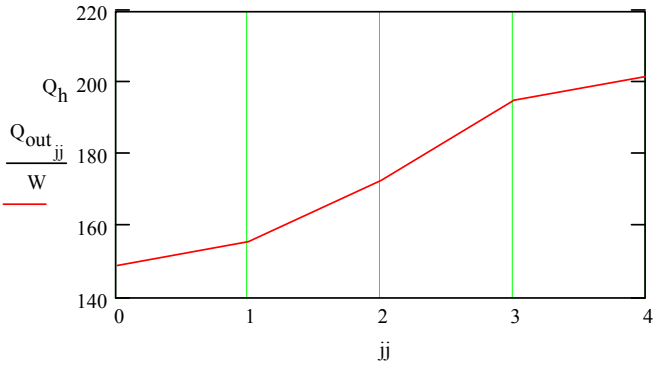

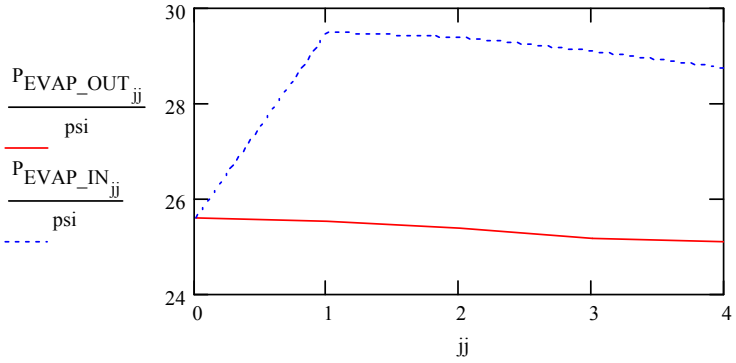

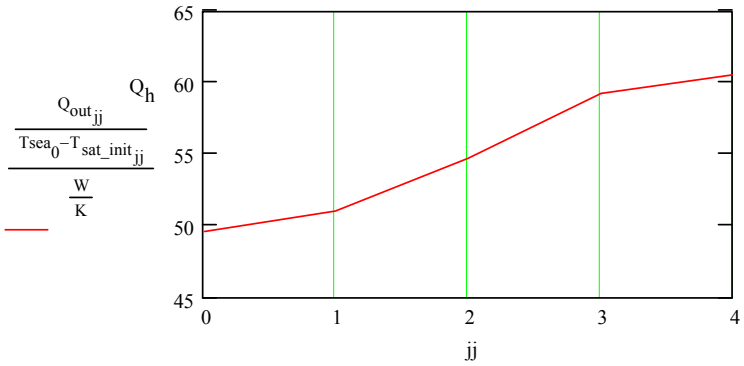

ITER = 4 jj := 0.. ITER

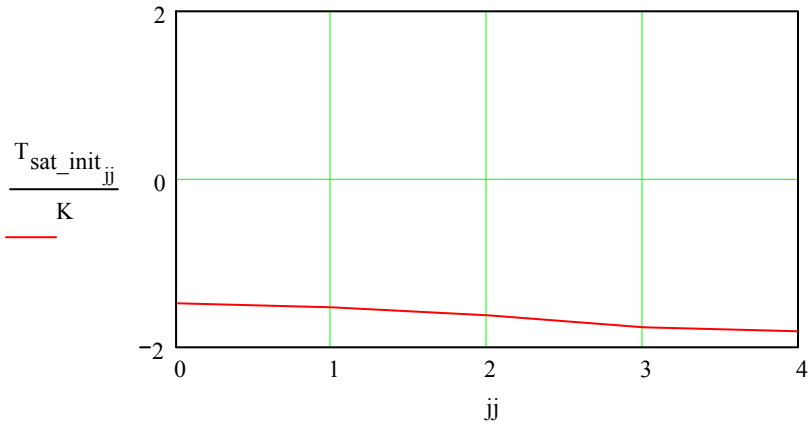

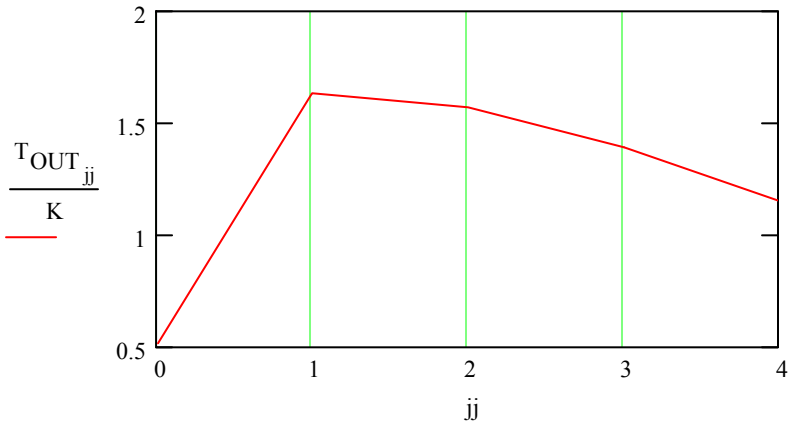

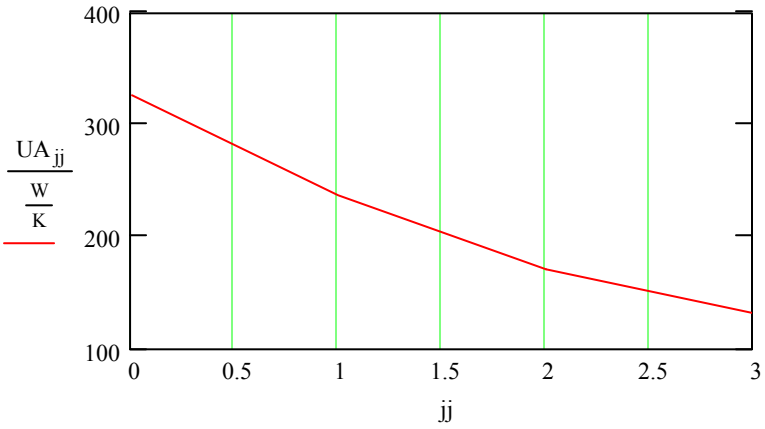

Summary:

$Tsea_0 = 1.512K$ $Tsea_{nn} = 1.702K$ $ITER = 4$ $ff_2 = 0$

$M_{DOT_{ITER}} = 1.314\frac{gm}{s}$ $GPM = 4\frac{gal}{min}$

$QQ_{nn} = 201.724W$ $w2 = 0.275in$

$P_{EVAP\_IN_{ITER}} = 28.715psi$ gauge pressure $Tsat_0 = -1.818K$ $t_{c2} = 0.03in$

$P_{EVAP\_OUT_{ITER}} = 25.095psi$ gauge pressure $Tsat_{nn} = 1.079K$ $n_{c2} = 3$

$P_{EVAP\_IN_{ITER}} - P_{EVAP\_OUT_{ITER}} = 3.620psi$ $L_f = 0.25in$

$\frac{max(QQ)}{Tsea_{nn} - mean(Tsat)} = 121.437\frac{W}{K}$ Q/(Tambin-Tsatavg) $t_2 = 0.05in$

$N_{n2} = 57$

$\frac{max(QQ)}{Tsea_{nn} - Tsat_1} = 68.069\frac{W}{K}$ Q/(Tambin-Tsatout)

$\frac{max(QQ)}{Tsea_{nn} - Tsat_{nn}} = 324.119\frac{W}{K}$ Q/(Tambin-Tsatin)

$SH := T134_0 - Tsat_0$ $SH = 2K$

$LMTD_{ITER-1} = 1.528K$ $UA_{ITER-1} = 132.019\frac{W}{K}$

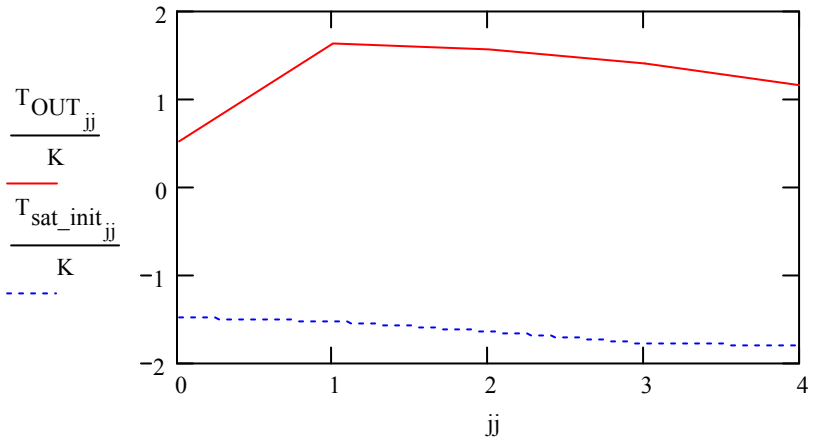

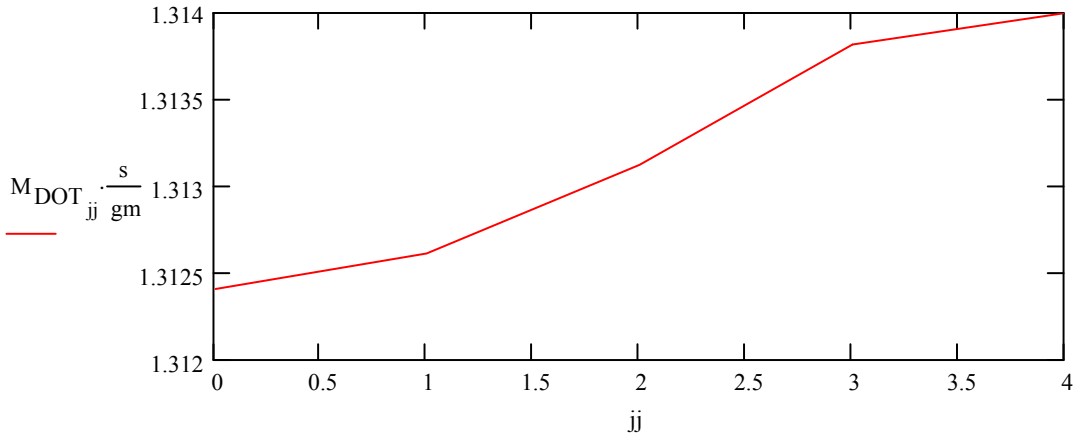

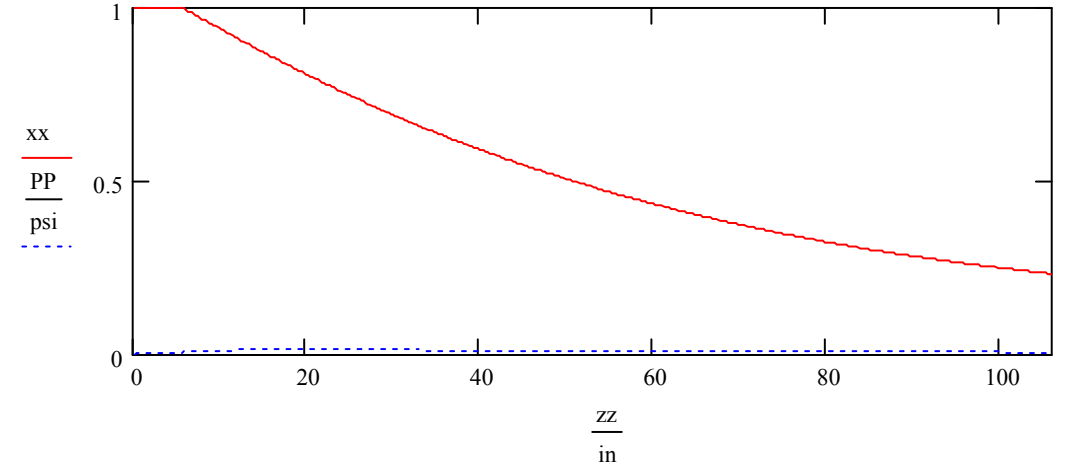

gauge pressure

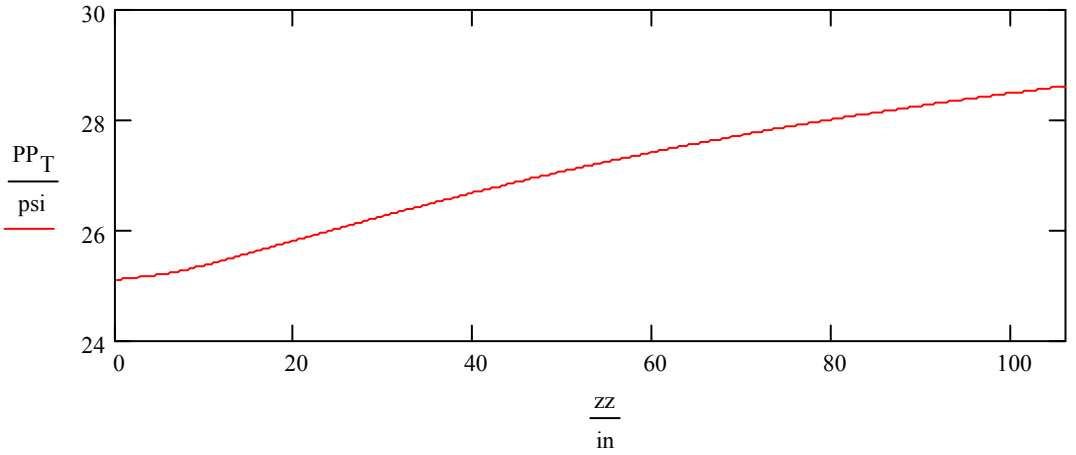

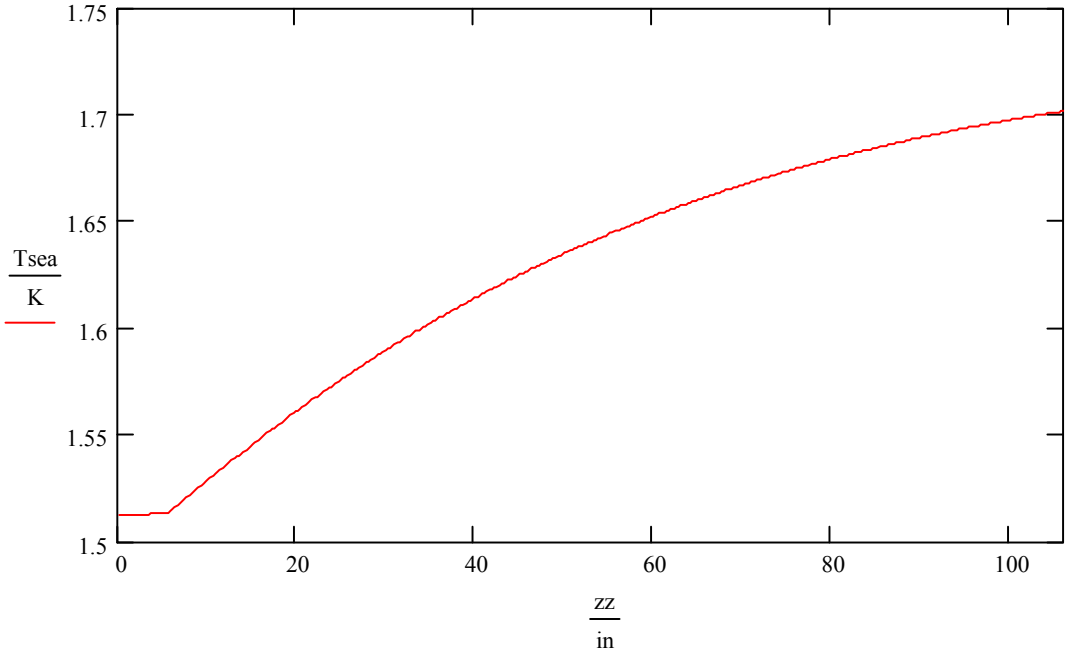

min(Tsat) = −1.818K max(Tsat) = 1.079K

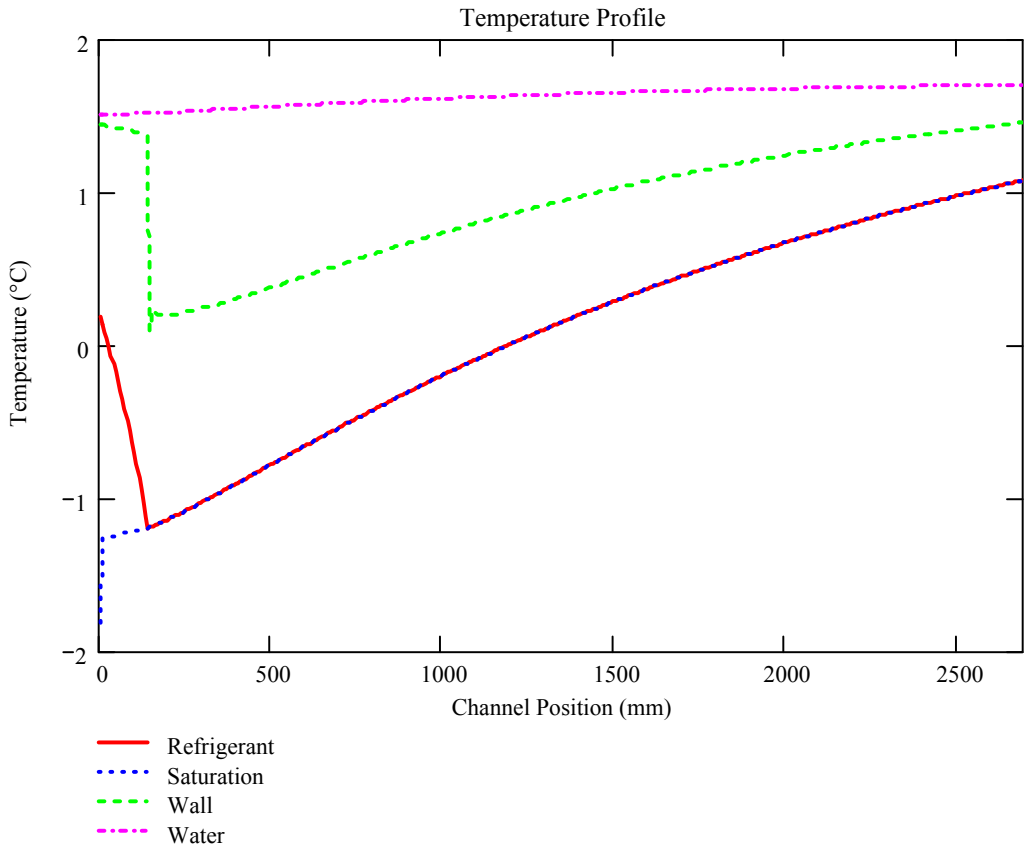

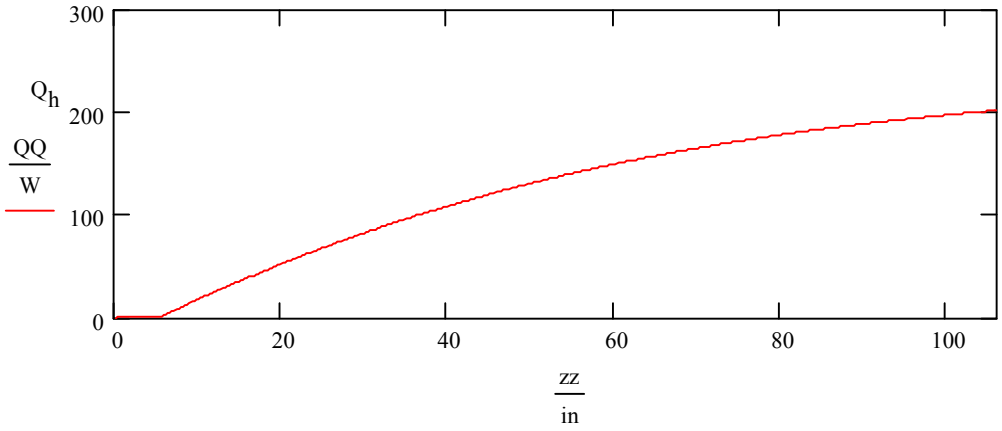

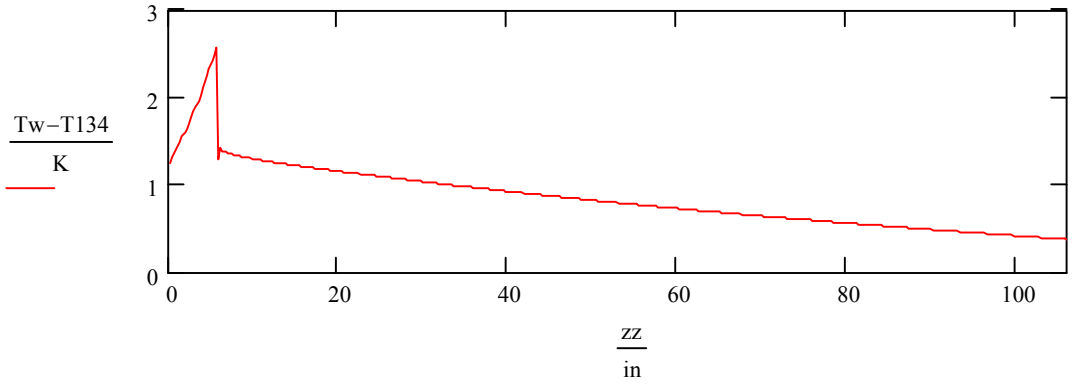

$$\Delta Z_2 := \frac{L_{ch}(w2, t_{c2}, n_{c2})}{nn} \qquad \Delta Z_2 = 0.265\text{in}$$

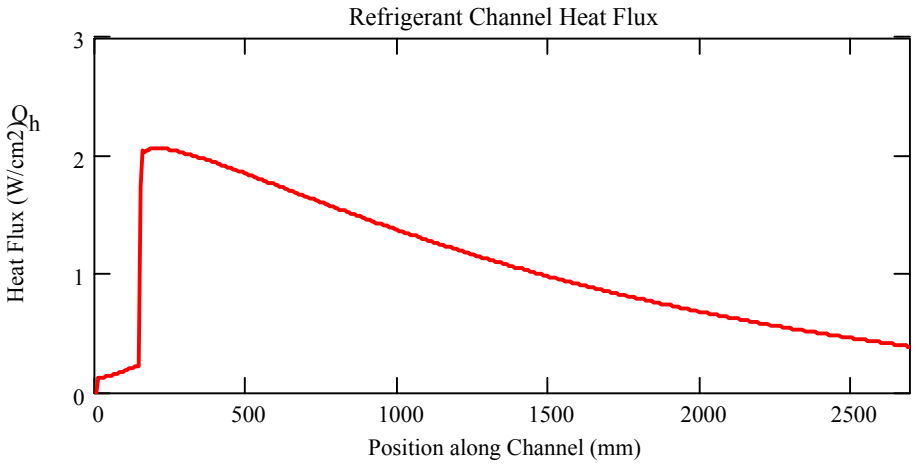

Create Functions to calculate Final W/K for a range of input geometry

$$w := \begin{pmatrix} 0.250 \\ 0.188 \\ 0.156 \\ 0.125 \end{pmatrix} \cdot in \quad t_c := \begin{pmatrix} 0.030 \\ 0.025 \\ 0.020 \\ 0.015 \end{pmatrix} \cdot in \quad n_c := \begin{pmatrix} 8 \\ 6 \\ 5 \\ 4 \\ 3 \end{pmatrix}$$

Iteration scheme to evaluate a range of geometries:

$$
\begin{aligned}
&\text{OUTPUT} := \left|\begin{array}{l}
\text{for } i \in 0..\text{rows}(w) - 1 \\
\quad \text{for } j \in 0..\text{rows}(t_c) - 1 \\
\quad\quad \text{for } k \in 0..\text{rows}(n_c) - 1 \\
\quad\quad\quad ii \leftarrow i \cdot \text{rows}(t_c) \cdot \text{rows}(n_c) + j \cdot \text{rows}(n_c) + k \\
\quad\quad\quad ANS_{ii,0} \leftarrow d_i \cdot in^{-1} \\
\quad\quad\quad ANS_{ii,1} \leftarrow L_c \cdot in^{-1} \\
\quad\quad\quad ANS_{ii,2} \leftarrow w_i \cdot in^{-1} \\
\quad\quad\quad ANS_{ii,3} \leftarrow t_{c_j} \cdot in^{-1} \\
\quad\quad\quad ANS_{ii,4} \leftarrow n_{c_k} \\
\quad\quad\quad ANS_{ii,5} \leftarrow hA_{water} \cdot \frac{K}{W} \\
\quad\quad\quad ANS_{ii,6} \leftarrow Vdot_{swim} \cdot \frac{min}{m^3} \\
\quad\quad\quad \text{break on error } CHX \leftarrow OUT\left(w_i, t_{c_j}, n_{c_k}, Vdot_{swim}, Q_h\right) \\
\quad\quad\quad Qevap \leftarrow \max\left(CHX_9\right) \\
\quad\quad\quad LMTD \leftarrow CHX_{12} \\
\quad\quad\quad UA \leftarrow \frac{Qevap}{LMTD} \\
\quad\quad\quad WperK \leftarrow WK\left(N_n, t, ff\right) \\
\quad\quad\quad DP \leftarrow CHX_{11} \\
\quad\quad\quad iter \leftarrow CHX_{14} \\
\quad\quad\quad ANS_{ii,7} \leftarrow Qevap \\
\quad\quad\quad ANS_{ii,8} \leftarrow \frac{Q_h}{h_{fg} + Cp_g \cdot Super + Cp_f \cdot Subcool} \cdot \frac{s}{gm} \\
\quad\quad\quad ANS_{ii,9} \leftarrow UA \\
\quad\quad\quad ANS_{ii,10} \leftarrow WperK \cdot \frac{K}{W} \\
\quad\quad\quad ANS_{ii,11} \leftarrow DP \\
\quad\quad\quad ANS_{ii,12} \leftarrow iter \\
ANS
\end{array}\right.
\end{aligned}
$$

APPENDIX C: DEPTH ANALYSIS

Evaporator Inner Cylinder

$d_o := 3.279\text{in}$ $d_i := 3.089\text{in}$

$l_s := 7.5\text{in}$

$t_s := \frac{d_o - d_i}{2}$ $t_s = 0.095\text{in}$

$A_s := d_o^2 \cdot \frac{\pi}{4}$

$a_s := \frac{d_o + d_i}{4}$ $d_s := 2 \cdot a_s$ $d_s = 3.184\text{in}$

Salt Water Properties:

$\rho_w := 1007 \frac{\text{kg}}{\text{m}^3}$ $D_w := 300\text{ft}$

$P_{ext} := \rho_w \cdot g \cdot D_w$ $P_{ext} = 130.969\text{psi}$

6061-T6 Aluminum Properties

$E_{al} := 10000000\text{psi}$

$\nu_{al} := 0.33$

$\sigma_{yp} := 40000\text{psi}$

Minimum thickness for a simple supported end cap subjected to external pressure [22]

Impeller stator housing:

$$t_{stator} := 2.5\text{in} \cdot \frac{1}{2} \cdot \sqrt{\frac{3 \cdot \left(\frac{3}{\nu_{al}} + 1\right) \cdot P_{ext}}{\frac{8}{\nu_{al}} \cdot \sigma_{yp}}} \qquad t_{stator} = 0.08\text{in}$$

Large stainless steel end cap with electrical connections:

$$t_{ss} := 3.109\text{in} \cdot \frac{1}{2} \cdot \sqrt{\frac{3 \cdot \left(\frac{3}{\nu_{al}} + 1\right) \cdot P_{ext}}{\frac{8}{\nu_{al}} \cdot 42100\text{psi}}} \qquad t_{ss} = 0.097\text{in}$$

Yield failure of externally loaded cylinder [17]

$$d_o \cdot \frac{1}{2} \cdot \left(1 - \sqrt{1 - \frac{2 \cdot P_{ext}}{\sigma_{yp}}} \right) = 0.005\text{in}$$

Minimum thickness for infinitely long cylinder [18]

$$\left(P_{ext} \cdot \frac{1 - \nu_{al}^2}{2 \cdot E_{al}} \right)^{\frac{1}{3}} \cdot d_o = 0.059\text{in}$$

Euler buckling for ideal cylinder:

$$F_{crE} := \frac{\pi^2 \cdot E_{al} \cdot \left[\left(\frac{d_o}{2} \right)^4 - \left(\frac{d_i}{2} \right)^4 \right] \cdot \frac{\pi}{4}}{(2 \cdot l_s)^2} \qquad F_{crE} = 5.287 \times 10^5 \text{ lbf}$$

$$P_{crE} := \frac{F_{crE}}{d_o^2 \cdot \frac{\pi}{4}} \qquad P_{crE} = 6.261 \times 10^4 \text{ psi}$$

$$\frac{P_{crE}}{P_{ext}} = 478.042$$

David Taylor Model Basin (DTMB) [20]:

$$P_{cr} := \frac{2.42 \cdot E_{al} \cdot \left(\frac{t_s}{d_s} \right)^{\frac{5}{2}}}{\left(1 - \nu_{al}^2 \right)^{\frac{3}{4}} \cdot \left[\left(\frac{l_s}{2 \cdot a_s} \right) - 0.447 \cdot \left(\frac{t_s}{2 \cdot a_s} \right)^{\frac{1}{2}} \right]} \qquad P_{cr} = 1780.873\text{psi}$$

$$\frac{P_{cr}}{P_{ext}} = 13.598$$

Thinness ratio [19]:

$$\lambda = \left[\frac{\left(\frac{l_s}{d_{avg}} \right)^2}{\left(\frac{t_s}{d_{avg}} \right)^3} \right]^{\frac{1}{4}} \cdot \sqrt{\frac{\sigma_{yp}}{E_{al}}}$$

PKD = 1.2

$P_{exp} := \frac{P_{cr}}{PKD}$ $P_{exp} = 1484psi$ $\frac{P_{exp}}{P_{ext}} = 11.3$ safety factor

Von Mises, simple supported cylinder [21]

number of circumferential waves or lobes into which the vessel buckles:

$n_b := 3$

$$P_{cr\_VM} = \frac{E_{al} \cdot \left(\frac{t_s}{r_{avg}} \right)}{n_b^2 - 1 + 0.5 \cdot \left(\pi \cdot \frac{r_{avg}}{l_s} \right)^2} \cdot \left[\frac{1}{\left[n_b^2 \cdot \left(\frac{l_s}{\pi \cdot r_{avg}} \right)^2 + 1 \right]^2} + \frac{t_s^2}{12 \cdot r_{avg}^2 \cdot (1 - \nu^2)} \cdot \left[\left(n_b^2 \right) - 1 + \left(\frac{\pi \cdot r_{avg}}{l_s} \right)^2 \right]^2 \right]$$

$P_{crVM} = 1884psi$

$\frac{P_{crVM} - P_{exp}}{P_{exp}} = 27\%$

$\frac{P_{crVM}}{P_{ext}} = 14.388$

APPENDIX D: DATA ACQUISITION

Measurement Devices:

Item	Manufacturer	Model Number
0-100 psi Pressure Transducer	Setra Systems, Inc.	2091-100P-G-2M-24-06
0-250 psi Pressure Transducer	Setra Systems, Inc.	2091-250P-G-2M-24-06
Water Flow Meter	Key Instruments	GS10910SNV
Refrigerant Flow Meter	Key Instruments	GS10830ANB
Type-T Thermocouple Probe	Omega Engineering, Inc.	TMQSS-062U-2
Thermocouple Wire	Omega Engineering, Inc.	TT-T-24-SLE-500
Data Acquasition	Omega Engineering, Inc.	OMB-DAQ-56
Data Acquasition Expansion Module	Omega Engineering, Inc.	OMB-PDQ2
Water Flow Meter	Key Instruments	FR4L66BNBN

Data Acquisition Layout:

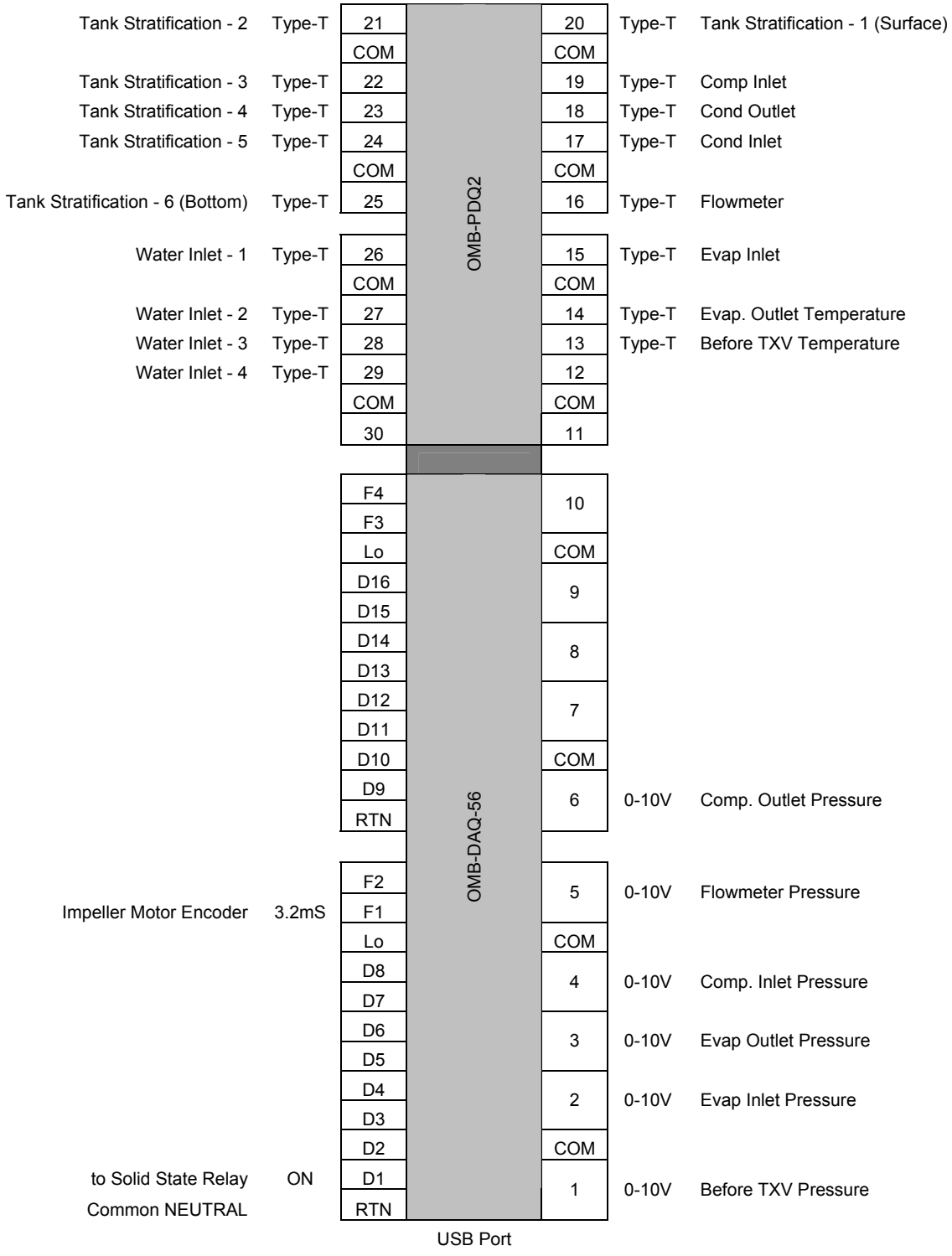

APPENDIX E: ERROR ANALYSIS

See Reference [24]

Temperature Measurements:

Accuracy = 1.0K Resolution = 0.00001

$B_{T1} := 0.1K$ $B_{T2} := 0.00001K$

$v := 200$ $S_T := 0.38K$ $t_{inf\_95} := 1.960$

$$u_T := \sqrt{B_{T1}^2 + \left[1.96 \cdot \left(\frac{S_T}{v^{0.5}}\right)\right]^2 + B_{T2}^2}$$

$$B_T := \sqrt{B_{T1}^2 + B_{T2}^2} \qquad P_T := 1.96 \frac{S_T}{v^{0.5}}$$

Water Flow Measurements

Accuracy = $0.1 \frac{gal}{min}$ Resolution = $0.2 \frac{gal}{min}$

$B_{V1} := 0.1 \frac{gal}{min}$ $B_{V2} := 0.2 \frac{gal}{min}$

$$B_V := \sqrt{B_{V1}^2 + B_{V2}^2}$$

Heat Rate Measurement Errror:

$Q = \rho_w \cdot Cp_w \cdot V_{dot} \cdot \Delta T$

$Cp_w := 4.216 \frac{J}{gm \cdot K}$ $\rho_w := 1000 \frac{kg}{m^3}$ $V_{dot} := 4 \frac{gal}{min}$ $\Delta T := 0.188K$

$$\frac{d}{dV_{dot}} Q = \rho_w \cdot Cp_w \cdot \Delta T$$

$$\frac{d}{d\Delta T} Q = \rho_w \cdot Cp_w \cdot V_{dot}$$

$$u_{Qw} = \sqrt{\left(B_V \cdot \frac{d}{dV_{dot}} Q\right)^2 + \left(B_T \cdot \frac{d}{d\Delta T} Q\right)^2 + \left(B_V \cdot \frac{d}{d\Delta T} Q\right)^2}$$

$$u_{Qw} := \sqrt{\left(B_V \rho_w \cdot Cp_w \cdot \Delta T\right)^2 + \left(B_T \cdot \rho_w \cdot Cp_w \cdot V_{dot}\right)^2 + \left(P_T \cdot \rho_w \cdot Cp_w \cdot V_{dot}\right)^2}$$

$u_{Qw} = 121W$

APPENDIX F: MOTOR EFFICIENCY

Motor Efficiency Calculator:

$mN := 10^{-3} \cdot N \quad ozf := \frac{lbf}{16} \quad rpm := \frac{1}{min} \quad krpm := 1000 rpm$

Motor Characteristics:

max continuous torque in air

$\tau_{maxcont} := 7 \cdot ozf \cdot in$

torque constant

$K_t := 2.5 \cdot \frac{ozf \cdot in}{A}$

motor resistance

$R_{motor} := 1 ohm$

static torque

$\tau_{static} := 1.164 ozf \cdot in$

damping

$f_{damping} := 0.224 \frac{ozf \cdot in}{krpm}$

voltage constant

$K_v := \frac{1}{2 \cdot \pi \cdot K_t} \quad K_v = 540.918 \frac{rpm}{V}$

motor constant

$K_m := \frac{K_t}{\sqrt{R_{motor}}} \qquad K_m = 2.5 \frac{ozf \cdot in}{\sqrt{W}}$

Operating Conditions:

$P_{shaft} := 1.9 W$

$n_{load} := 590 rpm$

$\tau_{load} := \frac{P_{shaft}}{2 \cdot \pi \cdot n_{load}} \qquad \tau_{load} = 4.355 ozf \cdot in$

Estimated Controller Resistance:

$R_{cont} := 0.005 \Omega$

Calculations:

$$\tau_{total}(n) := \tau_{load} + \tau_{static} + f_{damping} \cdot n$$

Current:

$$I_{load} := \frac{\tau_{total}(n_{load})}{K_t} \qquad I_{load} = 2.26A$$

no-PWM operating voltage:

$$U_{load} := \frac{n_{load}}{K_v} + I_{load} \cdot (R_{motor} + R_{cont}) \qquad U_{load} = 3.362V$$

theoretical stall torque

$$\tau_{stall}(U) := K_t \cdot \left(\frac{U}{R_{motor} + R_{cont}} \right)$$

theoretical free speed shaft speed:

$$n_0(U) := K_v \cdot U \qquad n_0(U_{load}) = 1818.805rpm$$

torque load as a function of shaft speed and voltage:

$$\tau_{load}(n, U) := \tau_{stall}(U) \cdot \left(1 - \frac{n}{n_0(U)} \right) - \tau_{static} - f_{damping} \cdot n$$

total torque as a function of shaft speed and voltage:

$$\tau_{total}(n, U) := \tau_{load}(n, U) + \tau_{static} + f_{damping} \cdot n$$

motor current:

$$I_{input}(n, U) := \frac{\tau_{total}(n, U)}{K_t}$$

motor input power:

$$P_{input}(n, U) := U \cdot I_{input}(n, U)$$

resistance heat losses in motor windings

$$P_{heat}(n, U) := I_{input}(n, U)^2 \cdot R_{motor}$$

shaft work

$$P_{output}(n, U) := 2 \cdot \pi \cdot \tau_{load}(n, U) \cdot n$$

Motor Efficiency:

$$\eta(n, U) := \frac{P_{output}(n, U)}{P_{input}(n, U)}$$

$$\eta(n_{load}, U_{load}) = 25.0\%$$

$x := 30 \cdot rpm, 40 \cdot rpm .. 3000 \cdot rpm$

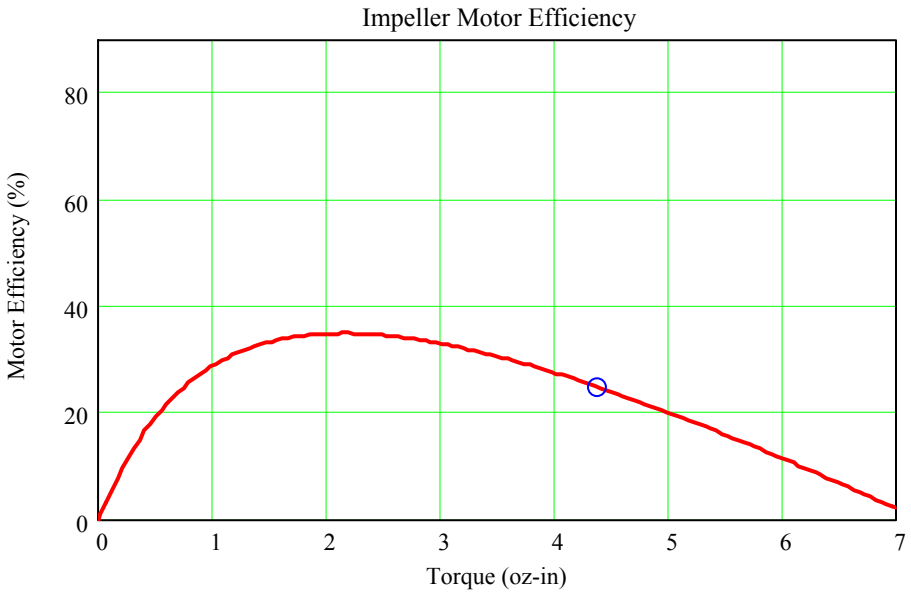

REFERENCES

[1] Bardy E, Molledndorf J and Pendergast D., Thermal conductivity and compressive strain of foam neoprene insulation under hydrostatic pressure *J. Phys. D: Appl. Phys.* 38 3832-40, 2005.

[2] Bardy E, Molledndorf J and Pendergast D., Regional and total body active heating and cooling of a resting diver in water of varied temperatures *J. Phys. D: Appl. Phys.* 41, 2008.

[3] Webb P, et al., Proposed Thermal Limits for Divers Office of Naval Research Contract N00014-72-C-0057, 1976.

[4] Incropera, F. P., and DeWitt, D. P., Introduction to Heat Transfer, Fourth Edition, John Wiley and Sons, Inc., New York, 2002.

[5] Ostrach, S., "An Analysis of Laminar Free Convection Flow and Heat Transfer About a Flat Plate Parallel to the Direction of the Generating Body Force," National Advisory Committee for Aeronautics, Report 1111, 1953.

[6] Kays W.M., and Crawford, M. E., Convective Heat Transfer, McGraw-Hill, New York, 1980.

[7] Carey, Van P. Liquid-Vapor Phase Change Phenomena, Second Edition, Taylor and Francis, United States. 2007.

[8] Lockhart, R. W., and Martinelli, R. C., Proposed correlation of data for isothermal two-phase, two-component flow in pipes, *Chem. Eng. Prog*., vol. 45, no. 1, pp. 39-48, 1949.

[9] Gnielinski, V., *Int. Chem. Eng.*, **16**, 359, 1976.

[10] Petukhov, B.S., in Irvine, T. F., and Hartnett, J.P., Eds., Advances in Heat Transfer, Volume 6, Academic Press, New York, 1970.

[11] Chen, J. C., Correlation for boiling heat transfer to saturated fluids in convective flow, *Ind. Eng. Chem. Proc. Design and Dev.,* Vol. 5, No. 3, pp. 322-339, 1966.

[12] Bennett, D. L., and Chen, J. C., Forced convective boiling in vertical tubes for saturated pure components and binary mixtures*, AIChE J*., vol. 26, pp. 454-461, 1980.

[13] Collier, J. G., Forced convective boiling, in Two-Phase Flow and Heat Transfer in the Power and Process Industries, A. E. Bergles, J. G. Collier, J. M. Delhaye, G. F. Hewitt, and F. Mayinger, Eds., Hemisphere, New York, 1981.

[14] Taitel, Y., and Dukler, A. E., Flow regime transitions for vertical upward gas-liquid flow:A preliminary approach through physical modeling, Paper presented at Session on Fundamental Research in Fluid Mechanics at the 70th AIChE Annual Meeting, New York, 1977.

[15] Forster, H. K., and Zuber, N., Dynamics of vapor bubbles and boiling heat transfer, *AIChE J*., vol. 1, pp. 531-535, 1955.

[16] Bennett, D. L., David, M. W., and Hertzler, B. L., The suppression of saturated nucleate boiling by forced convective flow, *AIChE Symp. Ser*., vol. 76, no. 199, pp. 91-103, 1980.

[17] Roark, R. and Young, W., Roark's Formulas for Stress and Strain, 7th Edition, McGraw-Hill, 2001.

[18] Bryan, G.H., Application of the Energy Test to the Collapse of a Long Thin Pipe under External Pressure, *Cambridge Philosophical Society Proceedings*, vol. 6, pp. 287-92, 1888.

[19] Ross, C. T. F., Pressure Vessels External Pressure Technology, Horwood Publishing Limited, pp.98-109, 2001.

[20] Windenburg, D.F. and Trilling, C., Collapse by Instability of Thin Cylindrical Shells under External Pressure, *Trans. ASME*, 11, 819-25, 1934.

[21] Von Mises, R., Der Kritische Aussendruck für Allseits Belastete Zylindrische Rohre, *Fest Zum 70. Gerburtstag von Prof. Dr A. Stodola, Zürich,* pp. 418-30, 1929 (also USEMB Translation Report No. 366, 1936).

[22] Avallone, E., Baumeister, T., Sadegh, A., Mark's Standard Handbook for Mechanical Engineers, 11th Edition, McGraw-Hill Professional, 2006.

[23] Davis, J. P., Surface Engineering for Corrosion and Wear Resistance, ASM International, 2001.

[24] Figliola, R. S., and Beasley, D. E., Theory and Design for Mechanic Measurements, 3rd Edition, John Wiley & Sons, Inc., New York, 2000.